Technical University of Denmark

DTU

Association Euratom - Risø National Laboratory annual progress report 2006

Michelsen, Poul; Singh, Bachu Narain

Publication date:
2007

Document Version
Publisher's PDF, also known as Version of record

Link back to DTU Orbit

DTU Library
Technical Information Center of Denmark

Association Euratom - Risø National Laboratory - Annual Progress Report 2006

Edited by P.K. Michelsen and B.N. Singh

RISØ

DTU

Author: Edited by P.K. Michelsen and B.N. Singh
Title: Association Euratom - Risø National Laboratory - Annual Progress Report 2006
Department: Optics and Plasma Research Department

Abstract (max. 2000 char.):

The programme of the Research Unit of the Fusion Association Euratom - Risø National Laboratory, Technical University of Denmark, covers work in fusion plasma physics and in fusion technology. The fusion plasma physics research focuses on turbulence and transport, and its interaction with the plasma equilibrium and particles. The effort includes both first principles based modelling, and experimental observations of turbulence and of fast ion dynamics by collective Thomson scattering. The activities in technology cover investigations of radiation damage of fusion reactor materials. These activities contribute to the Next Step, the Long-term and the Underlying Fusion Technology programme. A summary is presented of the results obtained in the Research Unit during 2006.

Contents

3 Fusion Technology 48

4 System analysis 70

5 ITER and Danish industry activities 71

Preface

In 2006 seven parties, EU, Japan, Russia, China, USA, Korea and India, signed the agreement to build and exploit ITER, and to place ITER in Cadarache in France. ITER is a major experimental facility for the development of fusion as an energy source. It is expected that ITER will be ready for scientific exploitation in 2016. The mission of ITER is to demonstrate that nuclear fusion can be exploited as an energy source. ITER represents an unprecedented international cooperation in the field of science and technology. It also represents a valuable opportunity for cooperation between public research organisations and private industry. Risø participates in the internationally coordinated activities to develop fusion and sees itself as having a key role in facilitating the participation of Danish industries in the international fusion programme.

The principle being pursued with ITER is the fusion of hydrogen isotopes to form helium. To make the fusion process run at a significant rate the hydrogen gas must be heated to high temperatures where it ionises and turns into a plasma. The plasma must be confined to achieve suitable densities and sustain the high temperature. ITER will use a magnetic field for the confinement. While fusion holds the promise of providing a sustainable source of energy, which is environmentally sound, it also presents considerable scientific and engineering challenges. Key issues in the final steps towards realising fusion energy production include:

Improving the plasma energy confinement, that is the ratio between the energy of the plasma and the heating power required to sustain the plasma energy. Improving energy confinement implies reducing energy transport out of the plasma, which principally is due to turbulence. So what we really need to do is to understand and control turbulence.

Channelling the energy of fast ions, produced in fusion reactions, into heating the bulk plasma without driving turbulence and without premature exit of the fast ions from the plasma. This requires understanding and control of the dynamics of the fast ions in interaction with other particles and with waves.

Development of materials, which maintain required mechanical properties under high and sustained neutron fluxes. Neutrons, produced in the fusion reactions, are not confined by the magnetic field. They pass through the first wall of the chamber surrounding the plasma, slowing down on impact with atoms in the wall, thereby giving rise to dislocations in the wall material, which affect the properties of the material.

Risø contributes to fusion research in all these areas: 1) codes, modelling turbulence and transport, are continually improved, and benchmarked against experiments. 2) Central to understanding the dynamics of fast ions is are temporally and spatially resolved measurements of the fast ion velocity distributions in the plasma. Risø, in collaboration with MIT (USA) and EURATOM partners, is exploiting and developing millimetre wave based collective Thomson scattering (CTS) diagnostics at the TEXTOR and ASDEX upgrade tokamaks in FZ-Jülich and the Max-Planck Institute for plasma physics in Garching (near Munich). Of particular note this year has been detailed measurements of fast ion populations in the TEXTOR which are in excellent agreement with Fokker-Planck modelling of the fast ion dynamics. Significant effort also goes into developing a fast ion CTS diagnostic for ITER. 3) In the field of irradiated materials Risø investigates the properties of copper alloys relevant to ITER, and of iron alloys, which will be an essential component of a commercial fusion power plant.

1 Summary of Research Unit activities

The activities in the Research Unit cover two main areas:

Fusion Plasma Physics, which includes:

- *Theoretical and numerical turbulence studies.* Turbulence and the associated anomalous transport is investigated using first principles based models and solving these by means of numerical codes in full toroidal geometry. These models are continuously being developed and benchmarked against experimental data and codes at other associations. The dynamics of bursts of fluctuations leading to profile relaxation have been studied in models for flux-driven interchange mode turbulence, where the back reaction of the turbulence on the equilibrium flows and profiles are accounted for.

- *Fast Ion Collective Thomson Scattering.* Risø has taken the lead in the development and exploitation of fast ion collective Thomson scattering diagnostics for TEXTOR, ASDEX Upgrade (AUG) and ITER. These projects are carried out in close collaborations with MIT, and with the TEC† and AUG teams.

Fusion Technology, which includes:

- Experimental and theoretical investigations of the effects of irradiation on the microstructural evolution and on the physical and mechanical properties of metals and alloys relevant to the Next Step, the Long Term and Underlying Fusion Technology Programme.

The **global indicators** for the Research Unit in 2006 are:

Professional staff:	14.0	man-years
Support staff:	8.66	man-years
Total expenditure - incl. mobility:	2.69	MioEuro
Total Euratom support:	0.66	MioEuro

---

† TEC: the Trilateral Euregio Cluster, a collaboration of FOM Institute for Plasma Physics, Holland; ERM/KMS, Belgium and Forschungszentrum Jülich, Germany.

2 Plasma Physics and Technology

2.1 Introduction

H. Bindslev
henrik.bindslev@risoe.dk

A plasma is a dense collection of free ions and electrons. The transitions from solids to fluids to gases are associated with increases in internal energy, the breaking of bonds and changes of physical properties. The same is true of the transition from a gas to a plasma; in fact the plasma is rightfully described as the fourth state of matter, its physics differing as much from that of gases as that of solids does. Just as solid state physics is involved in a broad range of applications, so it should be no surprise that plasmas have a wide range of applications, that their physics and chemistries are rich, and that the methods of generation and diagnosis are wide and complex.

Our activities in high temperature plasmas, aimed at developing fusion energy, are coordinated with the European EURATOM fusion programme through an agreement of association on equal footing with other fusion laboratories in Europe. Our EURATOM association facilitates extensive collaboration with other fusion research laboratories in Europe, crucial in the ongoing build-up of competencies at Risø, and gives us access to placing our experimental equipment on large fusion facilities at the Max-Planck Institute for Plasma Physics in Garching and at the Research Centre Jülich, both in Germany. Our association with EURATOM also provides the basis for our participation in the exploitation of the European fusion research centre, JET, located in England. With its organisation of national programmes as EURATOM associations, the European fusion programme is a successful example of a large *European Research Area.* Our activities in high temperature plasma research and the development of fusion energy are introduced in subsection 2.1.1, and described in further detail in subsection 2.2 discussing turbulence and transport in fusion plasmas, and in subsection 2.3 discussing our use of millimetre waves for investigating the dynamics of fast ions in fusion plasmas.

2.1.1 Fusion plasma physics

H. Bindslev
henrik.bindslev@risoe.dk
www.risoe.dk/euratom

Producing significant amounts of fusion energy requires a plasma with a temperature of 100 to 200 million degrees and densities of 1 to 2 times 10^{20} particles per cubic metre, corresponding to a pressure of 1 to 5 atmosphere. Unlike gases, plasmas can be confined and compressed by magnetic fields. At the required temperatures the plasma must be lifted off material walls to prevent the plasma from rapid cooling. This is done by suspending the plasma in a toroidally shaped magnetic field that also acts to balance the plasma pressure. The required temperature and densities have been achieved in the joint European fusion experiment, JET. The production of net energy adds the requirement that the energy in the plasma be confined at least on the order of six seconds. The confinement time is the characteristic time for cooling off if heating was switched off or, equivalently, the ratio of plasma energy to required heating power to sustain that energy content. Achieved confinement times are on the order of one second. Higher density could compensate shorter confinement time and visa versa, so a simplified statement of the target is that the product of temperature, density and confinement time should be six

atmosphere × seconds and is currently one atmosphere × seconds. Progress towards the goal principally involves improving the confinement time or, equivalently, reducing the energy transport in the plasma. The energy transport in fusion grade plasmas is principally due to turbulence, one of our main research activities reported in subsection 2.2. Significant progress towards the goal is expected with the next step fusion experiment, ITER. In ITER significant fusion rates are expected and with that the fast ion populations in the plasma will increase dramatically compared with present machines. The fast ions may then influence the plasma significantly. As a consequence, the dynamics of fast ions and their interaction with the rest of the plasma is one of the central physics issues to be studied in ITER. It is in fact also one of our main research topics in fusion as reported in subsection 2.3.

The fields of turbulence, transport and fast ions are closely knit. With steep gradients in plasma equilibrium parameters and with populations of energetic ions far from thermal equilibrium, fusion plasmas have considerable free energy. This energy drives turbulence, which in turn acts back on the equilibrium profiles and on the dynamics of the fast ions. The turbulence naturally gives rise to enhanced transport, but also sets up zonal flows that tear the turbulent structures apart and result in edge transport barriers; most likely at the root of the poorly understood, but experimentally reliably achieved, high confinement mode (H-mode). This non-linear interplay between turbulence and equilibrium also supports transient events reminiscent of edge localised modes (ELMs) where energy and particles are ejected from the plasma edge in intermittent bursts.

This set of topics is the focus of our fusion plasma physics research: With first-principles based codes we seek to model the interplay between plasma turbulence, transport and equilibrium. This modelling is tested against experimental data in collaboration with other fusion plasma physics institutes. To elucidate the physics of fast ions and their interplay with turbulence, waves and transient events, we are engaged in the diagnosis of confined fast ions by collective Thomson scattering (CTS) at the TEXTOR tokamak at the Research Centre Jülich and at the ASDEX upgrade tokamak in the Max-Planck Institute for Plasma Physics in Garching, both in Germany.

2.2 Turbulence and transport in fusion plasmas
O. E. Garcia, V. Naulin, A. H. Nielsen and J. Juul Rasmussen
volker.naulin@risoe.dk; jens.juul.rasmussen@risoe.dk

The transport of heat and particles across the confining magnetic field of fusion plasmas is one of the most important and interesting, but also most difficult areas of contemporary fusion research. It is well established that the "anomalous" transport component mediated by low frequency turbulence is far larger than both the classical and neo-classical collisional transport, at least in the edge region. Therefore it is utmost importance to achieve a detailed understanding of anomalous transport and the underlying turbulence for the design of an economical viable fusion reactor based on magnetic confinement devices. In spite of the dramatic progress in experiment, theory and computations during recent years the quantitative understanding is still sparse and any predictive capacity is at best rudimentary. Even fundamental phenomena such as transitions from low confinement regime (L-mode) to high confinement regime (H-mode), the profile resilience and the particle pinch that are routinely observed and classified experimentally have no generally accepted detailed explanations.

The activities within plasma turbulence and transport are mainly focussed on topics related to edge and scrape-off-layer (SOL) regimes of toroidal plasmas. It is generally acknowledged that the conditions near the edge of the plasma are dictating the global performance, a natural assumption since all transport has to go through the edge region. Theoretical and numerical investigations of first principle models form the majority of the work performed. We emphasize benchmarking of results and performance both with other codes and increasingly with experimental observations.

Our activities are fully integrated into the EURATOM fusion program, and we have active collaborations with several EURATOM laboratories on theoretical issues as well as on direct comparisons of our results with experimental observations. We have a strong standing within the EFDA-JET program, with V. Naulin as deputy task force leader of Task-Force Transport. We are actively participating in the Integrated Tokamak Modelling (ITM) Task Force on validation and benchmarking of codes as well defining the ITM data structures. In the spring of 2006 we where hosting a workgroup meeting of the IMP4 activity within ITM with participants from Germany, Austria, Switzerland, and Portugal. The theme was on global modelling of edge/SOL dynamics including issues as boundary conditions etc. Several of our numerical codes are in use at different European laboratories, where they are employed for specific purposes, ranging from experimental comparisons to education of students. The collaboration with the TCV group at CRPP, EPFL in Lausanne, has resulted in specifically good results (see Sec. 2.2.1). Detailed comparisons of the codes with experiment were performed for JET, where first results were presented at IAEA (see Sec. 2.2.2) and are emerging for other devices, amongst them ASDEX Upgrade and MAST.

The work carried out through 2006 included the following items:
- Investigations of the turbulence and transport at the edge and SOL of toroidal plasmas by applying the two dimensional, electrostatic edge-SOL turbulence code, ESEL. It is well established that turbulence and transport in the edge and SOL of toroidal plasmas are strongly intermittent and involve outbreaks of hot plasma. These structures, often referred to as "blobs", are formed near the last closed flux surface (LCFS) and propagate far into the SOL and into the wall shadow region. They have a profound influence on the pressure profiles in the SOL, the ensuing parallel flows, and the power deposition on plasma facing components. The ESEL code describes the perpendicular dynamics and transport events in the SOL. The profiles of density, electron temperature, and vorticity are evolved together with the fluctuations, without making a scale separation-ansatz, i.e., allowing relative fluctuation levels of order unity and profile variations by many orders of magnitude. In Sec. 2.2.1 we describe the latest results on the successful quantitative comparison between the experimental results from TCV (EPFL, Lausanne) and the ESEL code. Discussions of the comparisons with JET results are presented in the following section (2.2.2), while the initial comparisons with ASDEX Upgrade data are presented in Sec. 2.2.6. With the aim to estimate the amount of recycling generated by the out streaming plasma in the SOL we have initiated a collaboration with IPP Juelich, where we couple the ESEL code with the Monte Carlo code EIRENE, which calculates the recycling in local plasma conditions see Sec. 2.2.3.
- The involvement in the JET work programme is described in Sec. 2.2.2. It is focused on modelling and simulation and involves in addition to the investigation of turbulence and transport in the JET SOL described above also modelling of transient transport events in the plasma core.
- The basic dynamics of field aligned plasma filaments, including blobs, in the SOL is well described in terms of nonlinear interchange motions; see Sec. 2.2.4. The filaments are localized across the magnetic field and propagate radially through

the SOL with a velocity of approximately one tenths of the ion sound speed. The results reveal a scaling for the maximum radial velocity of the blobs and specifically the role of different parallel boundary conditions have been clarified.

- In order to extend our turbulence modelling in the edge/SOL we have derived a gyro-fluid model for the two dimensional interchange dynamics as a generalization of the ESEL code (see Sec. 2.2.5). In the initial investigations we have studied the influence of finite ion Larmor radius on the propagation of blobs and on the development of the interchange turbulence in edge/SOL. The basic characteristics are not altered by the finite ion temperature, but there are significant changes in the detailed dynamical evolution.

- The spontaneous formation of flows in turbulence is an ongoing topic in fusion research. We have investigated the dependence of Reynolds-, Maxwell- and geodesic transfer terms for varying values of q and magnetic shear using the 3 dimensional electromagnetic code TYR, and have observed a tendency for the spatial structure of the transfer to align with the rational surfaces. See Sec. 2.2.7.

- We have "exported" our codes (ESEL, TYR) to several laboratories within EURATOM, where they have been adapted and employed for specific purposes. The basic Hasegawa-Wakatani code is now in use at several laboratories and University Institutes for producing "synthetic" turbulence data for testing various diagnostic methods. As an example, Sec. 2.2.8 describes the testing of an experimental method for measuring the nonlinear energy transfer function in two-dimensional turbulence.

2.2.1 Fluctuations and transport in the TCV scrape-off layer

O. E. Garcia, J. Horacek (Association EURATOM-Institute of Plasma Physics, Prague, Czech Republic), R. A. Pitts (CRPP, EPFL, CH-1015 Lausanne, Switzerland), A. H. Nielsen, W. Fundamenski (EURATOM/UKAEA Fusion Association, Culham Science Centre, Abingdon OX14 3DB, United Kingdom), V. Naulin and J. Juul Rasmussen
odd.erik.garcia@risoe.dk

Fluctuations and particle transport in the scrape-off layer (SOL) of TCV plasmas have been investigated by probe measurements and direct comparison with two-dimensional ESEL interchange turbulence simulations at the outer midplane region.[1] The experiments demonstrate that with increasing line-averaged core plasma density, n_e, the radial particle density profile becomes broader in both scale length and radial extent, as seen in Figure 1. The particle and radial flux density statistics in this so-called far-SOL exhibit a high degree of statistical similarity with respect to changes in the line-averaged core plasma density. This is exemplified by the relative plasma fluctuation level presented in Figure 1, which has the same magnitude and radial variation for all n_e in the region with broad profiles.

From Figure 2 we further see that at the wall radius position the plasma fluctuations have the same asymmetric temporal waveform with a steep front and a trailing wake. Note that the bursty plasma fluctuations have characteristic amplitudes of nearly 4 times the root-mean-square value of the full time series. The probability density function (PDF) of the fluctuations, also presented in Figure 2, are strongly skewed and flattened with a similar shape for all values of the line-averaged core plasma density. The time-averaged values of the particle and radial flux densities at the wall radius are both found to increase quadratically with the line-averaged plasma density. As a consequence, the turbulence driven particle flux in the wall region can be parameterized in terms of an effective convection velocity, although there does not seem to be any simple flux parameterization in terms of effective convection or diffusion that is valid at all radial positions in the SOL and for all values of n_e.

The experimental measurements are compared with a two-dimensional ESEL interchange turbulence simulation, employing a simple description of open and closed field line regions.[1] The simulations reveal that plasma transport in the SOL is dominated by radial motion of filamentary structures, which appear as blobs in the plane perpendicular to the magnetic field. This is shown to result in broad plasma profiles, large relative fluctuation levels, asymmetric wave forms, skewed and flattened PDFs, and significant transport-driven parallel flows when estimated from pressure fluctuation statistics. Based on the good agreement between the turbulence simulation and experimental measurements across a range of fluctuation statistics, it is concluded that interchange motions are the salient mechanism underlying the collective dynamics observed in the TCV SOL and by inference in the same region of other tokamaks.

1. O. E. Garcia, J. Horacek, R. A. Pitts, A. H. Nielsen, W. Fundamenski, J. P. Graves, V. Naulin, J. J. Rasmussen, Plasma Phys. Control. Fusion **48**, L1 (2006).
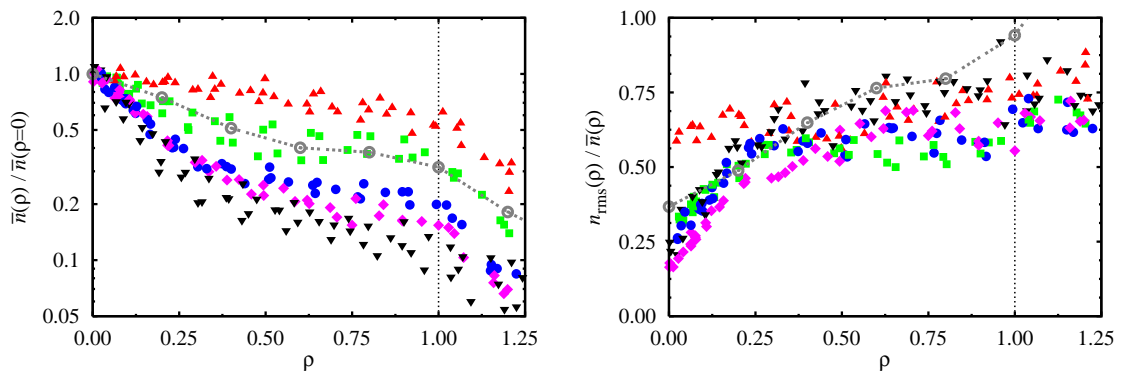
Figure 1. Radial variation of the average particle density (left) and its relative fluctuation level (right) at the outer midplane region of the TCV device for a range of different line averaged core particle densities. The broken lines with open circles are the results from ESEL interchange turbulence simulations.
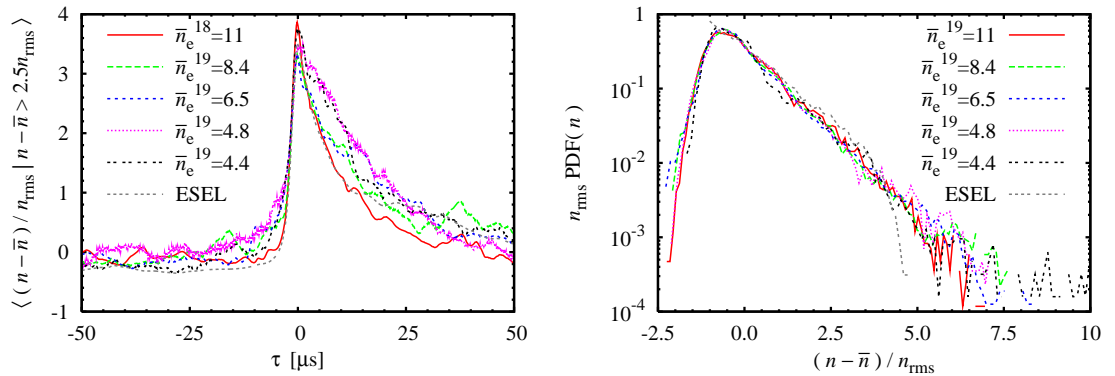
Figure 2. Conditional average (left) and the probability density function (right) of the particle density at the outer midplane region of the TCV device for a range of different line averaged core particle densities. The broken grey lines are the results from ESEL interchange turbulence simulations.

2.2.2 Participation in the JET work programme

O. E. Garcia, J. Stærk Larsen, J. Madsen, V. Naulin, S. Kragh Nielsen, A. H. Nielsen and J. Juul Rasmussen
volker.naulin@risoe.dk

The involvement of Risø in the JET work programme is focused on the topics of modelling and simulation. In 2006 the work included the following topics investigated with collaboration from the JET Programme:

2.2.2.1 Fast pulse propagation modelling

A fast response of plasma core to edge cooling has often been reported, leading to the suggestion that non-local features may be present in tokamak transport physics. Detailed comparison of cold pulse propagation with the propagation of heat waves originated from depositing modulated electron power in the plasma core is rarely available. Such comparison is crucial to identify whether the fast cold pulse propagation really deviates from a local paradigm or whether it is consistent with a highly non-linear (but local) transport in regions where the temperature inverse gradient length exceeds the threshold for turbulence on-set. In fact in a stiff plasma any perturbation will propagate much faster than predicted on the basis of the power balance heat diffusivity. On the other hand, if the cold pulse propagation is significantly faster than that of the modulation heat wave, this would reveal the anomaly and call for more sophisticated nonlocal models. Such experiments have been performed in JET low collisionality L- and H-mode plasmas. Edge cooling was induced by Ni laser ablation and heat modulation by ICRH in mode conversion scheme. By moving ICRH from on-axis to off-axis it was possible to vary the radius at which the threshold in R/L_{Te} was crossed. It was found that even in situations where the plasma is above threshold in most of the core, the core reaction to cold pulses is faster than would be predicted on the basis of the stiffness level deduced from power modulation. In addition, in situations where the plasma goes below threshold around mid-radius, it was even clearer that the cold pulse keeps propagating very fast whilst the modulation heat wave is slowed down and damped by the low transport level below threshold. This asymmetry of behaviour cannot be explained by local transport models, even taking into account the high non-linearity of models based on the critical gradient concept. Here new approaches have been explored to provide simplified models that couple an evolution equation for the level of the turbulence fluctuations to a transport equation. These models, based on the idea of turbulence spreading which provides the non-locality, are shown indeed capable of qualitatively explaining the experimental observations of an asymmetry of behaviour in the propagation of cold pulses and modulation.[1,2]

1. P. Mantica, X.Garbet, V.Naulin, M.Nora, J.Juul Rasmussen, T.Tala, A.Thyagaraja and JET EFDA contributors, 11th EU-US Transport Task Force Workshop, Marseille, France, 4th September 2006 - 7th September 2006.

2. J. Juul Rasmussen, V. Naulin, J.S. Lonnroth, P. Mantica, V. Parail, Proc. 33. European Physical Society conference on plasma physics and controlled fusion, Rome (IT), 19-23 Jun 2006. (Europhysics Conference Abstracts, vol. 32B) P1-076 (4 p.).
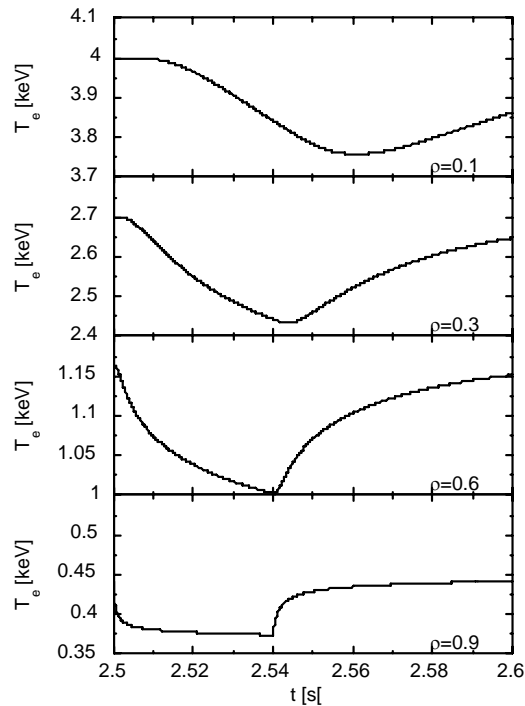
Figure 3. Fast pulse propagation in the turbulence spreading transport model, showing a faster core response then critical gradient models.

2.2.2.2. ESEL modelling of JET SOL

Understanding and modelling radial plasma transport originating at the transition from closed to open field lines is of vital importance for the development of fusion machines. The strongly intermittent turbulent transport fuels the Scrape-off layer (SOL) and dictates the density and temperature profiles across the SOL. It is further responsible for plasma contact with the vessel wall, which is detrimental for the operation of fusion reactors as it not only damages plasma facing components, but will lead to an increased influx of impurities into the core plasma due to main vessel recycling. Transport modelling for the SOL has in recent years made tremendous progress, but still struggles to include the effects of turbulent transport in the SOL with high levels of intermittency as reported from a large number of devices.

The two dimensional (2d), electrostatic edge-SOL turbulence code ESEL is used to simulate the perpendicular dynamics of transport events in the JET Scrape Off Layer (SOL) and the self consistent development of the SOL profiles at the outboard midplane. The code results are compared to probe measurements of the JET SOL. Qualitative agreement is shown amongst others for the plasma temperature and density profiles. The magnetic field direction independent part of the parallel flow velocity in the SOL can be reproduced by assuming that it is mainly due to the along the magnetic field lines localised blob structures, whose overpressure on the flux lines drives the flow. The code predict magnetic field independent parallel flows with velocities of 0.2 ion sound speed in good agreement with measurements. Moreover the correlation between parallel and perpendicular velocity fluctuations, shown in figure 4, is reproduced by the code, hinting that the blob structures are the main player in parallel momentum transport through the SOL.[1]
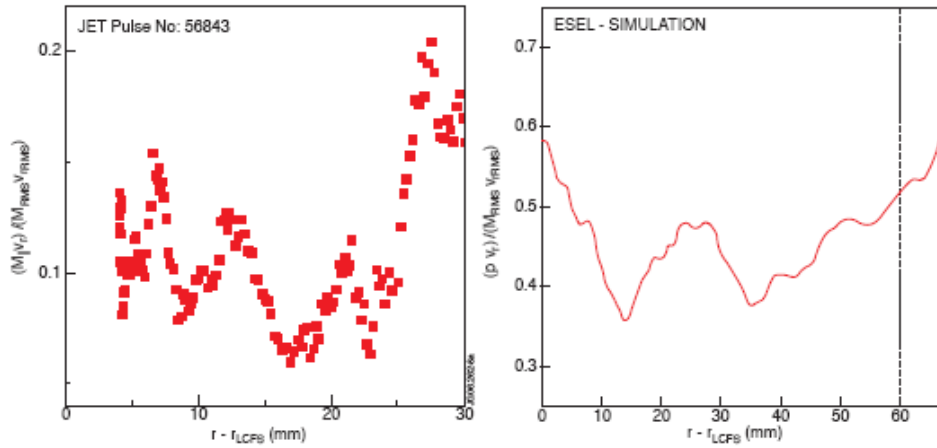
Figure 4. Correlation between parallel and radial velocity fluctuations over radial position from measurements (left) and inferred from simulation (right), with a peak some 30 mm outwards from the LCFS.

1. V. Naulin, W. Fundamenski, A.H. Nielsen, J. Juul Rasmussen, O.E. Garcia, B. Gonçalves, C. Hidalgo, M. Hron and JET EFDA contributors, **EFD-C(06)05/19.** IAEA 2006.

2.2.2.3 Evaluation of SOL probe data

The statistical signature of intermittency in the SOL is an important parameter to characterise transport in the SOL and to compare with simulations and theory. Data from the reciprocating probe at JET was analysed with respect to radial changes in the distribution function describing the fluctuations. The influence of several techniques to split between background and fluctuations was investigated and numerical tools for data processing developed.
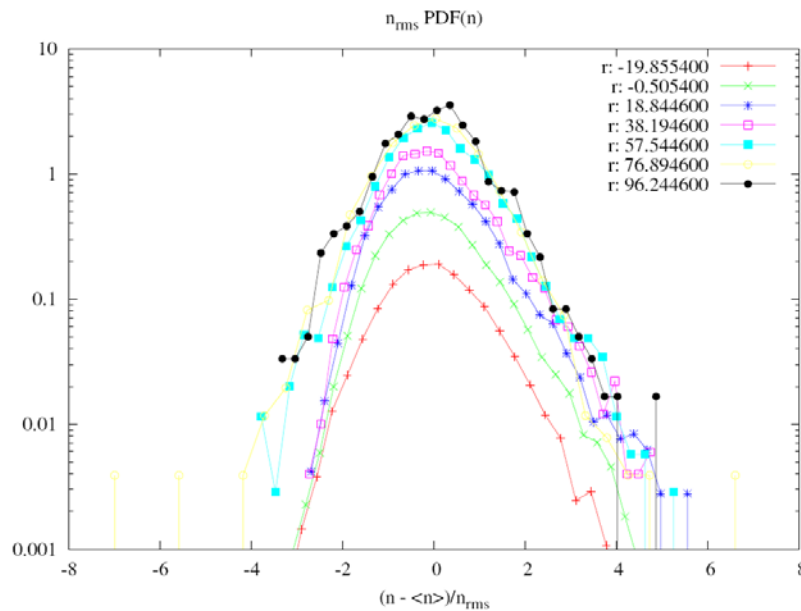
Figure 5. Density fluctuation PDF from probe measurements at different locations in the SOL.

2.2.3 ESEL-EIRENE coupling

O. E. Garcia, V. Naulin, A. H. Nielsen, J. Juul Rasmussen and D. Reiter*
(*IPP Juelich, Germany)
volker.naulin@risoe.dk

An important aspect of SOL transport is the amount of recycling generated by the outstreaming plasma. In collaboration with IPP Juelich the SOL turbulence code ESEL was therefore coupled to the Monte Carlo code EIRENE, which calculates the recycling in local plasma conditions. For initial testing feedback of the SOL source terms into the ESEL dynamics has been suppressed. Results obtained so far show, besides a high correlation of the sources with the blob like transport structures produced by ESEL, that the sources are dominated by the dynamical changes of the plasma. The expectation is therefore that recycling will not lead to large changes in the SOL dynamics, in some agreement with the good comparability of ESEL with SOL data.
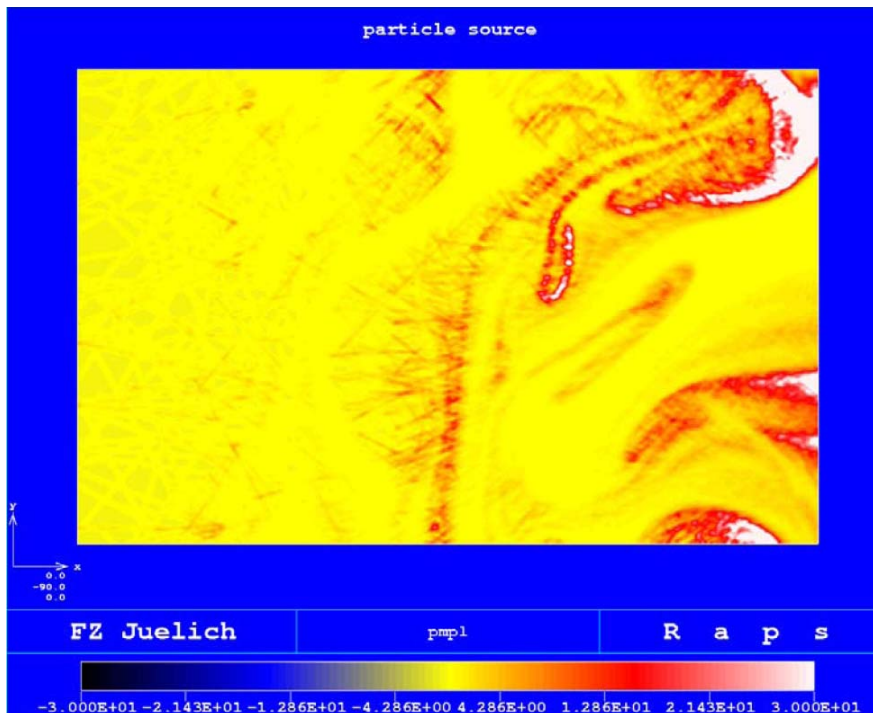
Figure 6. Particle source from recycling as found by the code EIRENE. Plasma conditions are from an ESEL simulation for JET parameters. Interaction with SOL structures can bee seen.

2.2.4 Radial interchange motions of plasma filaments

O. E. Garcia, N. H. Bian* (*School of Physics and Astronomy, The University of Manchester, Manchester M60 1QD, United Kingdom), W. Fundamenski** (**EURATOM/UKAEA Fusion Association, Culham Science Centre, Abingdon OX14 3DB, United Kingdom), V. Naulin, A. H. Nielsen and J. Juul Rasmussen
odd.erik.garcia@risoe.dk

Plasma structures elongated along and localized across magnetic field lines have been observed to propagate radially outwards in the scrape-off layer of many tokamak experiments. This is believed to be the cause of strong interactions between the plasma and the main chamber walls. Such blob-like structures have been found to prevail in virtually all experimental confinement and parameter regimes. The associated convective transport poses a serious problem for controlled particle and heat exhaust as well as particle migration in the next generation fusion experiments.

A comprehensive investigation of the physical mechanism and the velocity scaling for radial convection of isolated plasma filaments by interchange motions have been performed.[1,2] The inertial response to magnetic guiding center drifts results in the formation of dipolar electrostatic potential and vorticity fields and rapid radial acceleration of blob-like structures. As seen in Figure 7, the nonlinear evolution leads to the formation of a steep front and a trailing wake. This is a robust feature which is seen in all experimental probe measurements. Numerical simulations further demonstrate that the late dynamical evolution strongly depends on the amount of collisional diffusion and viscosity. However, an isolated structure is able to travel a radial distance many times its initial size in all experimentally relevant parameter regimes.

In the ideal limit, there is an inertial scaling for the maximum radial velocity of plasma filaments. This velocity scales as the acoustic speed times the square root of the structure size relative to the length scale of the magnetic field.[1,2] In Figure 7, this is manifested by the saturation of the maximum radial centre of mass velocity with increasing Rayleigh number, Ra, which measures the strength of the interchange drive relative to collisional diffusion and viscosity.

The role of parallel electric currents, represented by an effective sheath dissipation parameter, Λ, has also been investigated. When sheath dissipation is included in the numerical simulations, it significantly reduces the radial velocity of isolated filaments, as seen in Figure 7. Here the full line represents a well-known analytical blob-like solution, which clearly does not match the numerical results due to several flaws in the underlying assumptions of that particular solution. The new theoretical results have been compared favourably with observations of transient transport events in scrape-off layer plasmas, comprising both blob-like structures in low confinement modes and edge localized mode filaments in unstable high confinement regimes.[1,2]

1. O. E. Garcia, N. H. Bian, V. Naulin, A. H. Nielsen, J. J. Rasmussen, Phys. Plasmas **12**, 090701 (2005).

2. O. E. Garcia, N. H. Bian, W. Fundamenski, Phys. Plasmas **13**, 082309 (2006).
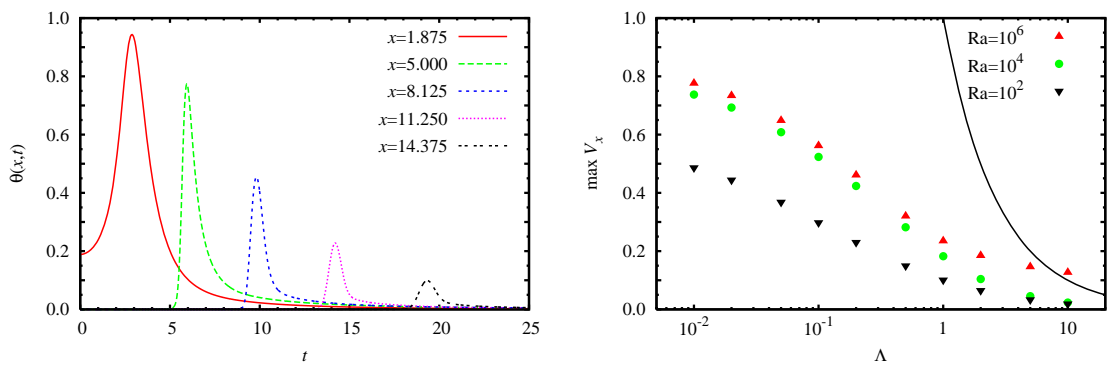
Figure 7. Left: Temporal evolution of the blob amplitude θ recorded by radially separated probes, where the radial position x is normalized by the initial blob size and time by the associated ideal interchange rate. Right: The maximum radial centre of mass velocity for a blob-like structure, initially at rest in an uniform background plasma, as function of the sheath dissipation parameter Λ (due to parallel electric currents) and the Rayleigh number (effective buoyancy over collisional dissipation).

2.2.5 A gyro-fluid model for turbulence and transport in the edge/SOL region of toroidal plasmas

J. Stærk Larsen, J. Madsen, O.E. Garcia, V. Naulin, A. H. Nielsen, J. Juul Rasmussen and A. Kendl (*Institute for Theoretical Physics, University of Innsbruck, A-6020 Innsbruck, Austria)*
jens.juul.rasmussen@risoe.dk

Turbulence and transport in the edge and scrape-off-layer (SOL) of toroidally magnetized plasmas are strongly intermittent and involve large outbreaks of hot plasma, as has now been revealed in several experiments, see also Sec. 2.2.1. These structures, often referred to as "blobs", have a significant influence on the pressure profiles in the SOL and may result in detrimental power deposition on plasma facing components. The basic dynamics of blobs are well described in terms of nonlinear interchange motions[1,2] in the limit of cold ions (see Secs. 2.2.4).

Motivated by the observations, in particular in large devices, where the ion temperature in the SOL is comparable to or even higher than the electron temperature we have developed a gyro-fluid model for the turbulent dynamics in the edge and SOL. This model accounts for finite ion temperatures and finite ion Larmor radius effects. The model is self-consistently derived from the variation of a fluid Lagrangian. The derivation is related to the approach in Ref. [3], but with important differences, the present model includes the full evolution of the pressure profile. In the first version the model is isothermal and describes the evolution of the electron and ion densities coupled through the polarization equation, where the full nonlinearities are retained. The model equations are implemented numerically by employing a new scheme for the solution of the polarization equation. It governs two-dimensional interchange dynamics at the outer mid-plane of toroidally magnetized plasma. Thus, it may be considered as a generalization of the Risø ESEL-code,[1] and the gyro fluid code has been named: GESEL.

We have applied the model to investigate the influence of finite ion temperature and finite Larmor radius effects on the propagation properties of isolated blob structures for various ratio of electron and ion temperature.[4] In figure 8 we show the evolution of the electron density (the ion density is evolving similarly) of the localized blob structure for different ion temperatures. Initially the ion and electron density perturbations are identically and the potential perturbation is vanishing in the limit of cold ions. This implies that there is no initial flow field, which, however, subsequently build up from the polarization of the blob structure due to the interchange mechanism and the densities will be advected radially outward (cf. [2]). The basic features of the blob propagation are not altered by finite ion temperatures and for $T_i = 0$ the propagation resembles the evolution for the cold ion fluid model. At finite ion temperature the blob acceleration increases, due to the enhanced polarization. Additionally, we observe an increasing concentration of the density at the front of the structure for increasing ion temperature preventing nonlinear fragmentation, which may result in enhanced localized power deposition on plasma facing components.
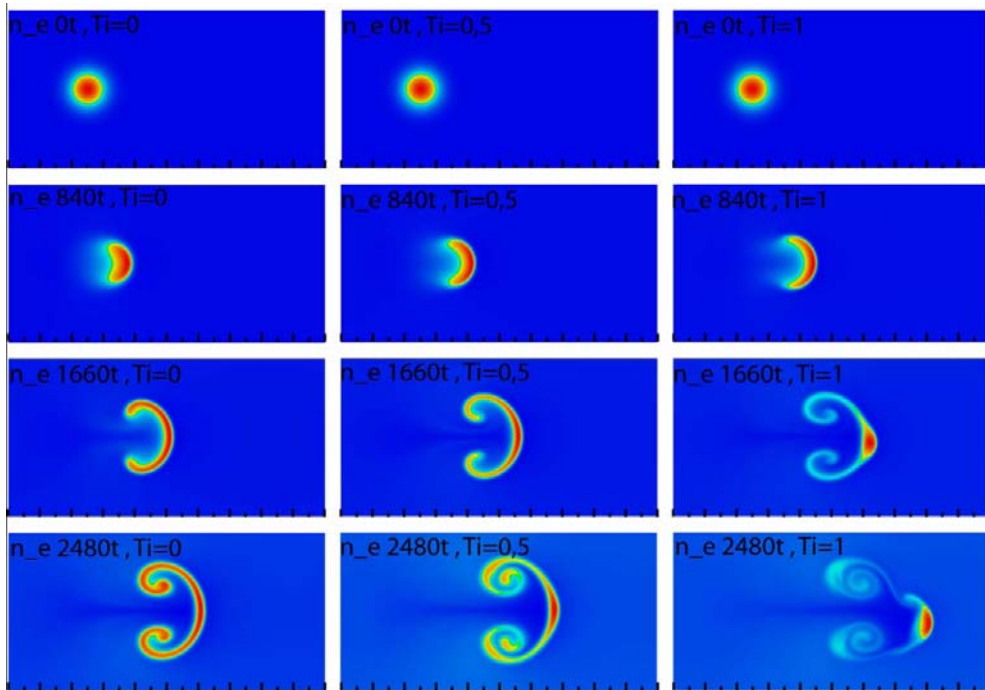
Figure 8. Evolution of the electron density for a blob initialized at (x,y) = (L/4, L/2) for three different ion temperatures normalized to the electron temperature. Time is increasing downwards.

Simulation of the turbulence and transport in the edge/SOL by using the gyro-fluid code GESEL has been initiated. The turbulence dynamics is strongly intermittent and dominated by radial propagation of blob-structures as in the case of cold ions. Preliminary results show that for high ion temperatures the bursting of blob structures tends to become more regular, i.e., blobs are generated and ejected at almost constant time intervals.

1. O.E. Garcia, V. Naulin, A. H. Nielsen, and J. Juul Rasmussen, Phys. Plasmas **12**, 062309 (2005).

2. O.E. Garcia, N. H. Bian, V. Naulin, A. H. Nielsen, and J. Juul Rasmussen, Phys. Plasmas **12,** 090701 (2005); O.E. Garcia, N. H. Bian, and W. Fundamensky, Phys. Plasmas **13,** 0082309 (2006).

3. D. Strintzi and B. Scott, Phys. Plasmas (2004) **11,** 5452.

4. J. Madsen, J. Staerk, O.E.; Garcia, V. Naulin, A.H. Nielsen, J. Juul Rasmussen, A. Kendl, Proc. 33. European Physical Society conference on plasma physics and controlled fusion, Rome (IT), 19-23 Jun 2006. (Europhysics Conference Abstracts, vol. 32B) P1-197 (4 p.)

2.2.6 Fluctuation measurements in the edge and scrape-off layer of ASDEX Upgrade and comparison with numerical simulations

O.E. Garcia, V. Naulin, A.H. Nielsen, J. Juul Rasmussen, R. Schrittwieser*, S. Konzett*, F. Mehlmann*, P. Balan*, C. Ionita* and A. Kend* (*Institute for Ion Physics, University of Innsbruck, Austria),
jens.juul.rasmussen@risoe.dk

The collaboration with the Plasma Physics Group at the University of Innsbruck on fluctuation measurements and characterisation is continued. The main aim is to contribute to the evaluation of the fluctuation data measured in the outer edge and SOL of toroidal devices by electrostatic probes and to compare these measurements with simulation results from the Risø ESEL-code. This will contribute significantly to the characterisation of turbulent fluctuations and in particular of the turbulent driven particle flux and Reynolds Stress, which governs the momentum transport. The investigations during 2006 have mainly been concentrated on measurements performed at ASDEX Upgrade in Garching, during L-mode as well as H-mode discharges.

The measurements are performed by means of a fast reciprocating probe at the midplane manipulator, with a probe head mounted with five pins, see Figure 9. Three pins measure the floating potential and its fluctuations and the remaining two pins are biased to ion saturation and swept, respectively. Electron temperatures were inferred from current-voltage characteristics. During a discharge typically a few reciprocations into the plasma were performed. The probe configuration allowed the calculation of the radial fluctuation-induced particle flux simultaneously with the Reynolds stress.

Initial evaluations of H-mode data indicate that the Reynolds stress and the fluctuations-induced particle flux show increased bursting behaviour during ELMs, revealing part of the ELM fine structure.[1]
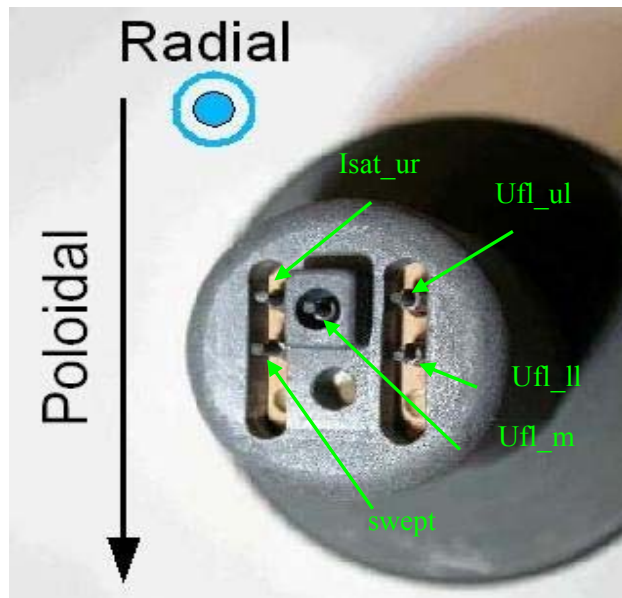

Figure 9. The five-pin probe head.

The potential and density (derived from the ion saturation current) fluctuations and the derived quantities in the L-mode was compared directly with numerical simulations. The statistical characteristics of particle density flux, Reynolds stress, and conditionally averaged waveforms obtained from the 2D interchange dynamics model, ESEL, with parameters from the experiment show reasonably good agreement with the experimental results. The limitations of the applicability of the ESEL code are revealed with respect to the frequency spectra. Investigations of the similarities and differences between ELM events (in H-mode) and the intermittent blob events modelled in the simulations are initiated.

1. P. Balan, C. Ionita, R. Schrittwieser, A. Herrmann, M.Maraschek, H.W. Müller, V. Rohde, V. Naulin, J. Juul Rasmussen, Proc. 33. European Physical Society conference on plasma physics and controlled fusion, Rome (IT), 19-23 Jun 2006. (Europhysics Conference Abstracts, vol. 32B) P1-128 (4 p.)

2.2.7 Influence of rational q's on the formation of poloidal flows

V. Naulin, J. Juul Rasmussen, A. H. Nielsen, O.E. Garcia, A. Kendl* and S. Konzett*
(*Institute for Theoretical Physics, University of Innsbruck, A-6020 Innsbruck, Austria)
volker.naulin@risoe.dk

The formation of flows out of turbulence is an ongoing topic in fusion research. A connection of sheared flows with enhanced confinement regimes as the H-mode or internal transport barriers (ITB) has often been proposed. Simulations in flux tube geometry have, however, until now failed to produce sheared flows strong enough to either suppress the instability or to absorb a relevant part of the fluctuation energy.

A geometric connection of the energy transfer rates from turbulence to flows can be observed in simulations. The spatial structure of the transfer seems to follow the rationals in the q-profile, even though this seems not to be a straightforward relationship. We investigate the dependence of Reynolds-, Maxwell- and geodesic transfer terms vor varying values of q and magnetic shear using the 3 dimensional electromagnetic code TYR.
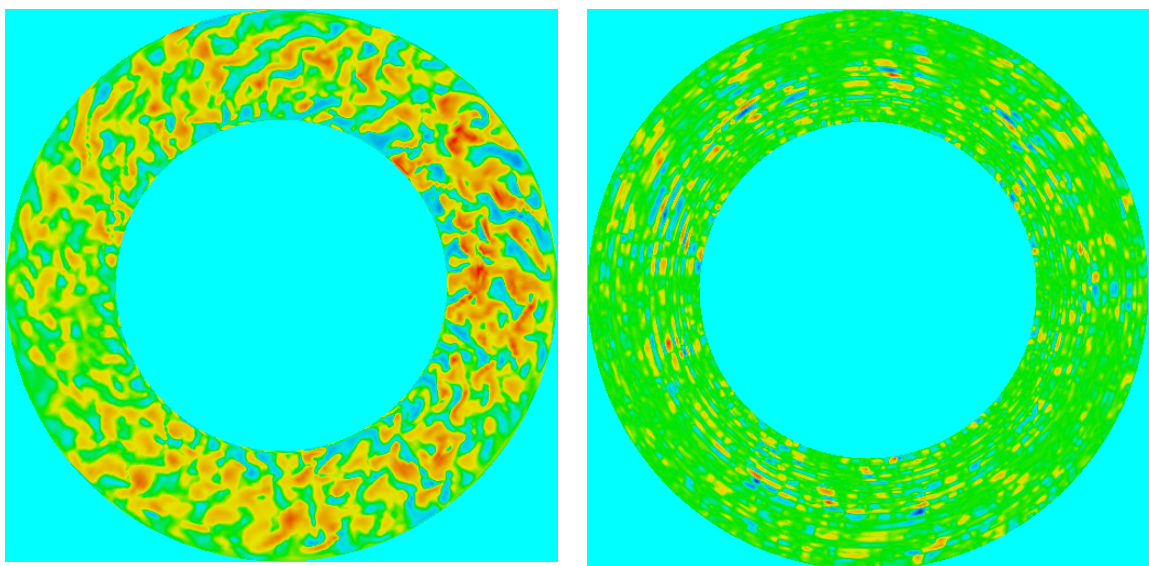

Figure 10. Temperature fluctuations (left) from the TYR code and Maxwell energy transfer term into flows (right). The structure seen in the energy transfer is localised near rational surfaces.

2.2.8 Principle experimental studies of the nonlinear energy transfer function in two-dimensional plasma turbulence

V. Naulin and P. Manz, M. Ramisch* U. Stroth* (*Institut für Plasmaforschung, University Stuttgart, D-70569 Stuttgart, Germany) and B.D. Scott* (**Max-Planck-Institut für Plasmaphysik, EURATOM Association, D-85748 Garching, Germany)*
volker.naulin@risoe.dk

Using bispectral methods developed by Ritz[1] and Kim[2], the turbulent energy cascade has been analysed in simulated and experimental data from toroidally confined magnetized plasmas. Tests on simulated Hasegawa-Wakatani turbulence show, that the scheme is appropriate for the envisaged study. In the analysis of 2D density and potential fluctuation data with only a few modes taken into account the analytically known growth rate and dispersion relation are recovered and clearly evidence on the expected dual cascade is found. Very similar results were found from the same analysis of experimental data from a 2D probe array. It is shown, that the density fluctuations, which are advected as a passive scalar with the vorticity, show power transfer in the direction of smaller scales, while the spectral power in potential fluctuations is transferred as an inverse cascade to larger scales.
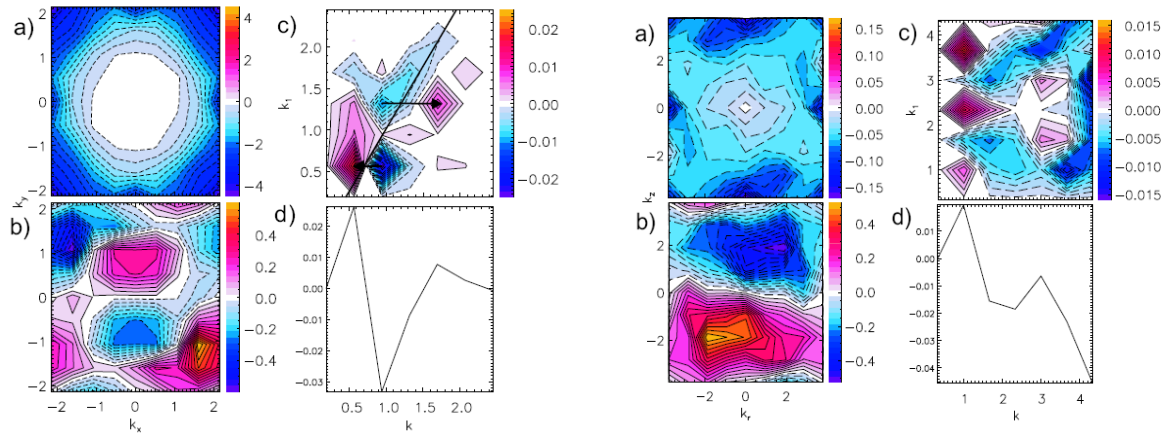
Figure 11. Growth rate (a) and dispersion relation (b) and energy transfer (c,d) of potential fluctuations from a Hasegawa-Wakatani equations simulation. Dashed and solid lines indicate negative and positive values, respectively. Arrows denote the direction of the energy transfer. Left from simulation and right from experiment.

1. C. P. Ritz, E. J. Powers, and R. D. Bengston, Phys. Fluids B: Plasma Phys. **1**, 153 (1989).

2. J. S. Kim, R. D. Durst, R. J. Fonck, E. Fernandez, A. Ware, and T. P. W., Phys. Fluids **3**, 3998 (1996).

2.3 Millimetre waves used for diagnosing fast ions in fusion plasmas

H. Bindslev, S.B. Korsholm (also at MIT Plasma Science and Fusion Center, Massachusetts, USA), F. Leipold, F. Meo, P.K. Michelsen, S. Michelsen, S.K. Nielsen, J.R. Pedersen and E.L. Tsakadze
soeren.korsholm@risoe.dk

Millimetre waves, corresponding to frequencies in the 100 GHz range, permit probing and imaging on the centimetre scale and transmission of signals with bandwidths in excess of 10 GHz. Coherent sources are now available from the micro- to Megawatt range, CW.

In the world of fusion, the millimetre waves are used extensively both as a diagnostic tool and for heating and manipulating the plasma locally as well as globally. Central to achieving these objectives is the fact that millimetre waves, like laser light, can be projected in narrow focused beams, but unlike laser light, the millimetre waves can interact strongly with the plasma.

At Risø we develop and exploit millimetre wave diagnostics for measuring the velocity distribution of the most energetic ions in fusion plasmas. The measurements are resolved in space on the centimetre scale and in time on the millisecond scale.

The most energetic (or fast) ions are the result of fusion reactions and auxiliary heating. Their interaction with the bulk plasma is the main mechanism by which the fusion plasmas reach and sustain the high temperatures of 100-200 million degrees Kelvin required for fusion. The considerable energy associated with the fast ions can also drive turbulence in the plasma, and degrade the confinement of the plasma and of the fast ions themselves. Understanding and controlling the dynamics of fast ions are central tasks in the development of fusion energy, and one of the main research topics for the next large fusion facility, ITER. It is a task we seek to contribute to by developing and exploiting the unique diagnostic capability of millimetre wave based collective Thomson scattering (CTS).

The group has developed fast ion CTS diagnostics for the TEXTOR and ASDEX Upgrade tokamaks, which are located at the Research Centre Jülich and at the Max-Planck Institute for Plasma Physics in Garching, both in Germany. These CTS projects are conducted in collaboration with the Plasma Science and Fusion Center at MIT (USA), the Max-Planck Institute for Plasma Physics in Garching and the TEC[1] consortium.

The upgraded CTS system for TEXTOR was brought into operation in 2005 and the first results were obtained. In 2006 experimental CTS campaigns have been performed. Unfortunately, some technical problems of mainly other systems limited the amount of data. An overview of the campaigns and results is found in subsection 2.3.1. Results of the campaign and data from the early CTS experiments in 2001 were published is Physical Review Letters in 2006 [2]. Examples of the results presented in the article are found in subsection 2.3.2.

In the course of the year a couple of auxiliary diagnostics for optimising the quasi optical transmission lines of the CTS systems were developed. The diagnostics are described in subsections 2.3.3 and 2.3.4. The use of the diagnostics for optimising the alignment of the transmission lines and finding the polarisation of the microwaves is described in subsections 2.3.5, 2.3.6, and 2.3.10 – 2.3.12. The ASDEX Upgrade CTS receiver system

was ready in 2004. In 2006 further tests and commissioning was carried out, details of which are given in subsections 2.3.9 – 2.3.13. Commissioning of the full system and first results depend on the operation of the new dual frequency gyrotron, and are expected in the spring of 2007. The optimal performance of the gyrotrons – being the powerful millimetre wave sources for the two CTS systems – is crucial to obtaining useful CTS data. A key issue is to have a clean single frequency spectrum being constant. The mode purity may be affected by other systems and also on the operation of the gyrotron, and for this reason detailed studies of the spectral behavior of the two gyrotrons have been performed. This is described in some detail in subsections 2.3.7 and 2.3.13.

A study by Risø, of the feasibility of measuring the fast ion phase space distribution in ITER by CTS was completed in 2003. The study revealed that a CTS system based on a 60 GHz probe has the highest diagnostic potential, and is the only CTS system expected to be capable of meeting all the ITER fast ion measurement requirements with existing or near term technology. Since then a detailed design has been under development. The focus in 2006 has been on detailed engineering design of in-vessel components. Especially, the antenna system on the high field side presents a challenge due to the limited space between and behind blanket modules. Results of this work are described in subsections 2.3.14 and 2.3.15.

1. TEC: the Trilateral Euregio Cluster, comprising Association EURATOM-Forschungszentrum Jülich GmbH, Institut für Plasmaphysik, Jülich, Germany; Association EURATOM-FOM, Institute for Plasma Physics, Rijnhuizen, The Netherlands; and Association EURATOM-ERM/KMS, Belgium.

2. H. Bindslev, S. K. Nielsen, L. Porte, J. A. Hoekzema, S. B. Korsholm, F. Meo, P. K. Michelsen, S. Michelsen, J.W. Oosterbeek, E. L. Tsakadze, E. Westerhof, P. Woskov, and the TEXTOR team, "Fast-ion dynamics in the TEXTOR tokamak measured by collective Thomson scattering", Phys. Rev. Lett., 97, article 205005 (2006).

2.3.1 Results of the CTS campaigns at TEXTOR during 2006

S.B. Korsholm (also at MIT), S.K. Nielsen, P. Woskov (MIT), F. Meo, F. Leipold, S. Michelsen, P.K. Michelsen, J.W. Oosterbeek, E.L. Tsakadze, J.R. Pedersen, E. Westerhof (FOM) and H. Bindslev
soeren.korsholm@risoe.dk

During 2006 three experimental campaigns using the collective Thomson scattering (CTS) system at TEXTOR have been performed. A number of physics and diagnostic development topics have been covered.

A key system upgrade utilised this year was a set of powerful motors for manipulating the CTS receiver mirror during a plasma shot. This enables sweeping the CTS receiver mirror orientation across the gyrotron probe beam. A result of such a sweep is seen in Figure 12, which originally appears in Ref. 1. The fact that the spectral power density of the fast ion signal is strongly dependent on the viewing direction provides clear evidence that we obtain fast ion data and not spurious gyrotron effects. The scanning mirror also have a very practical use, since after estimating the overlap location theoretically – the upgrade enabled search for optimal overlap between the probe and the receiving beam by the sweep. Such overlap searches were successfully conducted in 2006, and they clearly identify the viewing angle where maximum overlap occurs. This viewing angle is then used for successive discharges to study fast ion dynamics.
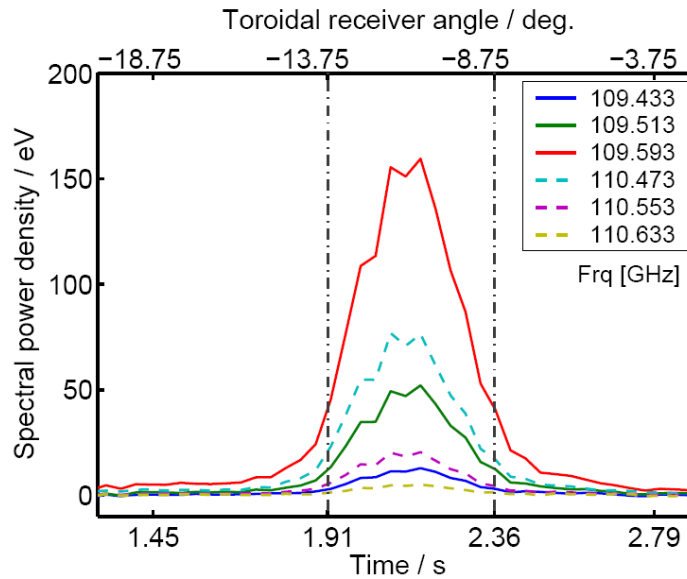
Figure 12. CTS spectral data recorded for an Ohmic plasma where the toroidal angle φ_r of the receiver viewing direction was scanned during the plasma shot. The plot shows CTS spectral power density in a number of channels vs. time and φ_r. Receiver and probe beams go through overlap for a variation of 5° of φ_r. With a distance from receiver antenna to scattering volume of 50 cm this corresponds to a width of the scattering volume of 4 cm in the direction perpendicular to the probe and receiver beam directions (perpendicular to k_i and k_s). In the direction of k^δ the extent of the scattering volume is approximately 5/2 times larger. TEXTOR shot number 100467. $\angle(k^\delta,B) = 110°$. Scattering volume at R = 1.8 m, z = 0 m.

As an example an ongoing physics study is focused on the evolution of the fast ion velocity distribution during NBI start up. Preliminary results have indicated that the fast ion distribution function is highly dynamic during the first ~50-100 ms after the beam turn-on. Results are presently being analysed and will be presented in the near future, while further studies of the effect will be made in May 2007. Another physics issue studied is the interaction between sawteeth and fast ions, which is also an ongoing study. Results of previous experimental CTS studies of sawteeth were presented in Ref. 1.

In parallel to the physics studies, one diagnostic development topic has been to study the interference between the gyrotron (probe of the CTS system) and the ICRH system. This issue is important, since the probing radiation for CTS needs to be spectrally clean having only a single frequency. High resolution frequency measurements of the 110 GHz gyrotron were carried out to better characterize the gyrotron used for CTS experiments, and to optimize the receiver notch filter tuning. These studies are further described in subsection 2.3.7.

One should note that the amount of useful data was cut short due to a number of various unfortunate events and systems failures. As an example we experienced interference between the gyrotron and the interferometer during the CTS experiments, causing loss of density control. Since the latter is important in the CTS experiments to ensure beam overlap and the location of the scattering volume, this was quite limiting on the amount of useful CTS data. A collaborative effort has lead to a quantification of the problem and identification to a solution that is now being implemented by IPP.

During 2006 the work on TEXTOR CTS has been described in invited talks on the HTPD meeting in Williamsburg, USA and on the 16th International Toki Conference, Japan, as well as in a number of conference contributions, and was published in three refereed journal articles [1-3]. Finally, the work was mentioned as Editors Choice in Science December 1st 2006. Examples of the data presented in Ref. 1 are found in subsection 2.3.2.

1. H. Bindslev, S.K. Nielsen, L. Porte, J.A. Hoekzema, S.B. Korsholm, F. Meo, P.K. Michelsen, S. Michelsen, J.W. Oosterbeek, E.L. Tsakadze, E. Westerhof, P. Woskov, *Fast-ion dynamics in the TEXTOR Tokamak measured by collective Thomson scattering*, Phys. Rev. Lett. (2006) 97, 205005.

2. P. P. Woskov, H. Bindslev, F. Leipold, F. Meo, S. K. Nielsen, E. L. Tsakadze, S. B. Korsholm, J. Scholten, C.Tito, E. Westerhof, J. W. Oosterbeek, F. Monaco, F. Leuterer, M. Muenich, D. Wagner, Frequency Measurements of the Gyrotrons used for CTS Diagnostics at TEXTOR and ASDEX Upgrade, Rev. Sci. Instrum., (2006) 77, 10E524.

3. S B Korsholm, H. Bindslev, F. Meo, F. Leipold, P.K. Michelsen, S. Michelsen, S.K. Nielsen, E.L. Tsakadze, P. Woskov, E. Westerhof, J.W. Oosterbeek, J. Hoekzema, F. Leuterer, D. Wagner, Current fast ion collective Thomson scattering diagnostics at TEXTOR and ASDEX Upgrade, and ITER plans (invited). Rev. Sci. Instrum. (2006) 77, 10E514.

2.3.2 Comparison between fast ion CTS measurements and numerical simulations

S.K. Nielsen, H. Bindslev, L. Porte (CRPP, EPFL) and J. A. Hoekzema (FZ Juelich)
stefan.kragh.nielsen@risoe.dk

Numerical Fokker-Planck simulations of the fast ions distribution function have been performed for TEXTOR parameters and have been compared with CTS fast ion measurements. The simulations have been done using measured electron density and temperature as input and having a fast ion population interacting with both the electrons and the bulk ions. The plasma in the simulation is homogenous. In TEXTOR discharge 89510 and in the simulation thereof the ion heating was turned off at time 2.2s and the slowing down of the fast ions can then be studied. The result is shown in Figure 13. More details of the comparison can be found in Ref. 1.
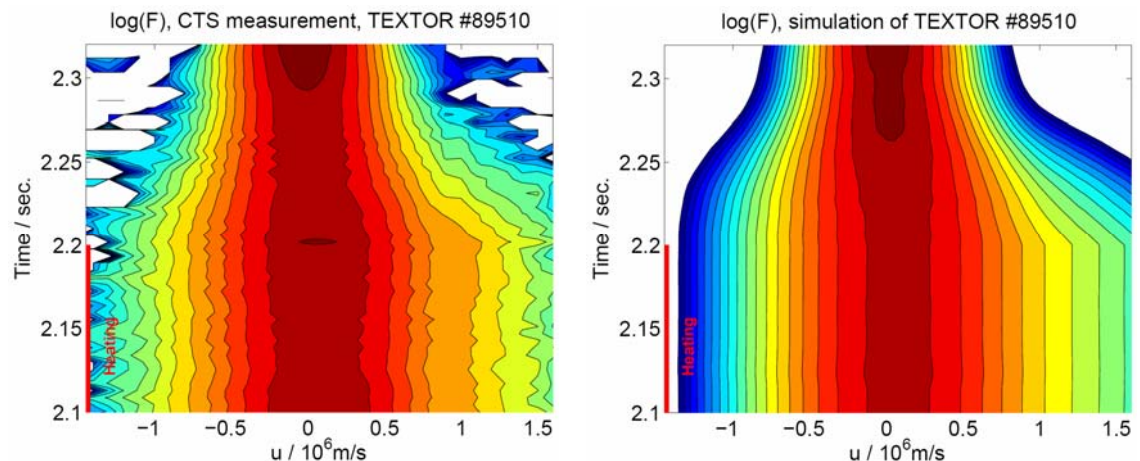

Figure 13. Comparison between measured ion distribution function and Fokker-Planck simulated ion distribution function. A good agreement is seen for the slowdown of the fast ions after t = 2.2 s with velocity around 1-1.5 10^6 m/s.

1. H. Bindslev, S. K. Nielsen, L. Porte, J. A. Hoekzema, S. B. Korsholm, F. Meo, P. K. Michelsen, S. Michelsen, J.W. Oosterbeek, E. L. Tsakadze, E. Westerhof, P. Woskov, and the TEXTOR team, "Fast-ion dynamics in the TEXTOR tokamak measured by collective Thomson scattering", Phys. Rev. Lett., 97, article 205005 (2006)

2.3.3 Technological advances – a novel micro-rig for measuring microwave antenna patterns

J.H. Holm, M. Jessen, S.K. Nielsen and S.B. Korsholm
soeren.korsholm@risoe.dk

When optimising a quasi-optical transmission line it is extremely useful to be able to measure the shape of the microwave beam; or in other words the antenna pattern. For this purpose a number of measuring rigs have been constructed in the group, all having in common that they carry a detector diode (working in the 100 GHz range) that measures the microwave power coming from the transmission line being diagnosed. In the treatment of the date a Gaussian beam shape is fitted to the spatially resolved measurements of the power, and by comparing this to theory this facilitates an optimisation of the transmission line. In the following we report on the newest measuring rig. Its predecessor – called the mini-rig (see subsection 2.3.4 of Ref. 1) – had outer dimensions of 43x61x6 cm^3 and a scanning area of 30x42 cm^2. While being extremely useful, it had some limitations due to its size. Hence a very compact version – called the micro-rig – was designed and built starting from scratch.

In Figure 14 the micro-rig is shown in operation measuring the antenna pattern of the CTS transmission line inside TEXTOR. The scanning area of the micro-rig is 25x25 cm^2, while the size of the rig itself is 40x40x8 cm^3. Note that it has no fixed frame – only the two axes of movement. The rig can be fitted with various waveguide antennae enabling measurements in different compact geometries. Examples of the measurements can be found in subsections 2.3.6, 2.3.10, and 2.3.11.
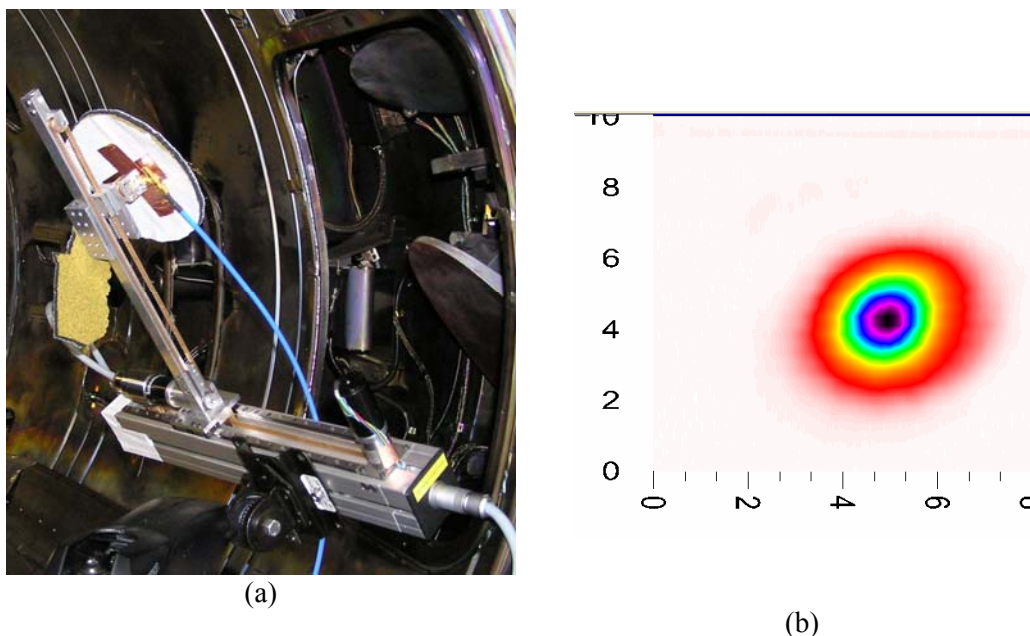

(a)

(b)

Figure 14. (a) The micro-rig in position inside TEXTOR for measuring the antenna pattern of the TEXTOR transmission line. (b) In-vessel beam pattern for a fully aligned transmission line.

1. Risø-R-1579(EN) Association Euratom - Risø National Laboratory Annual Progress Report 2005, http://www.risoe.dk/rispubl/ofd/ofdpdf/ris-r-1579.pdf, Edited by H. Bindslev and B.N. Singh.

2.3.4 Technological advances – a novel device for measuring elliptical polarization of microwave beams

F. Leipold, J.H. Holm, M. Jessen and S.K. Nielsen

frank.leipold@risoe.dk

A certain characteristic of microwave radiation (angle of ellipticity, ellipticity and direction of rotation (left or right hand)) can be achieved using a radiation source which provides linear polarized light (like a gyrotron) in conjunction with polarizer plates. Polarizer plates have parallel grooves in one direction causing different phase shifts upon reflection for two orthogonal electrical field vectors (parallel and perpendicular to the grooves). By reflection of linear polarized light on two consecutive polarizers, almost any type of light characteristics can be obtained by rotating the polarizer plates around their normal axis. Since the characteristics of the micro wave after reflection depend sensitively on the geometry of the grooves (and the machining accuracy), a measuring tool is required to verify the mathematical prediction.

For this purpose, a 2-channel microwave detector for detecting orthogonal electrical fields and measuring their relative phase shifts has been built. The measurement of the phase between both channels is important, because this is the only means for determining, whether light is left or right hand circular polarized. Figure 15 shows the sketch of this device. Two orthogonal orientated waveguides (WR-10 – in the frequency range of 110 GHz) are mounted together for detecting light in horizontal and vertical polarization direction. In a first stage, both signals are mixed with a frequency of 108 GHz coming from a common local oscillator. This mixes the frequency down to approximately 2 GHz. This frequency is still too high to be detected with an oscilloscope. Therefore, a second mixing stage is employed. Again the mixing frequency (approximately 1.8 GHz) must be provided by a common local oscillator. The signals are mixed down to a frequency range of approximately 200 MHz, which can be detected and evaluated by an oscilloscope. Before measurements, the device needs to be calibrated. This is done by feeding linearly polarised light at an angle of 45° into the device. This should give two identical signals in E_x and E_y.
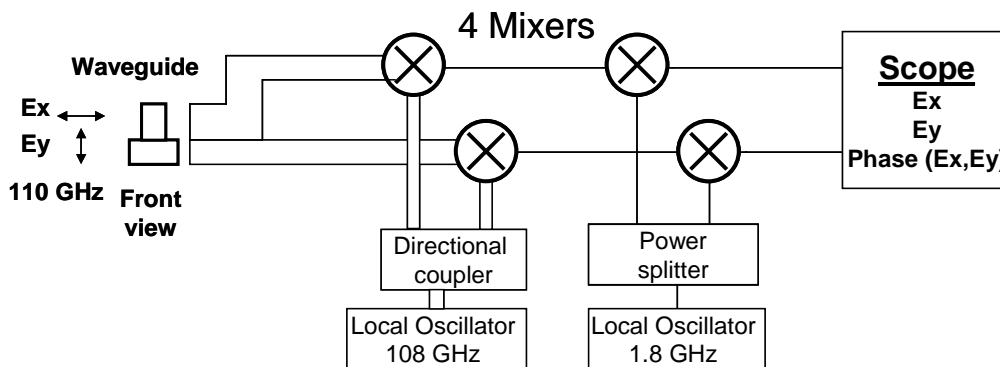

Figure 15. Sketch of the 2-channel detector.

2.3.5 Measurement of the microwave beam characteristics at the 110 GHz gyrotron at TEXTOR and comparison with the mathematical model

F. Leipold and S. Michelsen

frank.leipold@risoe.dk

The polarization measuring device described in subsection 2.3.4 was used to measure the effect of the gyrotron polarizers at TEXTOR. Figure 16 shows the arrangement of the beginning of the optical transmission line of the 110 GHz gyrotron at TEXTOR. The two polarizers UP1 and UP2 are identical. Due to the high incident angle ($\approx 45°$), the phase shift between the electrical field vector parallel and perpendicular to the grooves is a function of the angle of rotation of the polarizer. For the measurement, a Gunn diode is placed in front of UP1 and the detector is placed behind mirror M2 (see Figure 16).
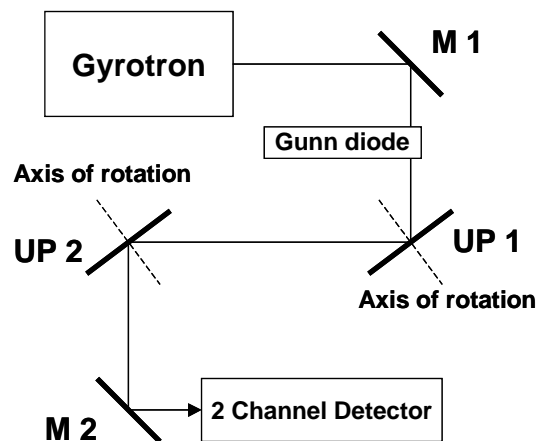
Figure 16. Setup to measure the microwave characteristic of the 110 GHz gyrotron at TEXTOR.

Figure 17 shows a comparison between measurement and calculation of the light characteristic after reflection at both polarizers for various angles of the polarizers. This good agreement between measurement and calculation verifies the mathematical model.

2.3.6 Alignment of the CTS transmission line at TEXTOR

S.K. Nielsen, J.H. Holm, M. Jessen, S. Nimb, S. Michelsen, E. Tsakadze and S.B. Korsholm (also at MIT)

soeren.korsholm@risoe.dk

During the summer opening of 2006 a repair to the flange of the CTS port was needed. Thus after re-installation of the flange, a re-alignment of the full transmission line was needed. The procedure for alignment includes the use of a diode laser and a microwave beam pattern measuring rig as e.g. the micro-rig described in subsection 2.3.3. The procedure is described in some detail in Ref. 1, and it is similar to what is described in subsection 2.3.4 of Ref. 2.
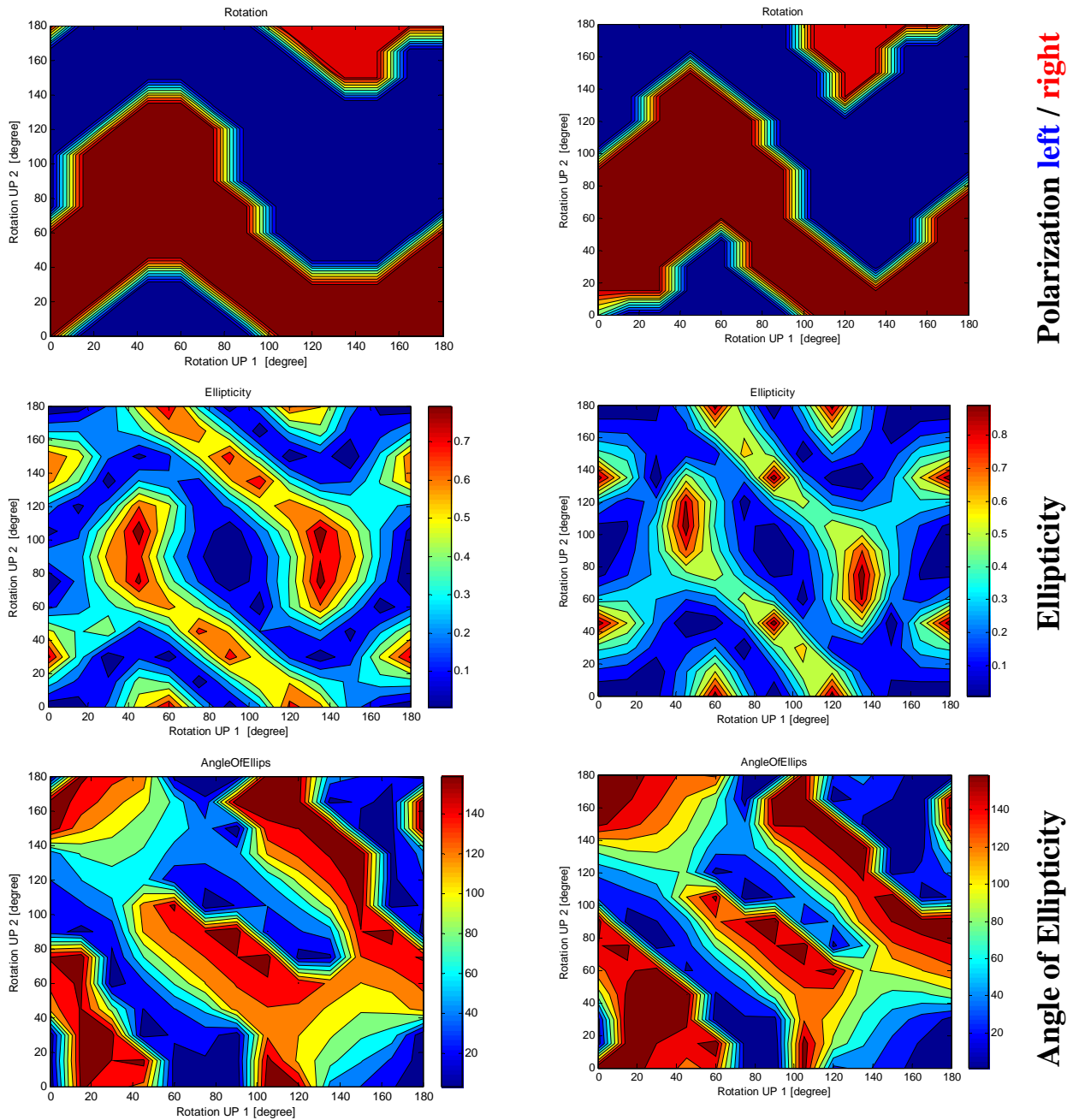
Figure 17. Comparison between measurement and calculation of light characteristic of the 110 GHz gyrotron at TEXTOR. Resolution: 15° steps.

Using the micro-rig the microwave beam shape was measured in a number of positions in the transmission line. From these measurements the Gaussian beam radius was found. A comparison between the measurements and the calculated theoretical values are presented in Figure 18. Mirror 1 (M1) is the moveable mirror closest to the plasma, while mirror 9 (M9) is the last mirror before the receiver horn. In the transition between the vacuum vessel and the outside the beam is transmitted through a circular corrugated waveguide. From Figure 18 one may see a very good agreement between measurements and theory.
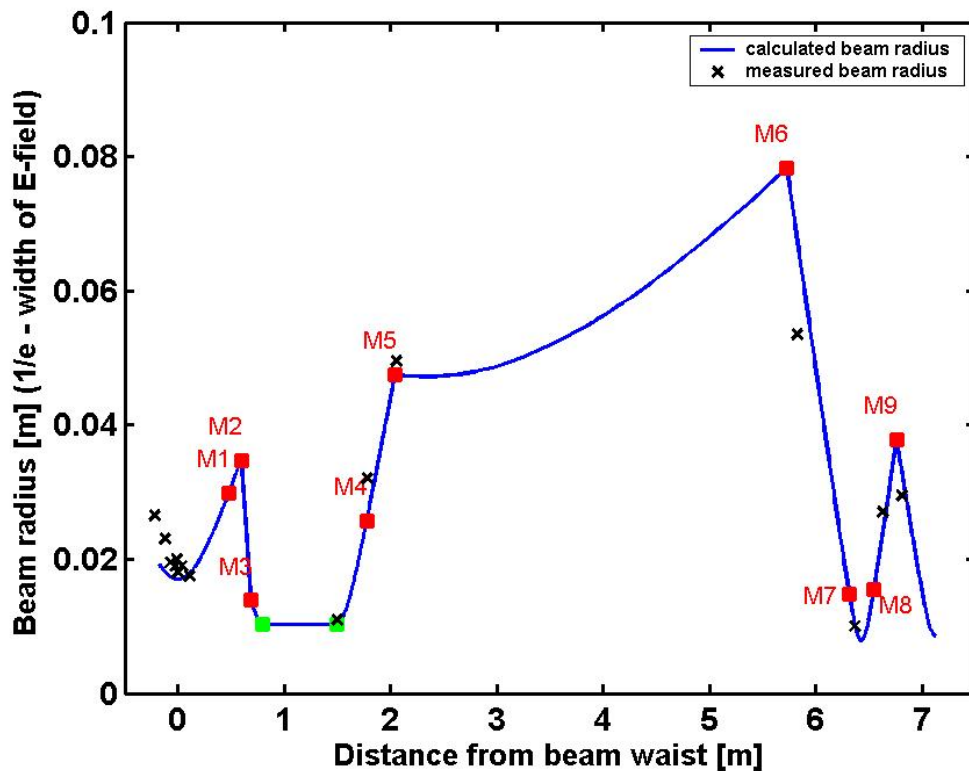
Figure 18. Comparison between calculated and measured beam radii for the TEXTOR CTS transmission line. Mirror 1 to 9 is marked by red squares and the circular corrugated waveguide entries are marked by green squares.

1. S. B. Korsholm, H. Bindslev, F. Meo, F. Leipold, P. K. Michelsen, S. Michelsen, S. K. Nielsen, E. L. Tsakadze, P. Woskov, E. Westerhof , FOM ECRH team, J. W. Oosterbeek, J. Hoekzema, F. Leuterer, D. Wagner, and ASDEX Upgrade ECRH team, *Current fast ion collective Thomson scattering diagnostics at TEXTOR and ASDEX Upgrade, and ITER plans (invited)*, Rev. Sci. Instrum, **77**, Art. No. 10E514 (2006).

2. Risø-R-1579(EN) Association Euratom - Risø National Laboratory Annual Progress Report 2005, http://www.risoe.dk/rispubl/ofd/ofdpdf/ris-r-1579.pdf, Edited by H. Bindslev and B.N. Singh.

2.3.7 High resolution frequency measurements of the TEXTOR gyrotron

P.P. Woskov (MIT), F. Leipold, F. Meo, S.B. Korsholm (also at MIT), S.K. Nielsen, J. Scholten (FOM), C. Tito (FOM), E. Westerhof (FOM), J.W. Oosterbeek (FZ Juelich)
soeren.korsholm@risoe.dk

High resolution frequency measurements of the 110 GHz gyrotron were carried out to better characterize this gyrotron for CTS diagnostics and to optimize the receiver notch filter tuning. The pulse starting frequency was found to be 109.970 ±0.005 GHz and chirped downward up to 27 MHz depending on pulse length and the on/off pulsing duty factor at the gyrotron operating settings that were found to produce maximum output power (~180 kW) with no spurious modes. The gyrotron spectrum during TEXTOR plasma shots was found to be generally clean with a line width of less than 120 kHz FWHM and occasionally present weak satellites at ~ ±17.5 MHz (< -30 dB). Perturbation of the gyrotron output spectrum at the ICRH frequency and harmonics was also observed to occur when both NBI and ICRH where operated at one scattering geometry setting [1]. This observation will be a topic of future studies. Figure 19 shows

the observed gyrotron output spectrum after downshifting to an IF frequency range when it was perturbed by the ICRH at 29 MHz and its harmonic during plasma shot #100472.
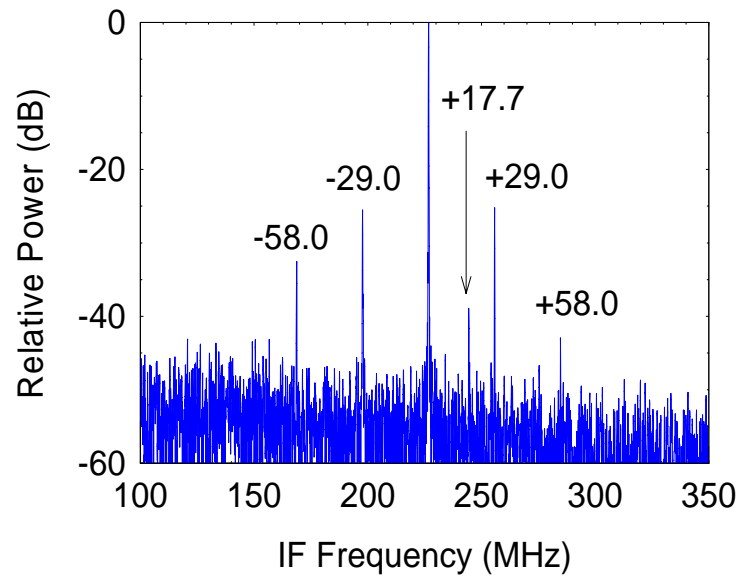

Figure 19. 110 GHz gyrotron forward power spectrum during shot #100472. The gyrotron line is mixed down to approximately 230 MHz in the spectrum.

1. P. P. Woskov, H. Bindslev, F. Leipold, F. Meo, S. K. Nielsen, E. L. Tsakadze, S. B. Korsholm, J. Scholten, C.Tito, E. Westerhof, J. W. Oosterbeek, F. Monaco, F. Leuterer, M. Muenich, D. Wagner, "*Frequency Measurements of the Gyrotrons used for CTS Diagnostics at TEXTOR and ASDEX Upgrade*", Rev. Sci. Instrum., **77**, 10E524 (2006).

2.3.8 Notch filter tuning

S. K. Nielsen and J. H. Holm
stefan.kragh.nielsen@risoe.dk

A key component of the CTS receiver is a set of two notch filters damping the stray radiation from the gyrotron by approximately 120 dB. With the original settings used in previous CTS experiments at TEXTOR, the notches were centered around 110.05 GHz and had a total 3 dB width of 300 MHz. The gyrotron was re-tuned in the beginning of 2006 and a higher output power was obtained at a slightly different frequency. Hence the notch filters were tuned to be centered on this new frequency, while the 3dB width was narrowed in order to receive more CTS signal. The tuning involved a tedious cavity optimization and was performed using the setup shown in Figure 20, while the result is shown in Figure 21. In order to get an absolute measure of the attenuation the gyrotron was used to measure the depth of the notch.

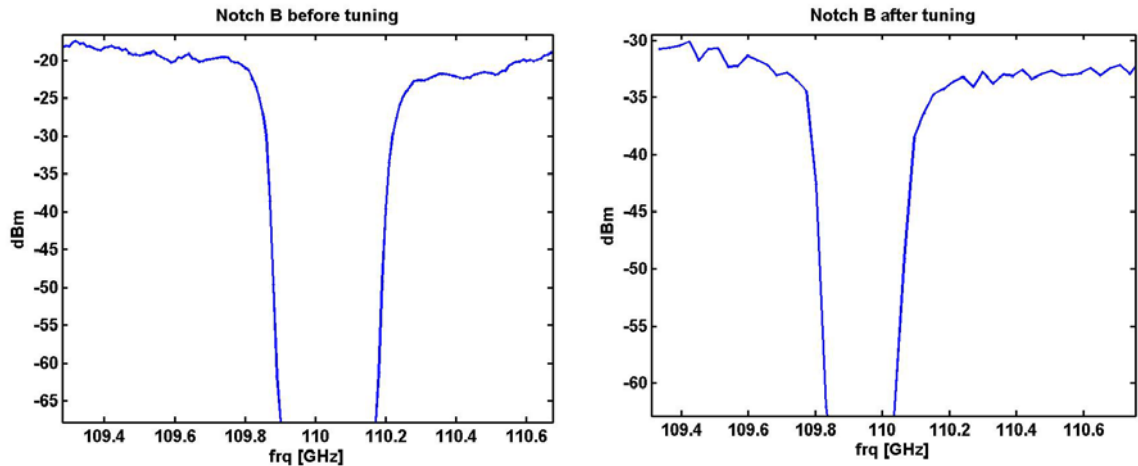Figure 20. Notch filter tuning setup.

Figure 21. (a) Relative transmission curve of Notch B before tuning. (b) Relative transmission curve of Notch B after tuning.

2.3.9 Overview of the Collective Thomson scattering diagnostic at ASDEX Upgrade

F. Meo, H. Bindslev, M. Jessen, J. Holm , S.B. Korsholm (also at MIT Plasma Science and Fusion Center, Massachusetts, USA), F. Leuterer (IPP Garching), P.K. Michelsen, S. Michelsen, S.K. Nielsen, S. Nimb, J.R. Pedersen and P.P. Woskov (MIT)
fernando.meo@risoe.dk

First CTS results were expect to take place in the 2006 ASDEX Upgrade AUG) campaign. However, due to the failure of the dual frequency gyrotron in Spring 2006, experiments were not possible. The gyrotron was sent back to the Institute of Applied Physics Russian Academy of Sciences in Nizhny Novgorod, for repair. A new gyrotron, originally planned to be the step tunable 4-frequency gyrotron, was installed and will be used as a dual frequency gyrotron. Commissioning is in progress and is expected to reach full power by spring 2007. In addition, one of the ASDEX Upgrade's fly-wheel generators was damaged by fire and thus no experiments were possible in 2006. It is expect that the ASDEX Upgrade campaign restart in spring 2007. However, there were significant improvements and understanding of the CTS system.

2.3.10 Alignment of the transmission line in the ASDEX Upgrade ECRH MOU

F. Meo, M. Jessen, J. Holm , F. Leuterer (IPP Garching) and S. Nimb
fernando.meo@risoe.dk

As stated in the 2005 report, the alignment procedure using the 2 way laser and the mini-rig technique has improved the throughput to 85 - 90%. However, due to space limitations, the last portion of the transmission line between sections 1 and 2 in Figure 23 was inaccessible. The beam quality at this most sensitive section was not known. However the more compact micro-rig (described in subsection 2.3.3) enabled the access and thus further improvement of the beam quality. The beam between the coupling mirror and the waveguide was measured at two different distances from the wave guide and shown in Figure 22.
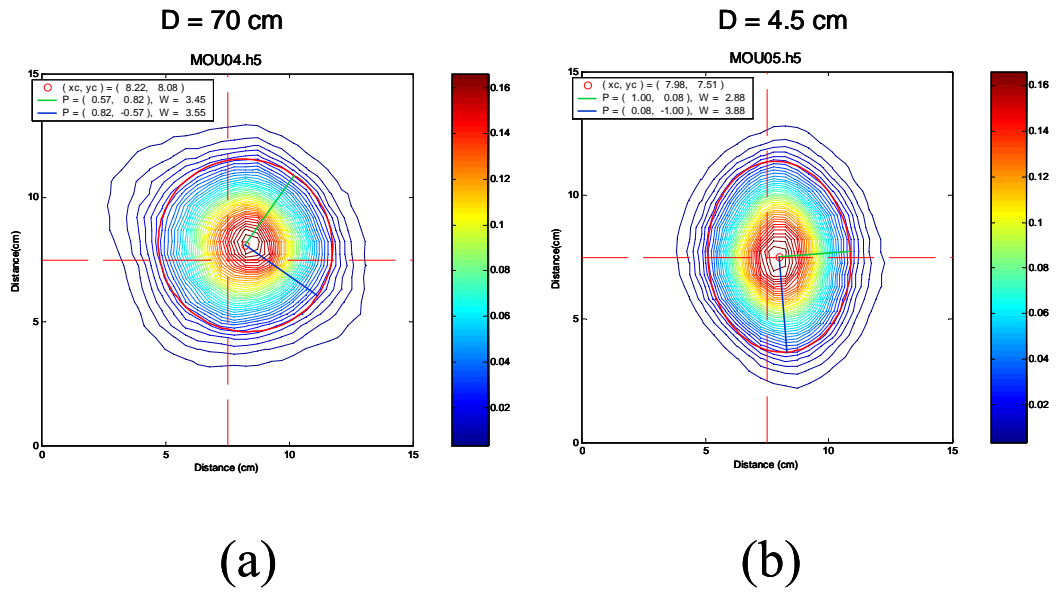
Figure 22. Beam pattern measure in front of the wave guide at two distances D from the waveguide. The laser reference that corresponds to the center of the line in the wave guide is shown with the red dashed lines.

The results in Figure 22 show the beam is astigmatic and slightly misaligned. The affect of the misalignment and/or astigmatism can be seen in the double structure in beam pattern measured at the end of the transmission line behind the ECRH antenna. The alignment was performed and corrected for astigmatism and misalignment of the beam section between the coupling mirror and the wave guide. Figure 23 shows an example of the beam measurements by the micro-rig at two different locations in the transmission line after alignment procedure was performed. The laser reference connecting the mirror centres are shown by the red cross hairs in Figure 23(a).
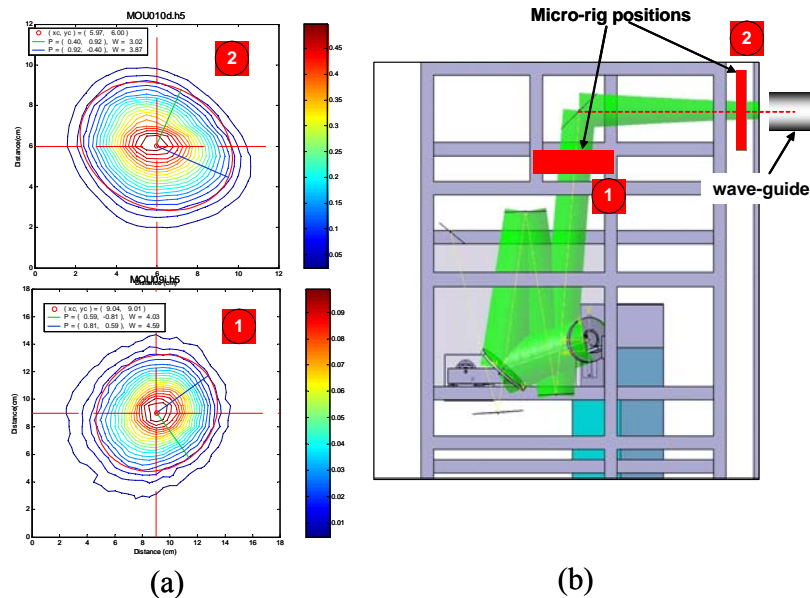

Figure 23. (a) Two examples of the beam pattern measurements of the MOU section of the CTS/ECRH transmission line. (b) A side view of the MOU box with the CTS/ECRH mirror set-up including the calculated beam (in green). Indicated are the two locations that correspond to the beam pattern measurements shown in (a).

2.3.11 ASDEX-Upgrade in-vessel beam measurements and comparison to laser mapping

F. Meo, M. Jessen, J. Holm and S. Nimb
fernando.meo@risoe.dk

The ECRH group have done mapping of the antenna settings to the launching angles using a laser. Beam pattern measurements were performed inside the AUG vacuum vessel to compare the laser position and the microwaves at different angle settings of the ECRH steerable antenna. Five antenna settings were chosen in the experiment that is plotted in Figure 24.

A high precision position measuring device operated and supplied by IPP (called the FARO system) measures the Cartesian global coordinates of any point inside the vessel. Measurements of the laser spots were carried out inside the vessel for each antenna position shown in Figure 24. The beam pattern was then measured by the micro-rig at different locations for the same antenna settings. One example of the measure beam pattern is shown in Figure 25 where the beam is close to Gaussian and no side lobes are present. The beam width from the fitted Gaussian of the measurements agrees well with the calculation. After each measurement, the micro-rig pickoff waveguide is positioned to the maximum intensity. The FARO system then measures the global coordinates of the waveguide position essentially measuring the microwave beam maxima. The vectors of the laser and the microwaves are constructed and compared for each antenna setting. The minimum distance between the viewing line from laser and microwaves as a function of distance from the first mirror is plotted in Figure 26. The colours in the figure represent a different ECRH antenna setting shown by the lines of the same colour in Figure 24. The solid lines are data for the aligned system. To investigate the sensitivity of any misalignment or astigmatism of the beam in the MOU section of the transmission, the measurements were also done for misalignment of the beam to the entrance of the wave guide in the MOU (dashed line in Figure 26), and changing the beam shape by rotating on of the CTS mirrors (dotted line in Figure 26). The data suggest that the maximum distance between the laser line of sight and the microwaves are smaller than 1.5 cm if the beam to the wave guide is less than 0.5 cm from the centre of the wave guide in the MOU. This will be the spatial error during the CTS experiments.

2.3.12 Measurement of the microwave beam characteristics at the 110 GHz through the gyrotron transmission line at ASDEX Upgrade

F. Leipold, F. Meo
frank.leipold@risoe.dk

The polarization measuring device described in subsection 2.3.4 was also used to measure the effect of the gyrotron polarizers at ASDEX Upgrade. The transmission line for a 140 GHz gyrotron will be used in the reverse direction for CTS measurements. Therefore, the transmission for a 110 GHz signal needs to be investigated. A Gunn diode was placed in the position of the first mitre bend pointing towards the gyrotron. The 2-channel detector was placed in front of the CTS receiver (Figure 27).
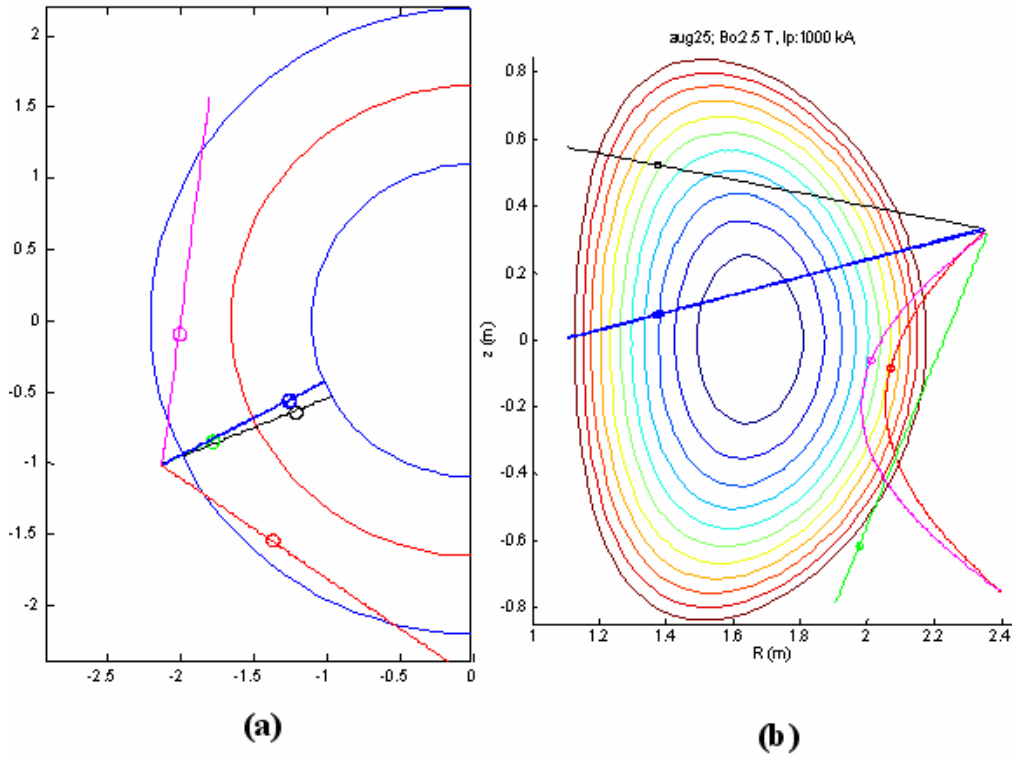
Figure 24. Launch angles for the in-vessel measurements. Top view (a) and poloidal view (b). The circles along the lines represent a distance of 1 m from the first mirror.
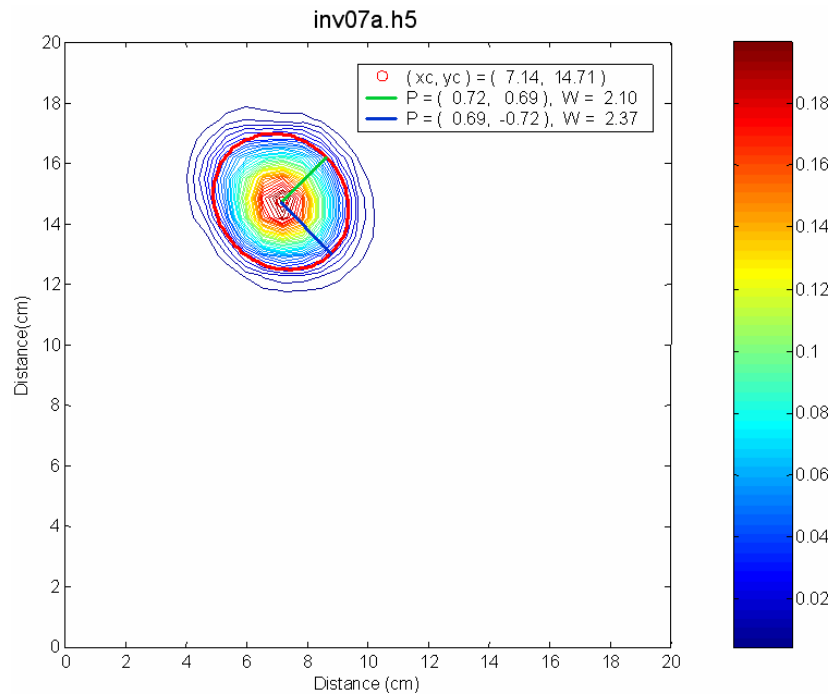
Figure 25. Beam pattern measured inside the vacuum vessel for antenna setting $(\alpha,\beta) = (9.3, -30)$ – magenta colour in Figure 24. The spatial resolution for these measurements is 0.6 cm.
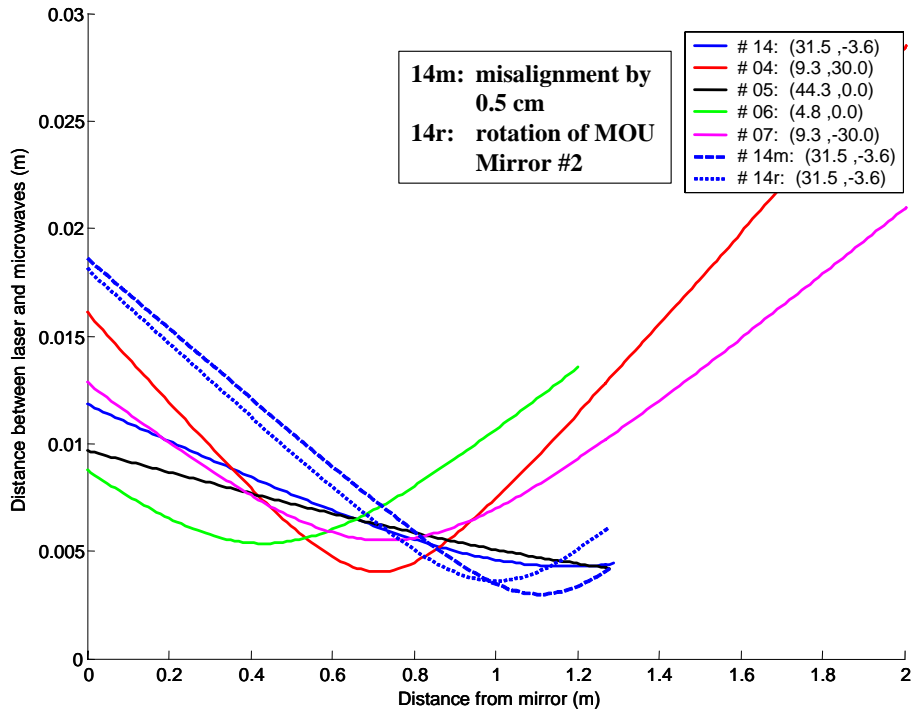
Figure 26. The distance between the measured laser line and the microwave line as a function of distance from the steerable mirror. The line colors correspond to the antenna settings also shown in Figure 24. The solid lines are "aligned" case. The dashed line is the case where the beam at the waveguide in MOU is misaligned by 0.5 cm. The dotted is the case where the beam shape was warped by rotating the MOU Mirror#2.
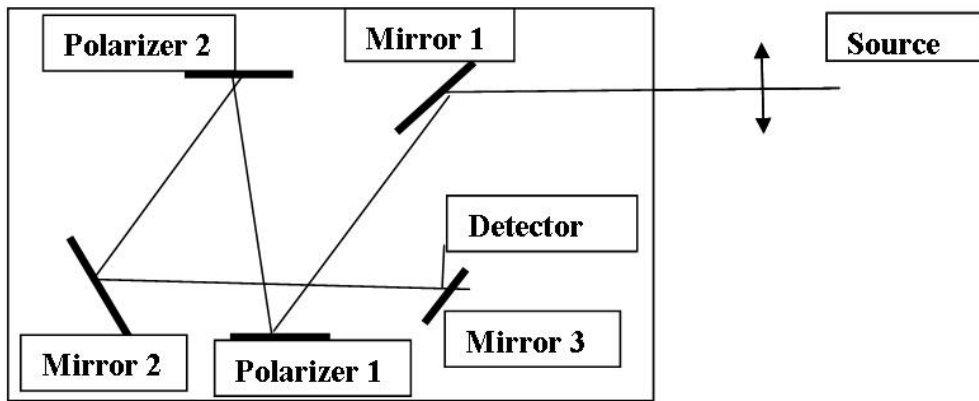
Figure 27. Transmission line at ASDEX.

The microwave polarization at the receiver was measured and calculated. Figure 28 shows a comparison between measurement and calculation of the light characteristic after passing the transmission line for various angles of the polarizers. This good agreement between measurement and calculation verifies the mathematical model. Note, that the polarizers, designated with λ/2 and λ/4 respectively have a phase shift of 180° and 90° for a frequency of 140 GHz and not for 110 GHz. The correct phase shifts applied in the calculations are scaled by 110GHz/140GHz to give 140° and 70°.
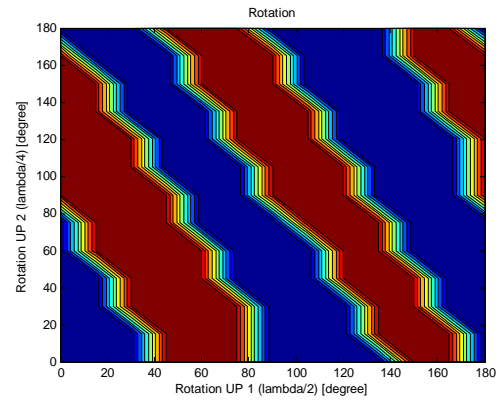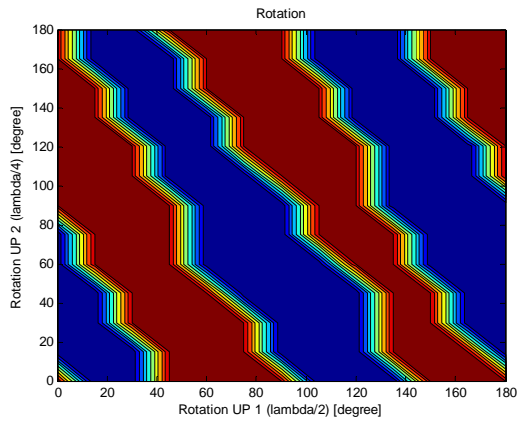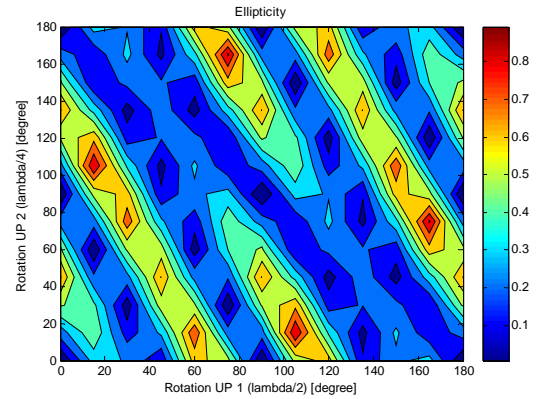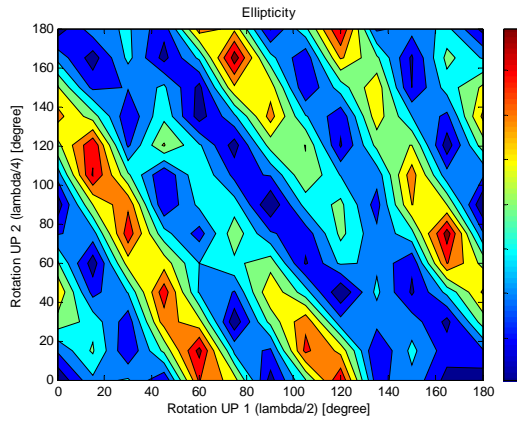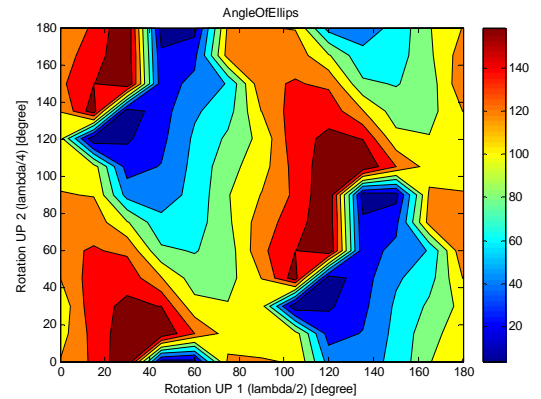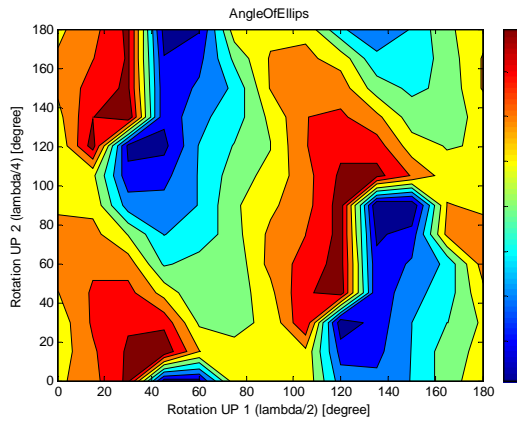
Figure 28. Comparison between measurement and calculation of linear polarized light through the transmission line of the ASDEX Upgrade gyrotron at 110 GHz. Resolution: 15° steps.

The agreement between measurements and calculations demonstrate the validity of the mathematical code to calculate the microwave characteristics for various polarizer settings.

2.3.13 Frequency measurements of the ASDEX Upgrade gyrotron

F. Meo and P.P. Woskov (MIT)
fernando.meo@risoe.dk

New frequency measurements during modulation were made in 2006 of the dual frequency gyrotron at ASDEX Upgrade. It is important to understand all the dynamics of the frequency drift for CTS. This has direct impact on the temporal resolution of the CTS. The experiments have revealed three frequency time constants during modulation where

$$\tau_{thermal} > \tau_{charge} > \tau_V$$

The time constant $\tau_{thermal}$ is the related to the thermal expansion of the cavity, τ_{charge} is the time constant related to the space charge, and τ_V is the time constant related to the voltage rise time. The time of the beam voltage rise time is about 0.5 ms. During this ramp, the tube is undergoing transitions through one or several modes. The thermal expansion time for a power level of 500 kW is about 1.5 sec. This was shown in the last report. However the most significant time behaviour that may affect the CTS experiments is one related to the space charge (τ_{charge}). The frequency measurements in Figure 29 demonstrate this. The measurements were performed while launching into the ECRH water load. The time window in the plot for a time > 4 sec well after the cavity has attained thermal equilibrium and the frequency drift due to cavity expansion has saturated.

The graph in Figure 29 shows the second intermediate time constant τ_{charge} during every gyrotron on-time. This intermediate frequency drift is believed to be caused by a build up of space charge (low density plasma) in the cavity [1]. The data suggests that the frequency time constant is weakly related to the duty cycle chosen or the power level. In addition, the τ_{charge} sometimes shows arbitrary behaviour at each gyrotron on-time as depicted by the green stars in Figure 29. Further studies are foreseen to minimize this type of frequency drift. In addition, studies are on-going to investigate the minimum frequency drift acceptable for CTS measurements.

1. Zaginaylov et al, IEEE Transactions on Plasma Science, **34**, No. 3, June 2006.
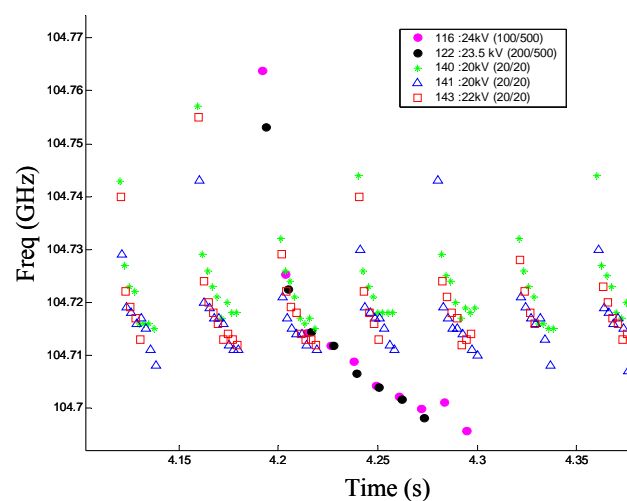
Figure 29. Frequency measurements of the Odyssey 1 gyrotron at ASDEX Upgrade for different beam voltage and different duty cycle.

2.3.14 Design work on a CTS diagnostic for ITER

S. Michelsen, H. Bindslev, S.B. Korsholm, F. Leipold, F. Meo, P.K. Michelsen,
A.H. Nielsen and E. Tsakadze
poul.michelsen@risoe.dk

In 2003 the Risø CTS group finished a feasibility study and a conceptual design of an ITER Fast Ion Collective Thomson Scattering System (Contract 01.654, Ref. 1). The purpose of the CTS diagnostic is to measure the distribution function of fast ions in the plasma. The feasibility study demonstrated that the only system, which can fully meet the ITER measurement requirements for confined fusion alphas, is a 60 GHz system. The study has shown that with two powerful microwave sources of this frequency (gyrotrons) both on the low field side, and two antenna systems, one on the low field side and one on the high field side, it should be possible to resolve the distribution function of fast ions both for perpendicular and parallel velocities with good spatial and temporal resolution.

In 2006 we have investigated alignment issues and made codes which could calculate the 3D shape of mirrors for astigmatic beams.

The mock-up of the ITER CTS high field side (HFS) receiver has been upgraded compared to the previous case as shown in Figure 30. Due to the available mm-wave components at the Risø CTS microwave lab (Gunn oscillator, detector, waveguides, etc.) the operation frequency of the CTS transmission line for the mock-up was chosen to be 110 GHz instead of 60 GHz. Therefore, the whole geometry was scaled down by the factor of 60/110 ~ 0.5455.
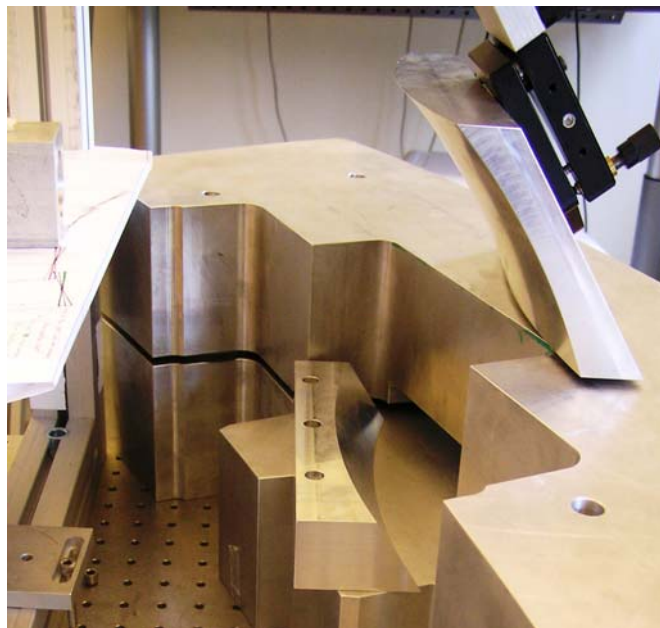
Figure 30. Setup for measurements. The mock-up is turned up side down, to allow easy adjustment of mirrors and the horn. The red line represents the centre position of the mm-waves.

The two mirrors produced the right astigmatic beam at the slot entrance, but the optical beam path was too long to use at ITER. It is still possible to investigate alignment effects, and it was showed that the horn could be offset about 3 mm, which is more than the uncertainty of remote handling of 2 mm. The angle through the slot should be below

2° according to the Computational Electro-Magnetic calculations if internal reflections in the slot should be prevented.

Calculations of misalignment influence on scattering geometry have shown that the probe beam is most critical since the offset should be below 2° degrees in the vertical direction and 4° in the horizontal direction. The receiver beam on the HFS is possible to offset -7° to 5° in the vertical direction and 6° in the horizontal direction. Here it is the geometry constrains which sets the limit and not the influence on the scattering geometry.

2.3.15 Four mirror receiver on the ITER high field side
F. Leipold, S. Michelsen, H. Bindslev, P.K. Michelsen and E. Tsakadze
poul.michelsen@risoe.dk

The high field side receiver system with 2 mirrors described above could produce the right beam at the slot entrance, but not in the available space as can be seen in Figure 30. After the new codes to calculate mirrors for astigmatic beams in 3D have been produced, it was possible to investigate more complex solutions. The performance and feasibility of a 4-mirror solution was therefore investigated. The resulting optimized geometry is shown in Figure 31. In this design it is possible to produce circular beams at the horn entrances within the available space. The spatial limitations are due to cooling pipes in the blanket and a blanket key mounted on the inner wall. The cut-out in the blanket module should also be minimized due to the neutron flux.
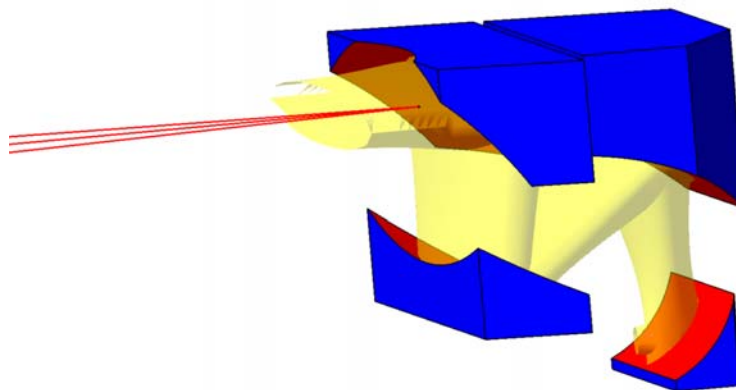
Figure 31. Mirror assembly to focus the elliptical beam at the slit in the blanket to a circular beam at the horn. The horn is not shown in the figure.

2.3.16 Neutronics calculations for the collective Thomson scattering diagnostic system for ITER
B. Lauritzen, E. Nonbøl and N. Dubois

The proposed collective Thomson scattering (CTS) diagnostic system for ITER consists of two separate systems measuring the fast ion velocity components in directions near parallel and near perpendicular to the magnetic field. One of these systems requires alterations to an inboard blanket module in the form of a cavity and a slot to accommodate the CTS receiver unit. The cut-off of the blanket implies increased neutron and gamma fluxes to the magnetic system, in particular to two of the inboard toroidal field (TF) coil legs.
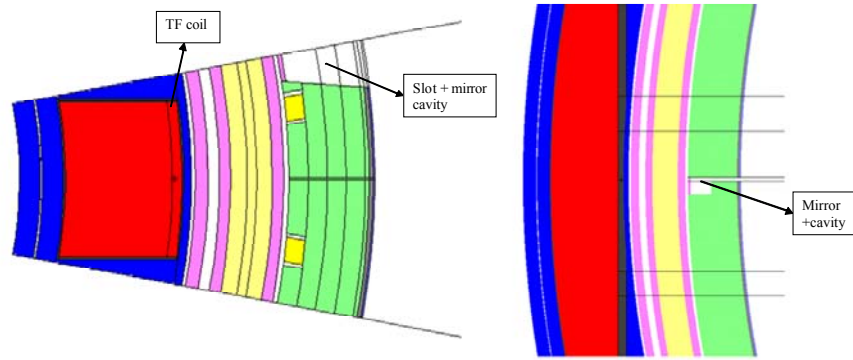
Figure 32. Simplified geometrical model of the tokamak. Horizontal (left) and vertical (right) cross sections showing the mirror cavity and slot.
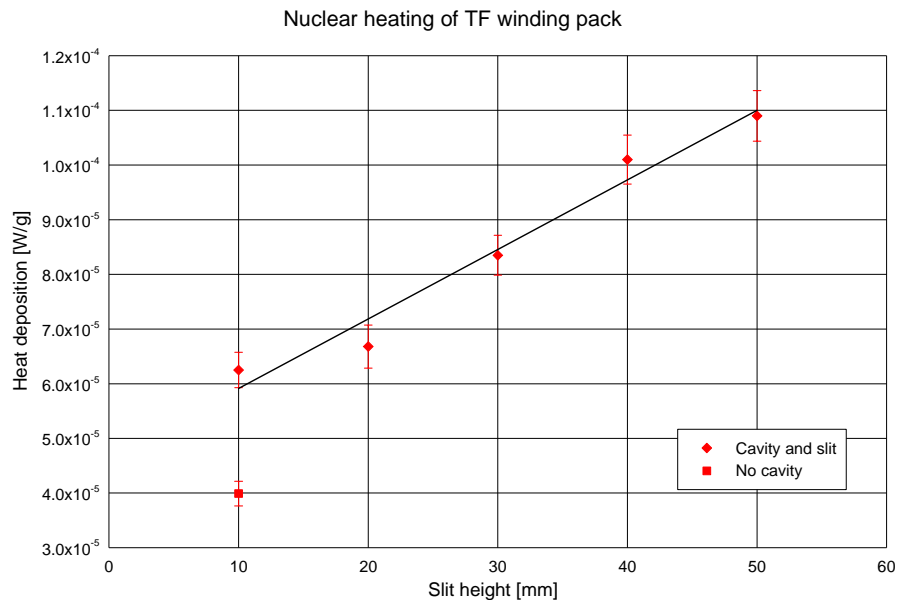
Figure 33. Local nuclear heating of the TF winding pack.

The neutron and gamma fluxes resulting from the proposed modification of the blanket module have been estimated. A geometrical model of the tokamak system including blanket, vacuum vessel, and TF coils were developed, allowing for 3D parametric Monte Carlo calculations using the MCNP-4C code. The model is a simplification of the ITER-FEAT model applied in 3D neutronics analyses of ITER components.

The simplified model is shown in Figure 32. The CTS receiver is placed inside a cavity on the back side of the blanket module (mirror cavity) and requires a horizontal slot (cut-off) facing the plasma. The vertical gap of the slot should be no less than 30 mm in order to satisfy the measurement requirements.
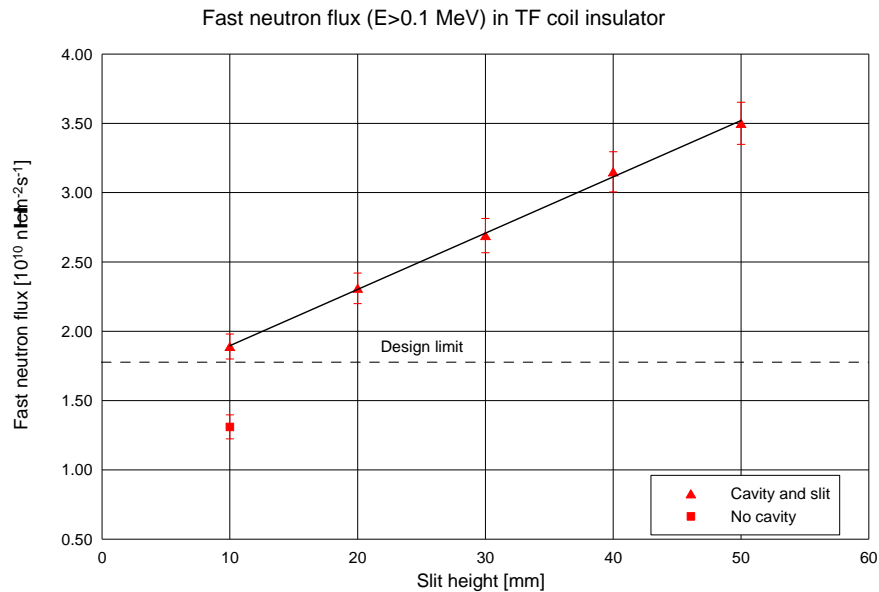
Figure 34. Fast neutron flux to the TF coil insulator.

In Figure 33 the local neutron and gamma heating of a 5x5x5 cm^3 segment of the TF coil is shown. The cavity itself causes an increase of the nuclear heating of approx. 50% while inserting a 30 mm slot increases the nuclear heating by additional 50%. The design limit of the local nuclear heating is approx 1.4×10^{-4} W g^{-1} which is higher than the estimated heat deposition [1]. In Figure 34, the fast neutron flux to the TF coil insulator is shown. In this case the mirror cavity and slot will cause an increase of the flux to above the design limit (1.8×10^{10} cm^{-2} s^{-1}). The fast neutron flux to the TF coil (not shown) remains below the design limit [1].

1. Nuclear Analysis Report, NAG-201-01-06-17-FDR.

2.4 Publications

International articles

Balan, P.; Ionita, C.; Schrittwieser, R.; Herrmann, A.; Maraschek, M.; Müller, H.W.; Rohde, V.; Naulin, V.; Juul Rasmussen, Fluctuation measurements in the SOL of ASDEX upgrade by Langmuir probes. In: Proceedings. 33. European Physical Society conference on plasma physics and controlled fusion, Rome (IT), 19-23 Jun 2006. (European Physical Society, Paris, 2006) (Europhysics Conference Abstracts, vol. 32B) P1-128 (4 p.)

Balan, P.; Ionita, C.; Schrittwieser, R.; Silva, C.; Figueiredo, H.F.C.; Varandas, C.A.F.; Juul Rasmussen, J.; Naulin, V., Emissive probe measurements in ISTTOK. In: Proceedings. 33. European Physical Society conference on plasma physics and controlled fusion, Rome (IT), 19-23 Jun 2006. (European Physical Society, Paris, 2006) (Europhysics Conference Abstracts, vol. 32B) P1-141 (4 p.)

Bindslev, H.; Nielsen, S.K.; Porte, L.; Hoekzema, J.A.; Korsholm, S.B.; Meo, F.; Michelsen, P.K.; Michelsen, S.; Oosterbeek, J.W.; Tsakadze, E.L.; Westerhof, E.; Woskov, P., Fast-ion dynamics in the TEXTOR tokamak measured by collective Thomson scattering. *Phys. Rev. Lett.* (2006) v. 97 p. 205005 (4 pages)

Brochard, F.; Windisch, T.; Grulke, O.; Klinger, T.; Naulin, V., Spatiotemporal investigation of nonlinear coupling and energy transfers indrift wave turbulence. In: Proceedings. 33. European Physical Society conference on plasma physics and controlled fusion, Rome (IT), 19-23 Jun 2006. (European Physical Society, Paris, 2006) (Europhysics Conference Abstracts, vol. 32B) P1-120 (4 p.)

Garcia, O.E.; Bian, N.H.; Naulin, V.; Nielsen, A.H.; Juul Rasmussen, J., Two-dimensional convection and interchange motions in fluids and magnetized plasmas. *Phys. Scr.* (2006) v. T122 p. 104-124

Garcia, O.E.; Bian, N.H.; Fundamenski, W., Radial interchange motions of plasma filaments. *Phys. Plasmas* (2006) v. 13 p. 082309 (16 pages)

Garcia, O.E.; Horacek, J.; Pitts, R.A.; Nielsen, A.H.; Fundamenski, W.; Graves, J.P.; Naulin, V.; Juul Rasmussen, J., Interchange turbulence in the TCV scrape-off layer. *Plasma Phys. Control. Fusion* (2006) v. 48 p. L1-L10

Garcia, O.E.; Naulin, V.; Nielsen, A.H.; Juul Rasmussen, J., Turbulence simulations of blob formation and radial propagation in toroidally magnetized plasmas. *Phys. Scr.* (2006) v. T122 p. 89-103

Juul Rasmussen, J.; Garcia, O.E.; Naulin, V.; Nielsen, A.H.; Stenum, B.; Bokhoven, L.J.A. van; Delaux, S., Generation of zonal flows in rotating fluids and magnetized plasmas. *Phys. Scr.* (2006) v. T122 p. 44-51

Juul Rasmussen, J.; Naulin, V.; Lonnroth, J.S.; Mantica, P.; Parail, V., Turbulence spreading transport simulations of JET plasmas. In: Proceedings. 33. European Physical Society conference on plasma physics and controlled fusion, Rome (IT), 19-23 Jun 2006. (European Physical Society, Paris, 2006) (Europhysics Conference Abstracts, vol. 32B) P1-076 (4 p.)

Korsholm, S.B.; Bindslev, H.; Meo, F.; Leipold, F.; Michelsen, P.K.; Michelsen, S.; Nielsen, S.K.; Tsakadze, E.L.; Woskov, P.; Westerhof, E.; Oosterbeek, J.W.; Hoekzema, J.; Leuterer, F.; Wagner, D., Current fast ion collective Thomson scattering diagnostics at TEXTOR and ASDEX Upgrade, and ITER plans (invited). *Rev. Sci. Instrum.* (2006) v. 77 p. 10E514 (7 pages)

Lamalle, P.U.; Mantsinen, M.J.; Noterdaeme, J.M.; Alper, B.; Beaumont, P.; Bertalot, L.; Blackman, T.; Bobkov, V.V.; Bonheure, G.; Brzozowski, J.; Castaldo, C.; Conroy, S.; Baar, M. de; Luna, E. de la; Vries, P. de; Durodie, F.; Ericsson, G.; Eriksson, L.G.; Govers, C.; Felton, R.; Heikkinen, J.; Hellsten, T.; Kiptily, V.; Lawson, K.; Laxåback, M.; Lerche, E.; Lomas, P.; Lysoivan, A.; Mayoral, M.L.; Meo, F.; Mironov, M.; Monakhov, I.; Nunes, I.; Piazza, G.; Popovichev, S.; Salmi, A.; Santala, M.I.K.; Sharapov, S.; Tala, T.; Tardocchi, M.; Eester, D., Van; Weyssow, B., Expanding the operating space of ICRF on JET with a view to ITER. *Nucl. Fusion* (2006) v. 46 p. 391-400

Lönnroth, J.-S.; Bateman, G.; Bécoulet, M.; Beyer, P.; Corrigan, G.; Figarella, C.; Fundamenski, W.; Garcia, O.E.; Garbet, X.; Huysmans, G.; Janeschitz, G.; Johnson, T.; Kiviniemi, T.; Kuhn, S.; Kritz, A.; Loarte, A.; Naulin, V.; Nave, F.; Onjun, T.; Pacher, G.W.; Pacher, H.D.; Pankin, A.; Parail, V.; Pitts, R.; Saibene, G.; Snyder, P.; Spence, J.; Tskhakaya, D.; Wilson, H., Integrated ELM modelling. *Contrib. Plasma Phys.* (2006) v. 46 p. 726-738

Madsen, J.; Staerk, J.; Garcia, O.E.; Naulin, V.; Nielsen, A.H.; Juul Rasmussen, J.; Kendl, A., Blob dynamics in a hot plasma. In: Proceedings. 33. European Physical Society conference on plasma physics and controlled fusion, Rome (IT), 19-23 Jun 2006. (European Physical Society, Paris, 2006) (Europhysics Conference Abstracts, vol. 32B) P1-197 (4 p.)

Mayoral, M.L.; Lamalle, P.U.; Eester, D. van; Lerche, E.A.; Beaumont, P.; Luna, E. de la; Vries, P. de; Gowers, C.; Felton, R.; Harling, J.; Kiptily, V.; Lawson, K.; Laxaback, M.; Lomas, P.; Mantsinen, M.J.; Meo, F.; Noterdaeme, J.M.; Nunes, I. Piazza, G.; Santala, M., Hydrogen plasmas with ICRF inverted minority and mode conversion heating regimes in the JET tokamak. *Nuclear Fusion* (2006) v. 46 p. S550-S563

Naulin, V.; Garcia, O.E.; Priego, M.; Juul Rasmussen, J., The application of passive tracers for investigating transport in plasma turbulence. *Phys. Scr.* (2006) v. T122 p. 129-134

Ratynskaia, S.; Rypdal, K.; Knapek, C.; Khrapak, S.; Milovanov, A.V.; Ivlev, A.; Juul Rasmussen, J.; Morfill, G.E., Superdiffusion and viscoelastic vortec flows in a two-dimensional complex plasma. *Phys. Rev. Lett.* (2006) v. 96 p. 105010 (4 pages)

Stroth, U.; Greiner, F.; Happel, T.; Holzhauer, E.; Mahdizadeh, N.; Manz, P.; Rahbarnia, K.; Ramisch, M.; Kendl, A.; Koehn, A.; Naulin, V.; Scott, B., Recent studies on turbulent transport in the torsatron TJ-K. In: Proceedings. 33. European Physical Society conference on plasma physics and controlled fusion, Rome (IT), 19-23 Jun 2006. (European Physical Society, Paris, 2006) (Europhysics Conference Abstracts, vol. 32B) O3-003 (4 p.)

Teliban, T.; Block, D.; Piel, A.; Naulin, V., A super-resolution method for spatio-temporal plasma diagnostics. *Plasma Phys. Control. Fusion* (2006) v. 48 p. 419-431

Tsakadze, E.L.; Bindslev, H.; Korsholm, S.B.; Leipold, F.; Meo, F.; Michelsen, P.K.; Michelsen, S.; Nielsen, S.K.; Woskov, P.; Hoekzema, J.A.; Oosterbeek, H.; Westerhof, E.; Leuterer, F., Progress on the fast ion millimetre wave CTS diagnostics on TEXTOR and ASDEX upgrade and status of the CTS design for ITER. In: Proceedings. 33. European Physical Society conference on plasma physics, Rome (IT), 19-23 Jun 2006. (European Physical Society, Paris, 2006) (Europhysics Conference Abstracts, vol. 30I) 4 p.

Windisch, T.; Grulke, O.; Klinger, T.; Naulin, V., Intermittent spatiotemporal turbulent structures in a linear helicon experiment. In: Proceedings. 33. European Physical Society conference on plasma physics and controlled fusion, Rome (IT), 19-23 Jun 2006. (European Physical Society, Paris, 2006) (Europhysics Conference Abstracts, vol. 32B) P1-121 (4 p.)

Woskov, P.; Bindslev, H.; Leipold, F.; Meo, F.; Nielsen, S.K.; Tsakadze, E.L.; Korsholm, S.B.; Scholten, J.; Tito, C.; Westerhof, E.; Oosterbeek, J.W.; Leuterer, f.; Monaco, F.; Muenich, M.; Wagner, D., Frequency measurements of the gyrotrons used for collective Thomson scattering diagnostics at TEXTOR and ASDEX Upgrade. *Rev. Sci. Instrum.* (2006) v. 77 p. 10E524 (4 pages)

Danish reports

Bindslev, H.; Singh, B.N (eds.), Association Euratom - Risø National Laboratory annual progress report 2005. Risø-R-1579(EN) (2006) 70 p. www.risoe.dk/rispubl/ofd/ofdpdf/ris-r-1579.pdf

Unpublished international conference proceedings

Balan, P.; Mehlmann, F.; Konzett, S.J.; Kendl, A.; Herrmann, A.; Ionita, C.; Maraschek, M.; Müller, H.W.; Garcia, O.E.; Naulin, V.; Nielsen, A.H.; Rohde, V.; Juul Rasmussen, J.; Schrittwieser, R., Investigation of fluctuations in the SOL of ASDEX upgrade by Langmuir probes. IEA large Tokamak IA workshop on edge transport in fusion plasmas, Krakov (PL), 11-13 Sep 2006. Unpublished. Presentation available

Garcia, O.E.; Fundamenski, W.; Bian, N.H.; Naulin, V.; Nielsen, A.H.; Juul Rasmussen, J., Radial motion of isolated blobs and ELM filaments in SOL plasmas. IEA large Tokamak IA workshop on edge transport in fusion plasmas, Krakov (PL), 11-13 Sep 2006. Unpublished. Presentation available

Garcia, O.E.; Pitts, R.A.; Horacek, J.; Nielsen, A.H.; Fundamenski, W.; Graves, J.P.; Naulin, V.; Juul RAsmussen, J., Turbulence simulations of interchange motions and intermittent transport in TCV scrape-off layer plasmas (poster). 17. International conference on plasma surface interactions in controlled fusion devices, Hefei Anhui (CN), 22-26 May 2006. Unpublished.

Giroud, C.; Angioni, C.; Bonheure, G.; Coffey, I.; Dubuit, N.; Garbet, X.; Guirlet, R.; Mantica, P.; Naulin, V.; Puiatti, M.E.; Valisa, M.; Whiteford, A.D.; Zastrow, K.-D.; Beurskens, M.N.A.; Brix, M.; Luna, E. de la; Lawson, K.; Lauro-Taroni, L.; Meigs, A.; O'Mullane, M.; Parisot, T.; Perez, C.; Zimmermann, O., Progress in understanding anomalous impurity transport at JET. 21. IAEA fusion energy conference, Chengdu (CN), 16-21 Oct 2006. Unpublished. Abstract available

Horacek, J.; Garcia, O.E.; Pitts, R.A.; Nielsen, A.H.; Fundamenski, W.; Graves, J.P.; Naulin, V.; Juul Rasmussen, J., Understanding SOL plasma turbulence by interchange motions. IEA large Tokamak IA workshop on edge transport in fusion plasmas, Krakov (PL), 11-13 Sep 2006. Unpublished. Presentation available

Juul Rasmussen, J., Theory and modelling at small associations. Workshop on fusion physics modelling, theory and support IT infrastructure, Brussels (BE), 6 Mar 2006. Unpublished.

Juul Rasmussen, J., Collapse dynamics, singularity formation and regularization (invited contribution). Symposium on fascinating nonlinear physics, Trieste (IT), 27 Aug 2007. Unpublished. Lecture notes available

Juul Rasmussen, J.; Garcia, O.E.; Naulin, V.; Nielsen, A.H., Intermittency and transport structures in edge/SOL turbulence. Edge physics meeting: JET TF-E and TF-T, 8-10 Feb 2006. Unpublished

Juul Rasmussen, J.; Garcia, O.E.; Naulin, V.; Nielsen, A.H., Turbulence and intermittent transport in magnetized plasmas (invited contribution). International workshop on frontiers of plasma science, Trieste (IT), 21 Aug - 1 Sep 2006. Unpublished.

Juul Rasmussen, J.; Garcia, O.E.; Naulin, V.; Nielsen, A.H.; Stenum, B.; Kendl, A., Generation and dynamics of large scale flows in magnetized plasmas. Task Force Transport (TF-T) seminar, Culham (GB), 21 FEb 2006. Unpublished.

Korsholm, S.B.; Bindslev, H.; Leipold, F.; Meo, F.; Michelsen, P.K.; Michelsen, S.; Nielsen, S.K.; Tsakadze, E.L.; Woskov, P.P.; Westerhof, E.; Oosterbeek, J.W.; Hoekzema, J.; Leuterer, F.; Wagner, D., Progress towards a fast ion collective Thomson scattering diagnostic for ITER. 48. Annual meeting of the Division of Plasma Physics, American Physical Society, Philadelphia, PA (US), 30 Oct - 3 Nov 2006. Unpublished. Abstract available

Korsholm, S.B.; Bindslev, H.; Woskov, P.; Hoekzema, J.; Leipold, F.; Leuterer, F.; Meo, F.; Michelsen, S.; Michelsen, P.K.; Nielsen, S.K.; Oosterbeek, J.W.; Tsakadze, E.L.; Wagner, D.; Westerhof, E., Current experiments on fast ion collective Thomson scattering at TEXTOR and ASDEX upgrade, and ITER plans (invited talk). 16. Annual conference on high-temperature plasma diagnostics, Williamsburg, VA (US), 7-11 May 2006. Unpublished.

Mantica, P.; Garbet, X.; Naulin, V.; Nora, M.; Juul Rasmussen, J.; Tala, T.; Thyagaraja, A., Fast core response to edge cooling in JET: Experiments and modelling. 11. EU-US Transport Task Force workshop, Marseille (FR), 4-7 Sep 2006. Unpublished.

Michelsen, P.K.; Bindslev, H.; Korsholm, S.B.; Larsen, A.W.; Meo, F.; Michelsen, S.; Nielsen, A.H.; Nimb, S.; Tsakadze, E., Fast ion collective Thomson scattering diagnostic for ITER (poster). 14. Joint workshop on electron cyclotron emission and electron cyclotron resonance heating, Santorini Island (GR), 9-12 May 2006. Unpublished. Paper available

Muller, S.H.; Diallo, A.; Fasoli, A.; Furno, I.; Labit, B.; Plyushchev, G.; Podesta, M.; Poli, F.M.; Naulin, V., Fluctuations, turbulence and transport in the TORPEX device. Theory of fusion plasma joint Varenna - Lausanne international workshop, Varenna (IT), 28 Aug - 1 Sep 2006. Unpublished.

Naulin, V., Turbulent transport and the plasma edge (invited talk). 17. International conference on plasma surface interactions in controlled fusion devices, Hefei Anhui (CN), 22-26 May 2006. Unpublished. Presentation available

Naulin, V.; Fundamenski, W.; Nielsen, A.H.; Juul Rasmussen, J.; Garcia, O.E.; Goncalves, B.; Hidalgo, C.; Hron, M., Turbulence modeling of JET SOL plasma. 21. IAEA fusion energy conference, Chengdu (CN), 16-21 Oct 2006. Unpublished. Abstract available

Nielsen, A.H.; Fundamenski, W.; Garcia, O.E.; Naulin, V.; Juul Rasmussen, J., Interchange turbulence simulations for JET relevant parameters. IEA large Tokamak IA workshop on edge transport in fusion plasmas, Krakov (PL), 11-13 Sep 2006. Unpublished. Presentation available

Nielsen, A.H.; Garcia, O.E.; Horacek, J.; Pitts, R.A.; Fundamenski, W.; Graves, J.P.; Naulin, V.; Juul Rasmussen, J., Comparison with experiment: Modelling TCV and JET SOL. Edge physics meeting: JET TF-E and TF-T, 8-10 Feb 2006. Unpublished.

Oosterbeek, J.W.; Bongers, W.A.; Classen, I.G.J.; Danilov, I.; Hoekzema, J.A.; Heidinger, R.; Graswinckel, M.F.; Korsholm, S.B.; Kramer-Flecken, A.; Kruijt, O.G.; Scholten, J.; Tito, C.; Tsakadze, E.; Vaessen, B.C.E.; Westerhof, E., Design of a dedicated ECE diagnostic for feedback control of instabilities by ECRH (poster). 14. Joint workshop on electron cyclotron emission and electron cyclotron resonance heating, Santorini Island (GR), 9-12 May 2006. Unpublished. Paper available

Pitts, R.A.; Horacek, J.; Fundamenski, W.; Nielsen, A.H.; Garcia, O.E.; Naulin, V.; Juul Rasmussen, J.; Wischmeier, M., Parallel SOL flow in TCV. 17. International conference on plasma surface interactions in controlled fusion devices, Hefei Anhui (CN), 22-26 May 2006. Unpublished. Presentation available

Staerk, J.; Madsen, J.; Naulin, V.; Garcia, O.E.; Kendl, A.; Nielsen, A.H.; Juul Rasmussen, J., Finite ion temperature effects on SOL turbulence and transport. 17. US - EU Transport Task Force meeting, Marseille (FR), 4-7 Sep 2006. Unpublished.

Tala, T.; Andrew, Y.; Crombe, K.; Vries, P.C. de; Garbet, X.; Hawkes, N.; Nordman, H.; Rantamki, K.; Strand, P.; Thyagaraja, A.; Weiland, J.; Asp, E.; Baranov, Y.; Challis, C.; Corrigan, G.; Eriksson, A.; Giroud, C.; Hua, M.-D.; Jenkins, I.; Knoops, H.C.M.; Litaudon, X.; Mantica, P.; Naulin, V.; Parail, V.; Zastrow, K.-D., Overview of toroidal and poloidal momentum transport studies in JET. 21. IAEA fusion energy conference, Chengdu (CN), 16-21 Oct 2006. Unpublished. Abstract available

Woskov, P.; Bindslev, H.; Leipold, F.; Meo, F.; Nielsen, S.K.; Tsakadze, E.L.; Korsholm, S.B.; Scholten, J.; Tito, C.; Westerhof, E.; Oosterbeek, J.W.; Leuterer, F.; Monaco, F.; Muenich, M.; Wagner, D., Gyrotron frequency measurements for fast ion CTS diagnostics at TEXTOR and ASDEX upgrade (poster). 48. Annual meeting of the Division of Plasma Physics, American Physical Society, Philadelphia, PA (US), 30 Oct - 3 Nov 2006. Unpublished. Abstract available

3 Fusion Technology

3.1 Introduction

The work reported in this section has been carried out in the Materials Research Department. The overall objective of the research activities in this area is to determine the impact of neutron irradiation on physical and mechanical properties of metals and alloys, so that appropriate materials can be chosen for their application in irradiation environment (e.g. in fusion reactor). Various experimental techniques are employed to study different aspects of the microstructural evolution during irradiation and the resulting consequences of the post-irradiation physical and mechanical properties of metals and alloys. Calculations and computer simulations are performed to understand the evolution of surviving defects and their clusters in collision cascades. The kinetics of defect accumulation during irradiation and the influence of irradiation-induced defects and their clusters on the deformation behaviour of irradiated metals and alloys are studied theoretically. In the following, the main results of these activities are highlighted.

3.2 Next step technology

3.2.1 In-reactor creep-fatigue cyclic testing of CuCrZr alloy[1]

B.N. Singh, S. Tähtinen, P. Moilanen* (*VTT Industrial Systems (Association EURATOM-TEKES), Espoo, Finland)), P. Jacquet** and J. Dekeyser** (**Reactor Experiment Department, SCK.CEN, Mol, Belgium)*

At present it seems almost certain that the precipitation hardened CuCrZr alloy will be used both in the first wall and divertor components of ITER. In the reactor vessel, this alloy will be exposed to a relatively high flux of 14 MeV neutrons and will experience thermo-mechanical cyclic loading as a result of the cyclic nature of the plasma burn operations of the system. Because of the "plasma-on" and "plasma-off" mode of operation, the deformation behaviour of the alloy is likely to be modified. This kind of cyclic loading would induce not only fatigue damage but also make the material creep during the operation. Not much is known at present about the impact of this complicated mode of deformation on the mechanical performance of metals and alloys particularly in the environment of intense neutron irradiation.. In order to make a realistic evaluation of the response of materials under these conditions, an experimental programme was initiated with the objective of carrying out creep-fatigue experiments directly in the environment of neutrons in the BR-2 reactor at Mol (Belgium). In order to carry out such tests, fatigue specimens and test modules were designed and fabricated. The main results of such in-reactor creep-fatigue tests carried out on CuCrZr HT1 alloy with a strain amplitude of 0.5 % were reported last year. In the following, the results of in-reactor creep-fatigue tests carried out on the same alloy with strain amplitudes of 0.25 % and 0.35 % and with a hold time of 10s are described.

---

[1] TW4 – TVM – COFAT 2
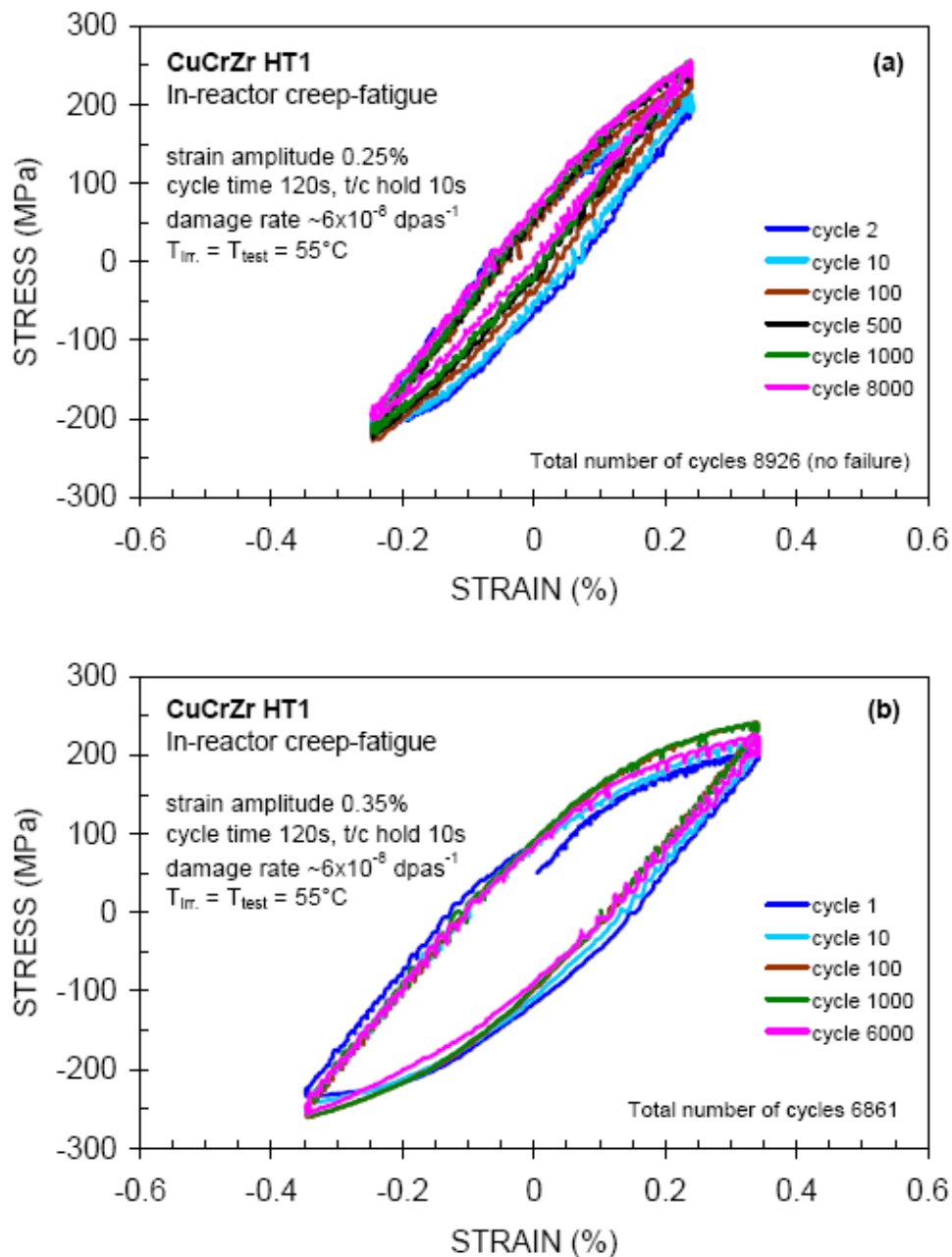
Figure 1. Cyclic deformation behaviour in the form of hysteresis loops for CuCrZr HT1 alloy obtained for different cycles during the in-reactor creep-fatique tests performed at 55°C and a holdtime of 10s both in the tension and compression sides of the cycles with a constant strain amplitude of (a) 0.25 % or (b) 0.35 %.

The test facility used in the present work consists of a pneumatic fatigue test module and a servo-controlled pressure-adjusting loop. The pressure-adjusting loop operates on a continuous flow of helium gas. The basic principle of the creep-fatigue test module is based on the use of two pneumatic bellows to introduce stress/strain and a linear variable differential transformer (LVDT) sensor to measure the resulting extension of the gauge length of the creep-fatigue specimen. The strain measured by the LVDT has been calibrated against the strain measured by strain gauges. The strain measured in the gauge length is used to control the pre-determined constant strain amplitude throughout the whole test. It should be pointed out that one bellows is used to induce tension whereas

the other bellows induces compression. Two such test modules were loaded into an instrumented irradiation rig. The temperature of specimens was measured by thermocouples placed immediately above the specimens. Thermocouples were also placed just above the bellows and LVDTs. Thus, each test module had three thermocouples so that its temperature during irradiations could be monitored at different positions in the irradiation rig. To avoid overheating of the specimens, water was circulated (600 litres per hour) from the top of the test assembly in the irradiation rig.

The irradiation rig containing the assembly of specimens, LVDTs, cooling system and thermocouples was lowered in the reactor core when the local neutron flux near the rig had reached a steady state level after the reactor start. It took about 10 minutes to reach a stable temperature of 55°C in both test modules. Creep-fatique specimens of CuCrZr HT1 were tested in the test module 1 (Test No.1) and test module 2 (Test No.2) with strain amplitudes of 0.25 % and 0.35 %, respectively. In both cases, time taken to reach from push to pull (i.e. compression to tension) was 50s giving the strain rate of $1x10^{-4}s^{-1}$ and $1.4x10^{-4}s^{-1}$ in the Test No.1 and Test No 2 respectively. In both tests a holdtime 10s was implemented both in the compression and the tension sides of the fatique cycle. Thus, the total time spent in each creep-fatigue cycle was 120s both in Test No.1 and Test No.2. The displacement dose per cycle was $7.2 x 10^{-6}$ dpa/cycle in both cases. The damage rate in both test modules was estimated to be ~ $6 x 10^{-8}$ dpa.s^{-1}

During in-reactor creep-fatigue tests the evolution of the stress and strain was continuously recorded during the cyclic loading. The cyclic deformation behaviour of CuCrZr specimen during the in-reactor creep-fatigue Test No. 1 and Test No. 2 is shown in Figures 1 in the form of hysteresis loops for different cycles during the tests with strain amplitudes of (a) 0.25 % and (b) 0.35 %. The symmetry and the stability of the loops demonstrate the validity of the in-reactor creep-fatigue tests. The average value of the maximum stress reached in the tension and the compression sides of a deformation cycle is plotted in Figure 2 as a function of number of cycles during Test No. 1 and 2. For comparison the results of reference tests carried out on unirradiate specimen at 80ºC with strain amplitudes of 0.3, 0.4 and 0.5 %. and with a holdtime of 10 s are shown in Figure 3. All tests on unirradiated specimens (Figure 3) were carried out until the end of life of the specimens. In-reactor Test No.1 at the stress amplitude of 0.25 % lasted for the whole reactor period. The Test No.2, on the other hand, produced crack in the specimen and the test was stopped after 6861 cycles. The total number of cycles in the Test No.1 at the time when the test was terminated at the end of the reactor period was 8926. During the in-reactor creep-fatigue deformation the total displacement dose accumulated on the specimens used in the Test No.1 and Test No.2 was 0.064 and 0.049 dpa, respectively. At the end of the reactor period the irradiation rig was removed from the reactor and transported to the hot cells where the deformed specimens were removed from the rig. Photographs of the deformed specimens including the gauge section are shown in Figure 4. It should be noted that the specimen tested with a strain amplitude of 0.25 % does not show any sign of any crack present at the surface of the specimen (Figure 4a). The specimen tested with a strain amplitude of 0.35 % (Test no.2) clearly show the presence of crack on the surface of the deformed specimen (Figure 4b). These observations are consistent with the results shown in Figure 2.
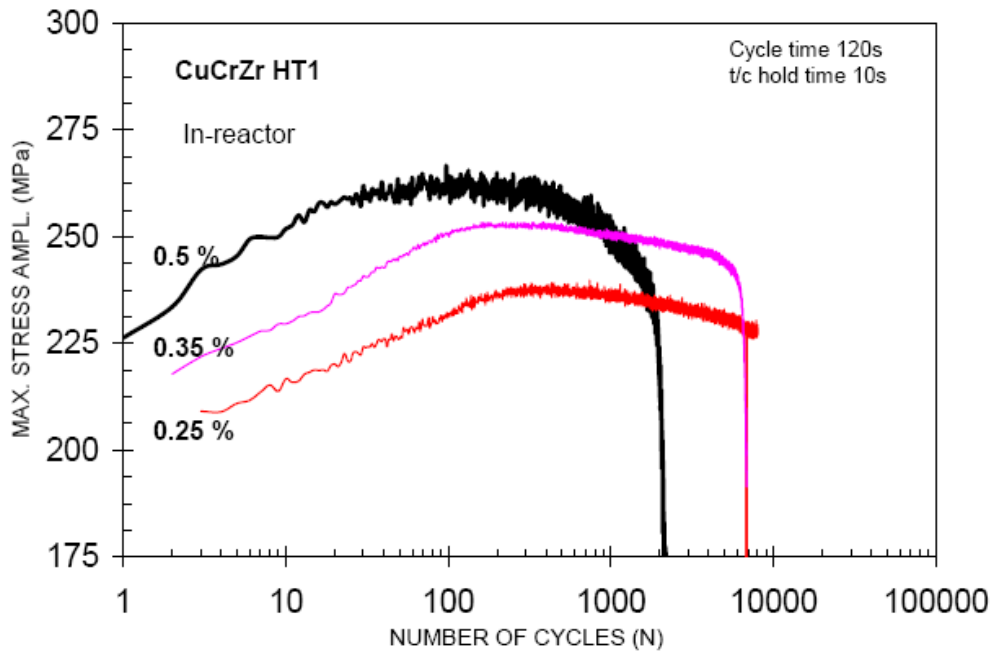
Figure 2.Variation of the maximum stress amplitude with the number of cycles during in-reactor creep-fatique tests at 55°C with strain amplitudes of 0.25 % and 0.35 % (Test No. 1 and 2,respectively) and with a holdtime of 10s. For comparision the results of earlier in-reactor creep-fatique test carried out at 90°C with a strain amplitude of 0.5% and a holdtime of 10s are also shown.
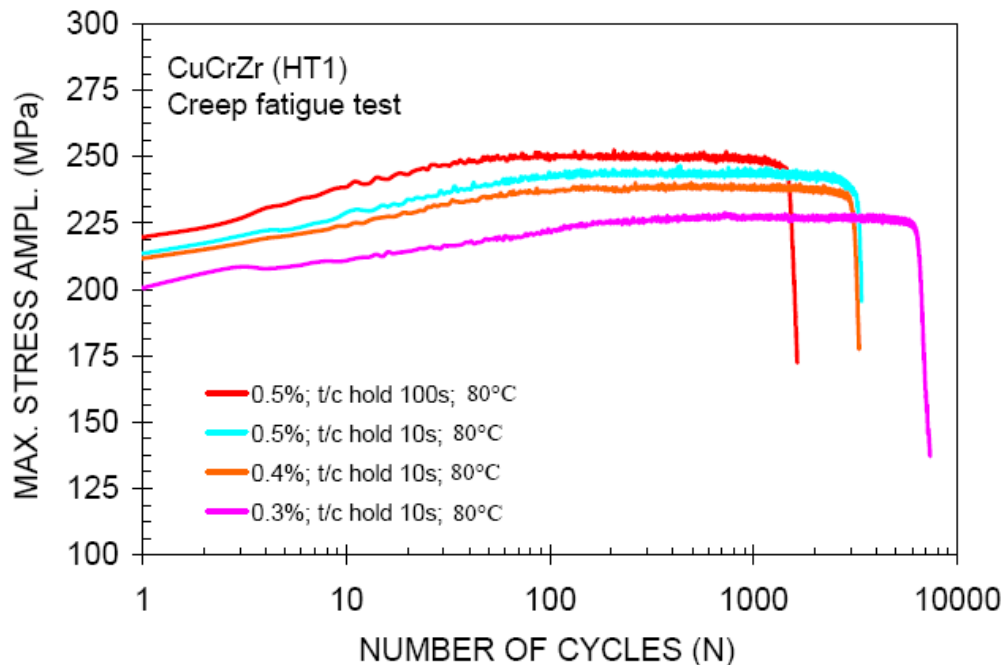
Figure 3. The same as in Figure 2 but for creep-fatigue tests carried out outside of reactor and on CuCrZr HT1 alloy in unirradiated condition. Tests were carried out at 80°C with a strain amplitudes of 0.3, 0.4 and 0.5 %.

It is reasonable to conclude that the present work has confirmed that it is possible to carry out well controlled and accurate in-reactor creep-fatigue tests. The most significant aspect of the present results is that the displacement damage produced by neutrons does not seem to affect the lifetime of the material exposed to creep-fatique condition in the field of neutron irradiation (compare results in Figure 2 and Figure 3).
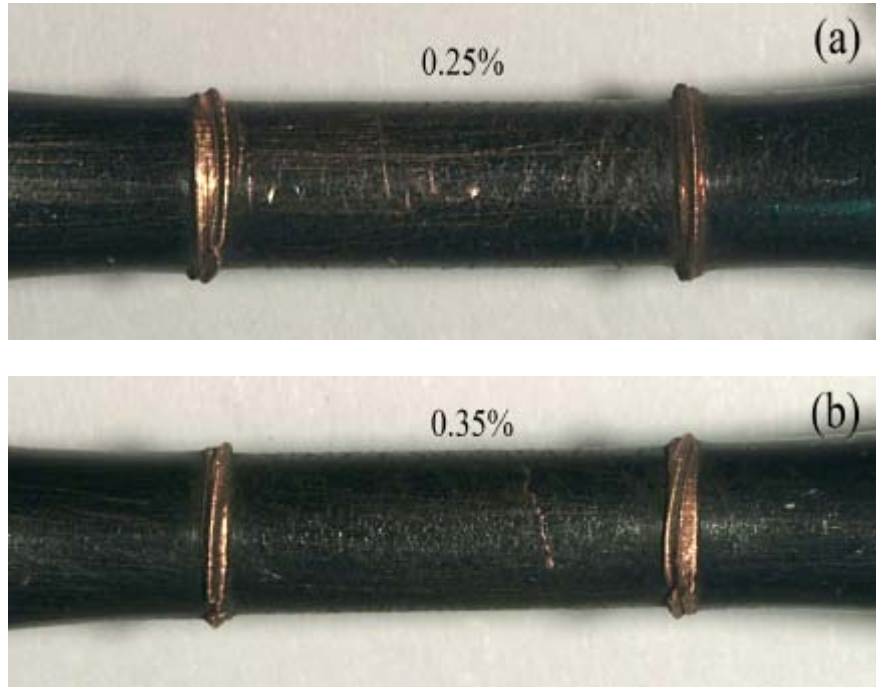
Figure 4. Photographs of the in-reactor creep-fatigue tested specimens with strain amplitude of (a) 0.25% (Test No. 1) and (b) 0.35 % (Test No. 2). Note the absence of any crack in Figure 4 (a) whereas a crack can be clearly seen in Figure 4 (b).

### 3.2.2 Testing of irradiated CuCrZr/SS joints produced under different blanket manufacturing conditions[2]
B.N. Singh and B.S. Johansen

Since the basic microstructure of the CuCrZr alloy (i.e. precipitate size and density, grain size, etc) is sensitive to thermo-mechanical treatments, it is expected that the mechanical properties of the base materials used in the joints of Cu-alloys (i.e. CuCrZr or DS Copper) with stainless steel (i.e. 316 LN) will be affected by manufacturing conditions used in the production of the first wall and divertor components. In recent years, experiments have illustrated that indeed the base material in the joints of both CuCrZr and DS-Copper(CuAl25) with stainless steel joints becomes softer after multiple HIPing thermal cycles. The effect of neutron irradiation on the mechanical properties of these base materials, on the other hand, is not known at present. It was therefore decided to investigate the effect of low dose neutron irradiation at 150°C on the tensile properties of CuCrZr alloy, DS copper (CuAl25) and 316(LN) stainless steel. Prior to irradiation, these alloys were subjected to various manufacturing heat treatments (see table 1).

---

2 TW4 – TVM - CUSSPIT

Table 1. Summary of manufacturing heat treatments.

Code	Material	HIP	Heat treatment	Ageing
T10-4	CuCrZr	1040°C/2h/140MPa	980°C/0.5h	560°C/2h
T13-2	CuCrZr	980°C/2h/140MPa	980°C/0.5h	580°C/2h
DS 15	CuAl25	1040°C/2h/140MPa	-	-
T11	SS316LN	1040°C/2h/140MPa	980°C/0.5h	560°C/2h

A number of tensile specimens of CuCrZr, DS-Cu(enAl25) and 316(LH) stainless steel with different heat treatments corresponding to different manufacturing conditions were irradiated with fission neutrons in the BR-2 reactor at Mol (Belgium) at 150°C to displacement doses of 0.001, 0.01 and 0.1 dpa. The irradiation was carried out in helium atmosphere and the irradiation temperature was achieved by controlling the gas-gap in the capsule containing specimens. The temperature was controlled by adjusting the water flow inside the irradiation thimble tube. Both irradiated an unirradiated reference specimens were tensile tested at 150°C at a strain rate of $1.3 \times 10^{-3} s^{-1}$ in vacuum.

The main results of tensile tests carried out on the irradiated as well as unirradiated CuCrZr specimens with different manufacturing conditions are summarized in Figure 5 in the form of stress-strain curves for CuCrZr alloy (a) HIPed at 1040°C (T10-4) and (b) HIPed at 980°C (T13-2). For both cases, stress-strain curves are shown for different displacement doses in the range of 0.001 to 0.1 dpa. The results show that the HIPing at 1040°C (Figure 5a) reduces the yield strength of the base material companed to the yield strength of the base material after HIPing at 980°C (Figure5b) even in the unirradiated condition. It should be noted that this difference is maintained even after irradiation upto a dose level of 0.1 dpa. The results shown in Figure 5 clearly demonstrate that irradiation at 150°C even to relatively low doses has significant effects both on the yield strength and the uniform elongation of the CuCrZr base material after HIPing at 1040°C and 980°C. In both cases irradiation causes a significant increase in the yield strength and correspondingly a significant decrease in the uniform elongation.

Figure 6 shows the stress-strain curves for DSCu125 HIPed at 1040°C (DS15) tensile tested at 150°C in the unirradiated as well as irradiated conditions. The effect of irradiation on mechanical properties is clearly visible even though the effect is not marked as in the case of CuCrZr alloy (Figure 5). The increase in the yield strength is for example not as large as in the case of CuCrZr alloy. The effect of irradiation to a dose level of 0.1 dpa causes almost a complete loss of uniform elongation indicating that the material looses it ability to work harden during deformation

In the case of stainless steel (316LN), the low dose irradiation causes increase in the yield strength but unlike in the case of copper alloys leads to very small descrease in the uniform elongation (Figure 7). Furthermore, even after irradiation to a dose level of 0.1 dpa, the material maintains its ability to work harden during post-irradiation deformation. It should be mentioned that the irradiation of SS316LN to a level of 0.1 dpa exhibits a tendency to introduce the phenomenon of yield drop immediately after the yield point during post-irradiation testing at 150°C even though the yield drop is very small.
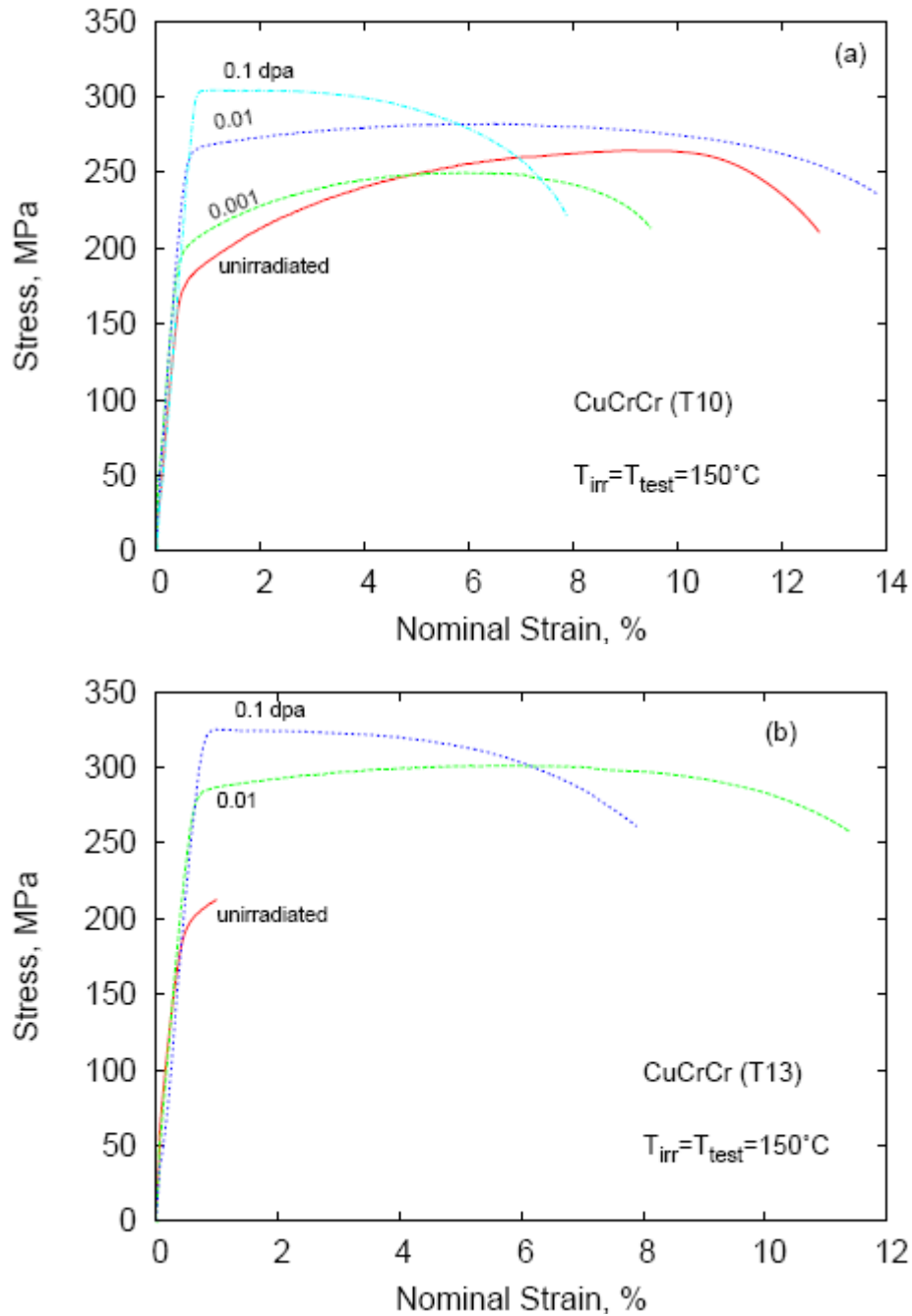
Figure 5. Stress-strain curves for unirradiated and irradiated CuCrZr alloy HIPed at (a) 1040°C (T10) and (b) 980°C (T13). Specimens with the manufacturing treatments T10 as well as T13 were irradiated at 150°C to doses of 0.001, 0.01 and 0.1 dpa. Specimens were tensile tested at 150°C. Note that the irradiation to a dose level of 0.1 dpa causes a significant reduction in the uniform elongation.
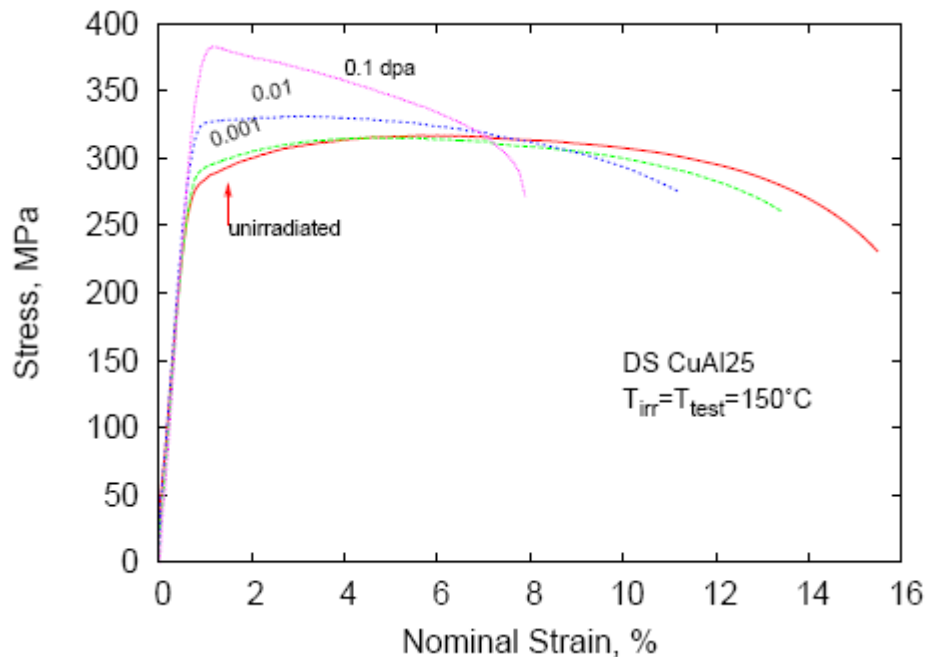
Figure 6. The same as in Figure 5 but for DSCuAl25. Note that irradiation to a displacement dose level of 0.1 dap reduces the uniform elongation almost to zero and tends to lead to plastic instability immediately after yielding.

Figure **7**. The same as in Figure 5, but for the base material SS316(LN). Note that even though both the yield and flow strength increase with increasing dose level, there is practically no reduction in the uniform elongation.

3.3 Long-term technology

3.3.1 Effect of helium implantation and neutron irradiation on cavity formation in iron and Eurofer-97[3]

M. Eldrup, B. N. Singh and P. Jung (*Forschungszentrum Jülich, Association EURATOM-FZJ, Germany)*

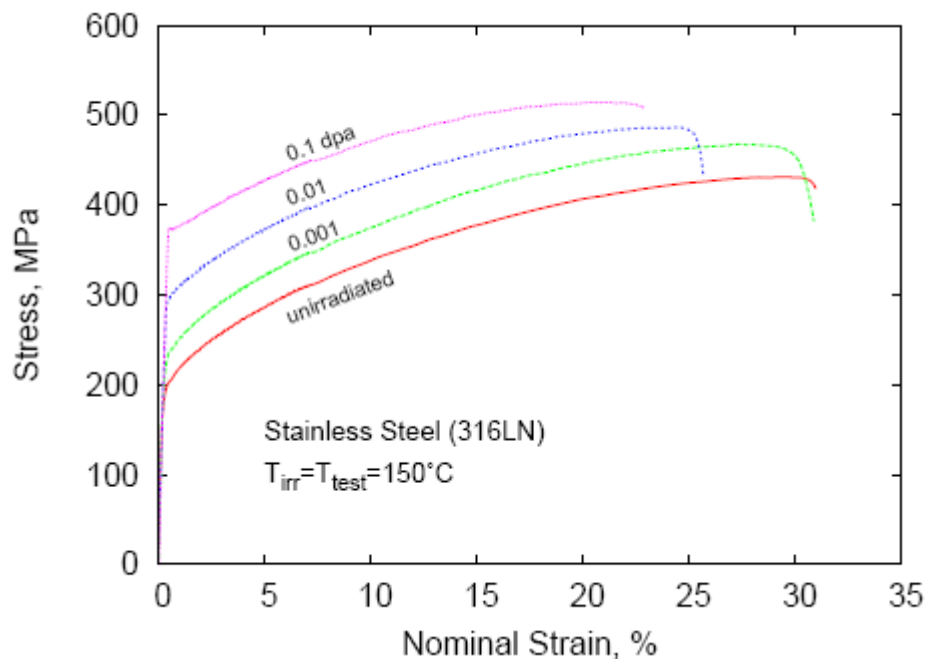Investigations of the effects of helium implantation and of neutron irradiation after helium implantation by Positron Annihilation Spectroscopy (PAS) have continued. While the He implantations carried out at Jülich have been completed, some of the neutron irradiations at SCK.CEN, Mol, Belgium have been delayed and the specimens delivered to Risø in the beginning of 2007. Helium implantation rates in the ranges of 6×10^{-4} to 6×10^{-3} appm He/s at 50°C and 1.2×10^{-3} to 1.2×10^{-2} appm He/s at 350°C were used for implantation of pure Fe and Eurofer-97 to doses of 1, 10 and 100 appm He. Some specimens have been investigated after both He implantation and neutron irradiation (in the range of 0.01 to 0.3 dpa). This work is continuing with the neutron irradiated specimens obtained in 2007. Careful examination and analysis of all measurements carried out so far show that the effects of both He dose and neutron displacement dose are clearly observed as has in part been reported earlier. However, the relatively small range of He implantation rates in combination with the unavoidable scatter on the experimental results has prevented a well-defined conclusion on the effects of He implantation rate.

Quantitative estimates of He bubble sizes and densities were found to agree with and thus support the results of theoretical calculations for He implantation at 350°C. For He implantation at 50°C, wide distributions of both He bubble sizes and densities of He in the bubbles are expected. Since both of these parameters influence the observed positron lifetimes, the extraction of quantitative estimates of cavity sizes and densities is more difficult than for 350°C implantations, although qualitatively the data clearly demonstrate that a high density of small (sub-nm) cavities are present in the as-implanted specimens.

In order to investigate the question of the character of the cavities which are created in iron during He implantation at a temperature of 50°C, an isochronal annealing experiment has been carried out of Fe implanted with 100 appm He. Both positron lifetime as well as Coincidence Doppler broadening (CDB) measurements were carried out in a collaboration with the Institute for Materials Research, Tohoku University, Japan (T. Toyama, Z. Tang, Y. Nagai, M. Hasegawa). Figure 8a shows the results of the positron lifetime measurements and Fig. 8b those of the CDB recorded simultaneously with the lifetime data. The green line is the signature of the presence of nano-voids after neutron irradiation. The deviation of the blue curve from the green line at the higher temperatures shows that the defects are different from nano-voids.

---

3 TW4–TTMS-007
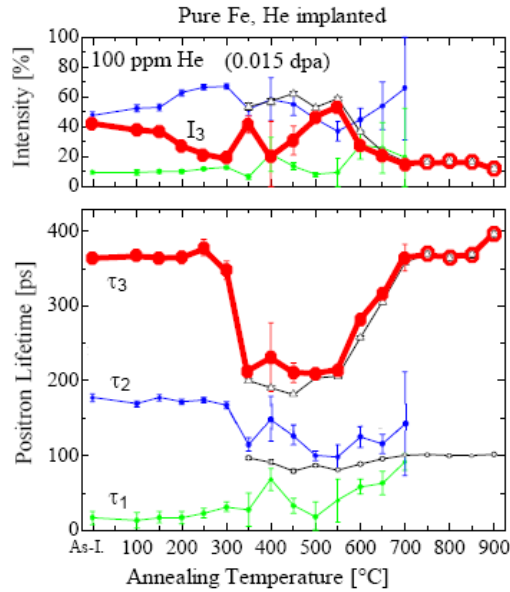
Figure 8a. Positron lifetime parameters as functions of annealing temperature for He implanted pure iron. The longest lifetime τ_3 and its intensity I_3 (enhanced red curves) are due to nano-voids and He bubbles. A sharp annealing stage is observed at about 300°C.
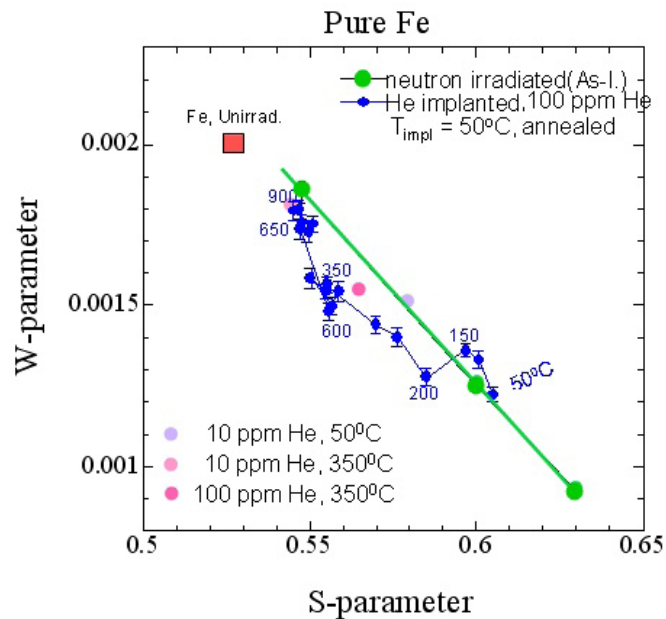
Figure 8b. So-called S-W plot derived from Coincidence Doppler broadening measurements. The data for samples with varying densities of the same type of defects will all fall on a straight line. This is exemplified by the green points for neutron irradiated Fe, which contain different densities of nano-voids (displacement doses of 10^{-4}, 10^{-3} and 10^{-2} dpa, respectively). The S-parameter increases with defects density, while the W-parameter decreases. The blue points are for He implanted and annealed Fe, with the blue numbers indicating the annealing temperatures.

3.3.2 In-reactor uniaxial tensile deformation of pure iron and Fe-Cr alloy4

B. N. Singh, S. Tähtinen, P. Moilanen* (*VTT Industrial Systems (Association EURATOM-TEKES), Espoo, Finland)), P. Jacquet** and J. Dekeyser** (**Reactor Experiment Department, SCK.CEN, Mol, Belgium)*

It is well known that neutron irradiation of iron and ferritic-martensitic steels at temperatures below 0.3Tm (where Tm is the melting temperature in Kelvin) causes a decrease in the uniform elongation and leads to plastic flow localization. This is a matter of concern from the point of view of application of these materials in the structural components of a fusion reactor. It should be recognized, however, that this conclusion and the concern are based exclusively on the results of post-irradiation tests. Clearly, the microstructure as well as the test conditions during a post-irradiation mechanical test are fundamentally so different from those expected during deformation of materials in the reactor environment that the results of the post-irradiation tests may not be representative of in-reactor deformation behaviour.

In fact, the in-reactor tensile tests performed recently on pure copper and a CuCrZr alloy have demonstrated that indeed the deformation behaviour observed in the in-reactor dynamic tests is significantly different from that in the case of a post-irradiation test[5]. However, since the dynamic behaviour of dislocation is likely to be different in bcc iron and steel from that in the fcc copper, it is of a particular interest to investigate the in-reactor deformation behaviour of bcc iron and steel. The results of these investigations would be valuable not only from technological points of view but may also be very useful for understanding and modeling the deformation behaviour of bcc materials under the condition of dynamic deformation in reactor environment. It was therefore decided to determine experimentally the deformation behaviour of pure iron and Fe-Cr alloy during uniaxial tensile tests performed directly in a fission reactor (i.e. in the environment of fission neutrons). Details of the necessary preparations for such experiments and the results of out-of-reactor tensile tests on unirradiated pure iron and Fe-Cr alloy were reported last year. In the following, a brief description is given of the in-reactor experiments and of the results obtained during in-reactor tensile tests.

The test facility used for carrying out these in-reactor tensile tests was essentially the same as the one used for copper and CuCrZr alloy5. The basic principle of the tensile test module is based on the use of a pneumatic bellow to introduce stress and a linear variable differential transformer (LVDT) sensor to measure the resulting displacement (i.e.strain) produced in the specimen. To accommodate the test modules and the necessary instrumentation to perform the uniaxial tensile tests in the reactor, special irradiation rigs were designed and constructed. In addition to measuring the stress and strain during the test, the temperature profile in each module was measured by three thermocouples placed at different positions (LVDT, specimen, ballons) in the rig. Three dosimeters were placed at the specimen level in the rig to determine the neutron fluence during the test.

The irradiation rig was designed to accommodate two complete test modules containing specimen, bellow, LVDT, thermocouples and dosimeters such that two independent tensile tests could be performed at the same time. An additional tensile specimen was attached to each test module which was irradiated in unstressed condition but with the same neutron flux and at the same irradiation temperature as for the in-reactor tensile test specimen. These specimens were used for the post-irradiation investigations.

In the first set of in-reactor tensile tests in this series, two tensile specimens of Fe-Cr alloy were loaded in two different test modules number 1 and 2. Both test modules together with necessary instrumentation were loaded into an irradiation rig. The test on the specimen loaded in the test module 1 was called Test No.1 and in the test module 2 was called Test No.2. Both tests were carried out at 53°C at a strain rate of $1 \times 10^{-7}s^{-1}$. The displacement damage rate during the tests was $\sim 6 \times 10^{-8}$ dpa/s.

In the case of Test No.1, the tensile test was initiated soon after the ambient temperature in the irradiation rig had reached a stable value of 53°C in about 16 min. Thus the tensile test was initiated after 16 min. of irradiation (i.e. after 5.8×10^{-5} dpa) in the absence of applied stress on the specimen. The test was continued until a clear sign of initation of fracture was observed. The stress and strain was continuously measured and recorded. The test was stopped at a dose level of 7×10^{-2} dpa.

The specimen in the test module 2 (Test No.2) was first irradiated in the unstressed condition for about 70 hours to give a displacement dose of 1.5×10^{-2}dpa. The specimen was then loaded manually to a stress level close to the estimated yield stress and then tensile test was initiated with a strain rate of $1 \times 10^{-7}s^{-1}$. The test was continued until a clear sign of the initiation of fracture was observed. At a dose level of 9.8×10^{-2}dpa the test was stopped. Soon after the irradiation rig was removed from the reactor core.

The second set of in-reactor tensile tests in this series was performed on pure iron. Prior to in-reactor tensile tests, the specimens were annealed at 650°C for 2h in vacuum. The annealed specimens were coated with a thin layer of platinum ($\sim$ 10 nm thick) to protect the specimens against water corrosion during the test. Two such tensile specimens of pure iron were loaded in two different test modules (number 3 and 4). Both modules containing specimens and the necessary instrumentation loaded into a irradiation rig. Both Test No. 3 and Test No. 4 (in the test modules 3 and 4, respectively) were carried out at 53°C with at damage rate of $\sim 6 \times 10^{-8}$ dpa s^{-1} and a strain rate of $1 \times 10^{-7}s^{-1}$.

After the irradiation rig was lowered in the reactor core, it took about 101 min. to start the Test No.3. Thus the specimen in the Test No. 3 received a displacement dose of 3.65×10^{-4}dpa in the absence of applied stress. The test was continued until the specimen fractured. The specimen in the test module 4(Test No.4) was irradiated without stress for about 70h to give a displacement dose of 1.5×10^{-2}dpa. After this irradiation the tensile test was started with a strain rate of $1 \times 10^{-7}s^{-1}$. Unfortunately the test module 4 developed some mechanical problem and the specimen in the test module could not be strained. After several unsuccessful attempts to make the straining system to function properly, the Test No.4 had to be abandoned.
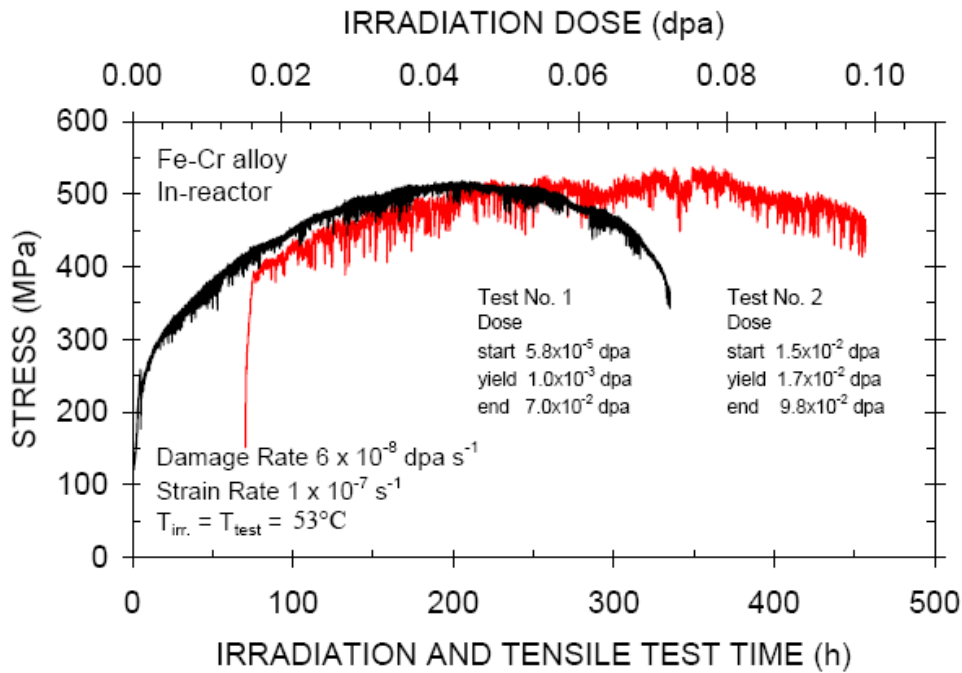
Figure 9. Continuously measured evolution of the stress response as a function of irradiation and tensile test time during the in-reactor tensile tests of Fe-Cr alloy at 53°C with the pre-yield doses of 1.0×10^{-3} dpa (Test No 1.) or 1.7×10^{-2} dpa (Test No.2).

As indicated earlier, the evolution of stress and strain during these in-reactor tests were continuously measured and recorded. Figure 9 shows the raw results on the evolution of stress as a function of irradiation and tensile test time (and displacement dose) for the Test No.1 and Test No.2 on Fe-Cr alloy. As can be seen in Figure 9, the actual tensile test on the specimens in the Test No.1 and Test No. 2 were initiated at different times after the specimens were brought in the reactor. Since the specimens in Test No. 1 and Test. No 2 received different levels of displacement doses while they were still at zero stress level, during subsequent tensile tests they yielded at different stress levels. It is interesting to note that even though the initial rate of hardening in the Test No. 1 is higher than that in the Test No.2, the level of maximum stress reached in both tests is about the same. Figure 10 shows the true stress – true strain curves for Test No. 1 and 2 on Fe-Cr alloy. Apart from the differences in the yield stress and initial hardening rates, the evolution of flow stress in the Test no. 1 and 2 is very similar. It is somewhat surprising that the uniform elongation in the case of Test No.2 is higher than that in the case of Test No. 1. Similar conclusions can be drawn from the results shown in Figure 11 describing the variation of irradiation induced hardening, $\Delta\sigma_f$, with true strain.
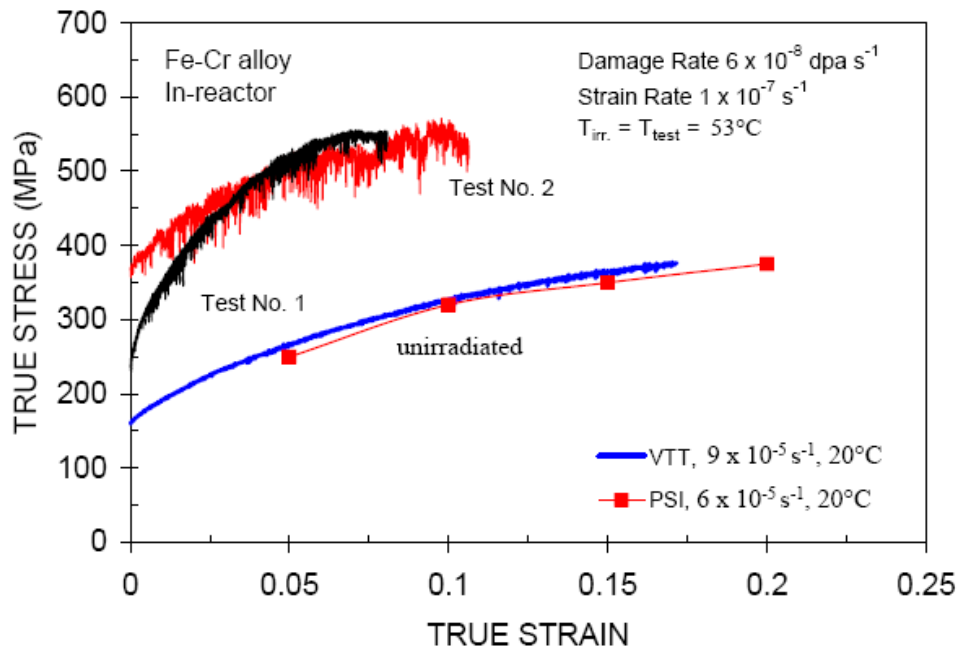
Figure 10. True stress – true strain curves for the in-reactor tensile Test No. 1 (with pre-yield dose of 1.0x10^{-3} dpa) and Test No. 2 (with pre-yield dose of 1.7x10^{-2} dpa) on Fe-Cr alloy. The results for the out-of-reactor tests on the uirradiated Fe-Cr alloy are also shown. Note that even though the higher pre-yield dose leads to a higher yield stress, the maximum flow stress (i.e. the ultimate strength) reached in both tests is almost the same.

Figure 11. The increase in flow stress due to irradiation, $\Delta\sigma_f$, as a function of true plastic strain for in-reactor Test No. 1 and 2 on Fe-Cr alloy. Note that the reate for increase in $\Delta\sigma_f$ with strain is higher in the case of the low pre-yield dose (i.e. Test no.1.) than that in the case of the higher pre-yield dose (i.e. Test No. 2). However, the maximum level of increase in $\Delta\sigma_f$ is about the same in both cases.

Figure 12. True stress – true strain curves for the in-reactor tensile tested pure iron at 53°C and for the out-of-reactor tensile tested pure iron at 20°C. Note that the magnitude of uniform elongation is significantly reduced due to irradiaton even though the increase in the yield stress and the flow stress due to irradiation is not very high.

Figure 12 shows the true stress – true strain curves for the unirradiated and in-reactor tensile tested specimens of pure iron. It can be easily seen that the magnitude of hardening during the in-reactor test is considerably lower than that in the case Fe-Cr alloy. The effect of irradiation on increase in the flow stress, $\Delta\sigma_f$, during the in-reactor Test No. 3 is shown in Figure 13 as a function of true strain. Note that the increase in hardening in the Fe-Cr alloy (Figure 11) during in-reactor tensile test is almost five times higher than that in the case of pure iron. It is interesting to note that in spite of the fact that the level of irradiation-induced hardening in Fe-Cr alloy is high, the Fe-Cr alloy specimens yield higher uniform elongation compared to the level of uniform elongation obtained in the case of pure iron specimen.

Photographs of Fe-Cr specimens used in the in-reactor tensile Test No. 1 and 2 are shown in Figure 14(a) and 14(b), respectively, after they were removed from the reactor. Figure 14(c) shows the photograph of Fe specimen used in the in-reactor Test No. 3. It can be seen in Figure 14 that the specimen tested in Test No. 1 (with a pre-yield dose of $\sim 1 \times 10^{-3}$ dpa) (Figure 14a) shows more extensive necking than the specimen used in the Test No. 2 (with a pre-yield dose of 1.7×10^{-2} dpa). The necking behaviour seen in Figure 14(a) or 14(b) is consistent with the test results shown in Figure 9.
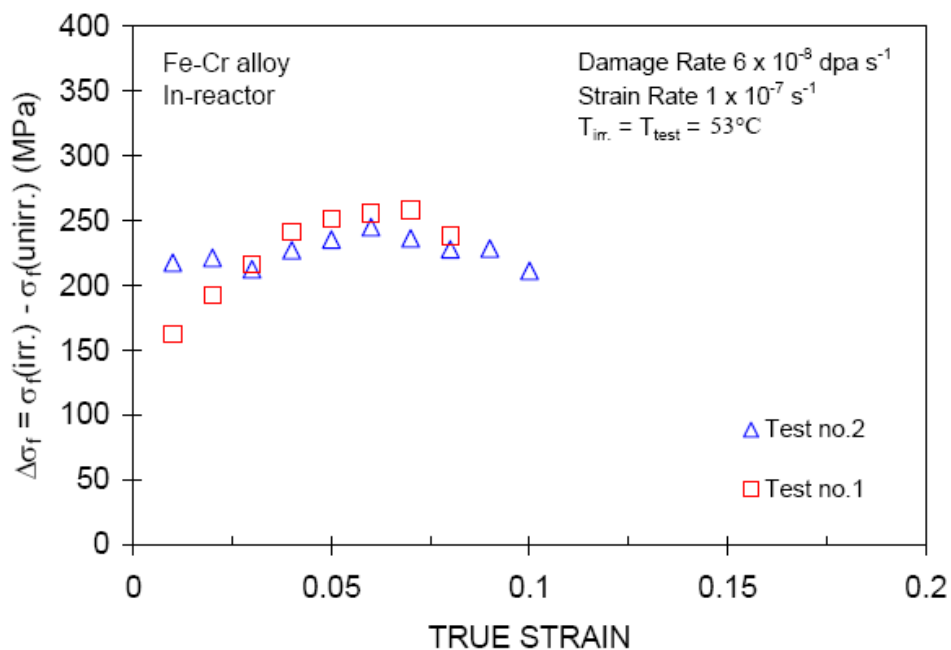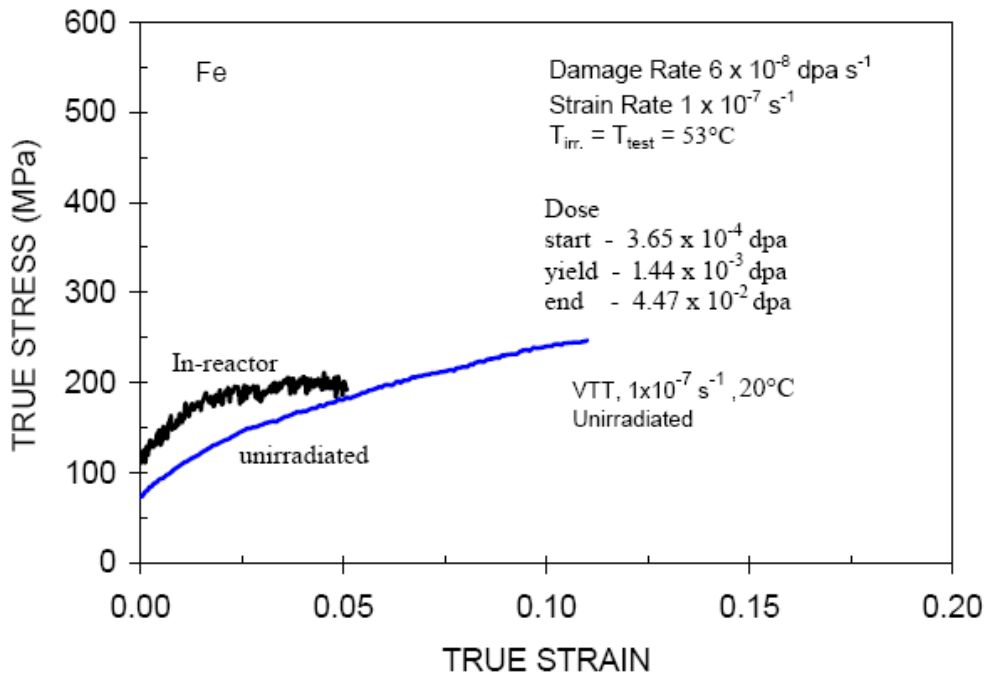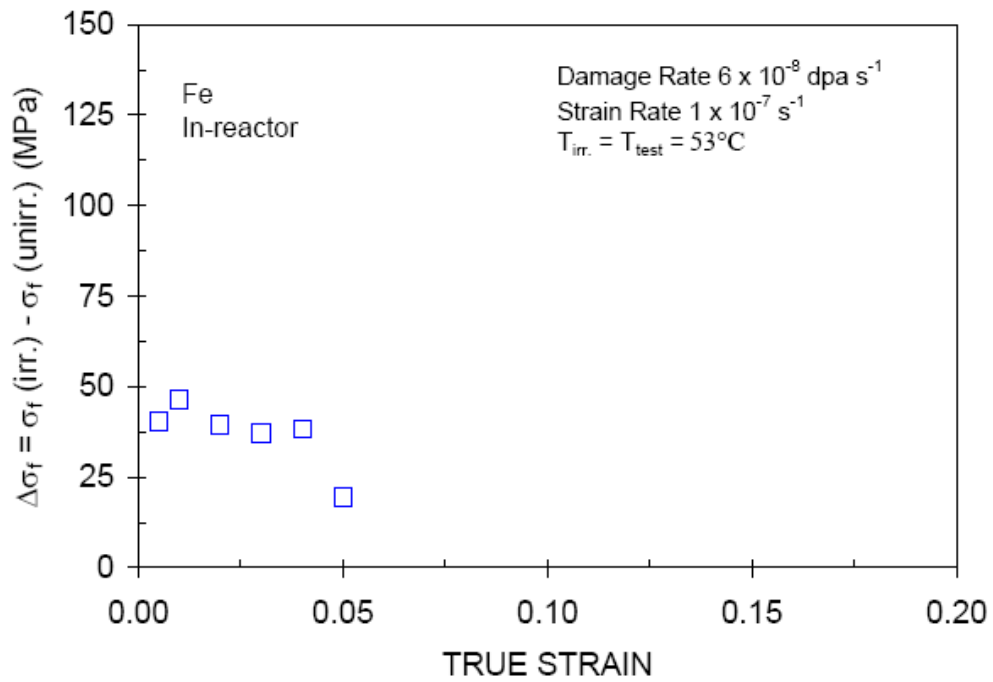
Figure 13. The increase in flow stress due to irradiation, $\Delta\sigma_f$ as a function of true plastic strain for the in-reactor tensile tested pure iron. Note that the magnitude of , $\Delta\sigma_f$ begins to decrease with strain already at a very low level of plastic strain.
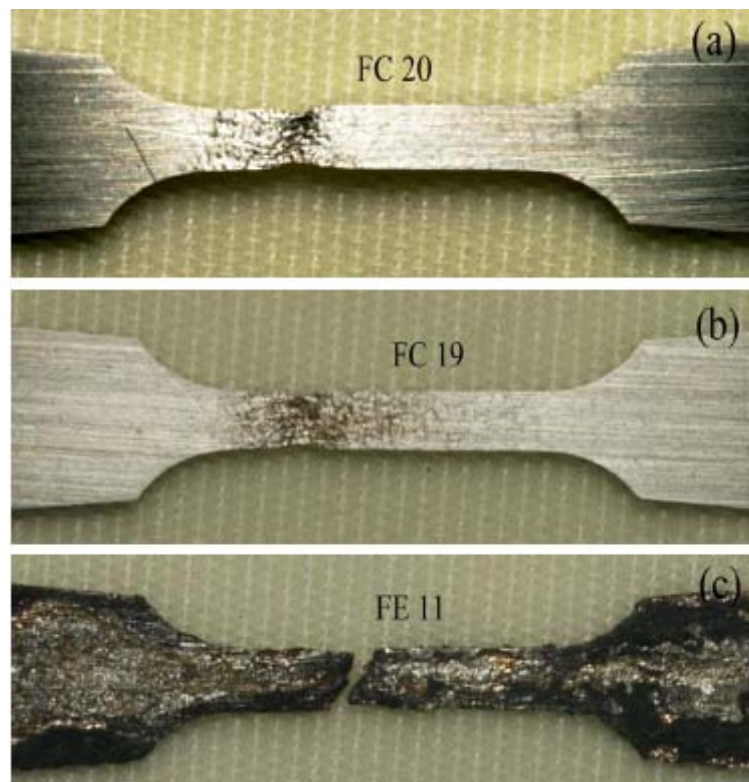

Figure 14. Photographs of in-reactor tensile tested specimens Fe-Cr alloy of (a,b) and pure iron(c); specimens (a) FC20, (b)FC19 and (c)FE11 were tested in Test No. 1,2 and 3.

3.4 Underlying technology

3.4.1 Mechanisms operating during plastic deformation of copper under concurrent production of casades and dislocations.

H. Trinkaus (*Forschungszentrum Jülich, Jülich, Germany) and B.N. Singh*

In-reactor tensile tests (IRTs) on pure Cu and CuCrZr alloy have revealed a deformation behaviour which differs significantly from that observed in conventional post-irradiation tensile tests (PITs). In contrast to PITs where the deformation behaviour is commonly observed to be characterised by yield drop and plastic instability and by pronounced localisation of plastic deformation in cleared channels, in IRTs, the materials deform uniformly and homogeneously. A prominent feature observed in IRTs is that an increase in the pre-deformation dose results in an increase in the level of hardening in its whole evolution from the yield stress to the on-set of fracture - as if the materials "remembered" the impact of the pre-yield damage level over the whole test period. These features have motivated us to start a comprehensive analytical analysis of the possible mechanisms underlying them.

In IRTs as well as in PITs, dislocations have been observed to be decorated with dislocation loops. We report here on an investigation of the effect of dislocation decoration on the yield stress and the post-yield flow stress in IRTs, using the small loop approximation within the isotropic elastic continuum approach in our analytical estimates. As in our previous treatment of PITs, we attribute dislocation decoration to the trapping of clusters of self-interstitial atoms (SIAs) in the form of glissile loops in the far ranging stress fields of dislocations. During pre-yield irradiation, small cascade induced glissile loops reach dislocations at rest by one-dimensional diffusion whereas dislocations moving during deformation are primarily supplied with loops by sweeping. The fate of matrix loops swept by a moving dislocation depends on their glide direction relative to the glide plane of the dislocation. Loops gliding parallel and transversely to the glide plane ("aligned" and "non-aligned" loops) join the loop cloud accompanying the dislocation and approach the dislocation where they are annihilated, respectively, provided their motion is not blocked by their interaction with other matrix clusters. In the latter case, bound pairs of clusters are left behind the dislocation.

An analytical description of this complex dynamic decoration process requires substantial simplifications. We have approximated the region of decoration around a dislocation by a 2D space of decoration defined by the surface perpendicular to the glide plane and tangential to the dislocation line, and have introduced the "coverage" of this surface with the decorating SIAs projected on it as a measure for the degree of decoration. For describing the evolution of this "coverage", α, under pre-yield and post-yield irradiation, we have formulated rate equations where the production terms are defined by the diffusion fluxes of cascade induced glissile loops and the swept apparent matrix loop fluxes, respectively. For the case of post-yield deformation and irradiation, we have taken into account alignment of "non-aligned" matrix loops, annihilation of SIAs in loops with vacancies in stacking fault tetrahedra (SFTs) and blocking of aligned loops by matrix clusters, characterising the strength of these reactions by appropriate cross sections. An important additional term describes the reduction of the (average) degree of decoration by the expansion of the decorated space during dislocation evolution. We have derived and parametrically studied approximate solutions of these rate equations.
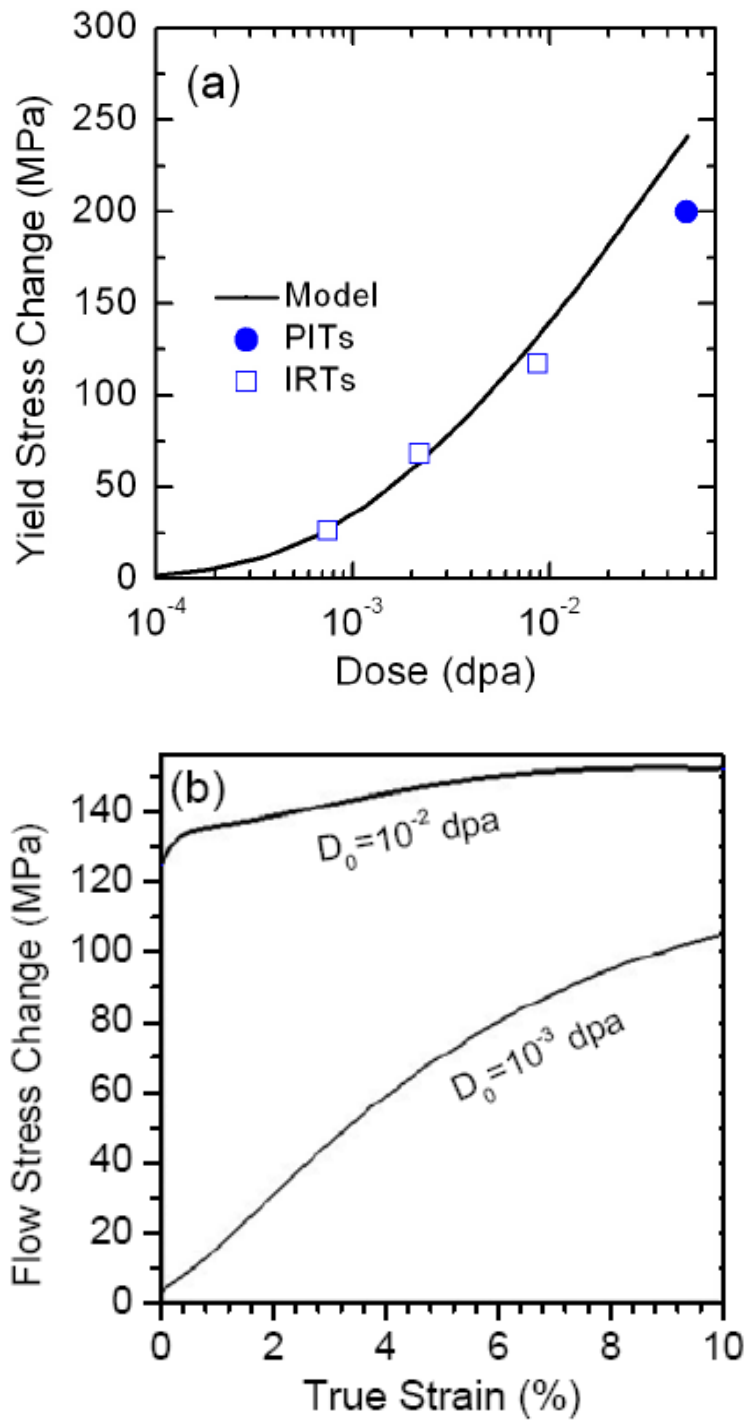
Figure 15. Contributions of temporary and definitive blocking of members of loop clouds decorating dislocations to (a) yield stress change as a function of dislocation dose and (b) flow stress change as function of true plastic strain calculated for the in-reactor test conditions for copper. Dose rates and strain rates where chosen according to the in-reactor test condition. Note the strong effect of the pre-yield dose (D_o) on the flow stress.

During yielding and post-yield deformation, temporary or definitive blocking of members of the loop cloud by their mutual interaction and their interaction with matrix clusters encountered is associated with forces on the dislocations which contribute to yield and flow stresses, respectively. Assuming that all dislocations are equally and homogeneously decorated and start to move at the same stress level, we may write these contributions, σ_y and σ_f, as bi-linear functions of the respective densities of the defects accumulated near the dislocations and in the matrix , α and c_m , respectively, both depending on dose:

$$\sigma_y = \eta\,\alpha^2\mu, \qquad\qquad \sigma_f = \varphi\,\alpha c_m\,\mu\,,$$

where η and φ are factors depending weakly on the size of the clusters involved, and μ is the shear modulus. Figures (15a) and (15b) illustrate the dependence of σ_y and σ_f on pre-yield dose and strain, respectively. In view of the simple nature of our approximations used, the experimentally observed trends, particularly the pronounced effect of the pre-yield dose on the flow stress, may be considered to be roughly reproduced by our approach - except for the flow stress at low pre-yield dose and strain which is substantially lower than observed. In this low dose/low strain range, the interaction of the matrix clusters with the moving loop cloud is obviously not the mechanism controlling the flow stress. On the other hand, this mechanism would explain the apparent memory of the deforming material concerning the impact of the pre-yield damage level on the flow stress over the whole test periods.

3.4.2 Molecular dynamics simulations of dislocation dynamics in the environment of radiation – induced microstructure.

Yu. N. Osetsky(*computer Science and Mathematics Division, Oak Ridge National Laboratory, Oak Ridge, U.S.A) and B.N. Singh*

In-reactor deformation experiments (both tensile and creep-fatigue tests) have clearly illustrated that the mechanical performance and lifetime of materials exposed concurrently to deformation and irradiation are substantially different from those exhibited under post-irradiation deformation conditions. The mechanical response of materials during in-reactor deformation experiments gets very complicated because of the simultaneous operation of two interactive kinetics: one due to irradiation-induced defect production rate and the other due to dislocation generation rate due to deformation. Under these conditions a large variety of interactions are likely to occur between moving dislocations and glissile and sessile clusters of interstitials and vacancies. The energetics of these interacations are likely to determine the dynamics of dislocations and buildup of dislocation and defect microstructure. This in turn will determine the buildup of stress and strain (i.e.mechanical response) in the material during in-reactor deformation experiments.

As reported in the previous subsection 3.4.1, analytical calculations are in progress to estimate the mechanical response of materials under the conditions in the in-reactor experiments. It should be emphasized, however, that in these analytical calculations the energetics of various interactions between dislocations and defect clusters are evaluated using the linear elasticity theory. These evaluations may not be very accurate for the cases of close distance interactions between dislocations and defect clusters. In order to make the results of analytical calculations of the yield and the flow stress more reliable and quantitative it is necessary to use the molecular dynamics (MD) simulations to evaluate the appropriate mechamism and the relevant rate constants for various cluster-cluster and cluster-dislocation interactions. Such simulation activities are in progress.

In the present work MD simulations have been performed to investigate the nature of some of the basic interactions between moving dislocations and defect clusters (e.g. SIA loops and vacaney SFTs) produced during in-reactor deformation experiments. Interactions of both edge and screw dislocations were simulated in fcc copper crystals containing 3-8x10^6 atoms at temperatures in the range of 0 to 600 K. In these simulations the EAM-type many-body interatomic potential was used. Simulations were performed using periodic boundaries along the glide direction and the dislocation line. The dislocation velocity used in these simulations was in the range of 2 to 200 m/s and the local strain rate varied in the range of 10^6 to 10^{8}s^{-1}. The results obtained thus a suggest that under the dynamic conditions of concurrent dislocations generation and damage productions, the mobile edge as well as screw dislocations are likely to enhance the recombination of interstitial and vacancy components of the irradiation-induced defects. In the case of edge dislocations, the recombination is enhanced primarily due to intereaction between glissile SIA clusters deposited into the existing stacking tault tetrahedron by the edge dislocation dragging the SIA clusters. In the case of screw dislocations, the enhancement of recombination occurs via annihilation of the opposite sign of helices formed due to interaction with interstitial and vacancy defects.

The result of interaction of moving dislocations with SIA loops is different for edge dislocations compared to that of the screw dislocations. A moving edge dislocations either absorbs the loops (with intersecting Burgers vector) or drags the loops (with Burgers reactor parallel to the dislocation line) along the glide direction. The screw dislocations, on the other hand, either change the Brugers of the loops to the Burgers vector of the dislocation line or shear the loops. Most commonly both types of dislocation shear SFTs particularly large ones. The present simulations suggest that in order to understand the removal of loops and SFTs from cleared channels the interactions of both edge and screw dislocations with loops and SFTs in the cleared channels have to be considered.

3.5 Publications and conference proceedings

International articles

Lucon, E.; Benoit, P.; Jacquet, P.; Diegele, E.; Lässer, R.; Alamo, A.; Coppola, R.; Gillemot, F.; Jung, P.; Lind, A.; Messoloras, S.; Novosad, P.; Lindau, R.; Preininger, D.; Klimiankou, M.; Petersen, C.; Rieth, M.; Materna-Morris, E.; Schneider, H.C.; Rensman, J.W.; Schaaf, B. van der; Singh, B.K.; Spaetig, P., The European effort towards the development of a demo structural material: Irradiation behaviour of the European reference RAFM steel EUROFER. 7. International symposium on fusion nuclear technology - ISFNT-7 Part B, Tokyo (JP), 22-27 May 2005. Fusion Eng. Des. (2006) v. 81 p. 917-923

Zinkle, S.J.; Singh, B.N., Microstructure of neutron-irradiated iron before and after tensile deformation. Symposium on microstructural processes in irradiated materials, San Francisco, CA (US), 13-17 Feb 2005. J. Nucl. Mater. (2006) v. 351 p. 269-284

Danish reports

Bindslev, H.; Singh, B.N (eds.), Association Euratom - Risø National Laboratory annual progress report 2005. Risø-R-1579(EN) (2006) 70 p.

International reports

Moilanen, P.; Saarela, S.; Tähtinen, S.; Singh, B.N.; Jacquet, P., In-reactor creep-fatigue tests in BR2 test reactor - design, construction and calibration of loading devices. VTT-R-09316-06 (2006) vp.

Unpublished international conference contributions

Singh, B.N., Exploration of materials response to irradiation with energetic particles: Progress and perspectives. 23. Symposium on effects of radiation on materials, San Jose, CA (US), 13-15 Jun 2006. Unpublished.

Tähtinen, S.; Moilanen, P.; Jacquet, P.; Dekeyser, J.; Singh, B.N., In-reactor mechanical testing - a novel approach to the study of deformation behaviour in neutron environment. 23. Symposium on effects of radiation on materials, San Jose, CA (US), 13-15 Jun 2006. Unpublished.

Trinkaus, H.; Singh, B.N., Analytical treatment of defect accumulation and plastic deformation of metals under concurrent production of cascades and dislocations. 23. Symposium on effects of radiation on materials, San Jose, CA (US), 13-15 Jun 2006. Unpublished.

Osetsky, Y.N.; Singh, B.N., Atomic-scale properties of radiation defects and their reactions with dislocations. 23. Symposium on effects of radiation on materials, San Jose, CA (US), 13-15 Jun 2006. Unpublished.

Wen, M.; Wang, Z.; Ghoniem, N.M.; Singh, B.N., Systematic comparison between experiments and dislocation dynamics modeling of the effects of irradiation on the deformation of Cu. 23. Symposium on effects of radiation on materials, San Jose, CA (US), 13-15 Jun 2006. Unpublished.

Matsukawa, Y.; Zinkle, S.J.; Bilde-Sørensen, J.B.; Singh, B.N., Crystallographic analysis of surface slip bands in neutron irradiated pure copper. 23. Symposium on effects of radiation on materials, San Jose, CA (US), 13-15 Jun 2006. Unpublished.

Toyama, T.; Tang, Z.; Eldrup, M.; Nagai, Y.; Jung, P.; Hasegawa, M.; Singh, B.N., On the annealing behaviour of helium implanted Fe and Cu. 14. International conference on positron annihilation - ICPA-14, Hamilton (CA), 23-28 Jul 2006. Unpublished.

Singh, B.N., In-reactor deformation: Experiments, results and implications. International workshop on fundamental aspects of radiation damage, Barcelona (ES), 12-14 Sep 2006. Unpublished.

Trinkaus, H.; Singh, B.N., Mechanisms controlling plastic deformation of metals under concurrent production of cascades and dislocations. International workshop on fundamental aspects of radiation damage, Barcelona (ES), 12-14 Sep 2006. Unpublished.

Singh, B.N., Characterization of surface slip bands in neutron irradiated and deformed copper using electron backscatter diffraction technique. International workshop on fundamental aspects of radiation damage, Barcelona (ES), 12-14 Sep 2006. Unpublished.

Singh, B.N., Effect of helium implantation on neutron irradiation. International workshop on fundamental aspects of radiation damage, Barcelona (ES), 12-14 Sep 2006. Unpublished.

Victoria, M.; Dudarev, S.; Boutard, J.L.; Diegele, E.; Lässer, R.; Almazouzi, A.; Caturla, M.J.; Fu, C.C.; Källne, J.; Malerba, L.; Nordlund, K.; Perlado, M.; Rieth, M.; Samaras, M.; Schaeublin, R.; Singh, B.N.; Willaime, F., Modelling irradiation effects in fusion materials. 24. Symposium on fusion technology (SOFT), Warsaw (PL), 11-15 Sep 2006. Unpublished.

Boutard, J.-L.; Diegele, E.; Alamo, A.; Singh, B.N.; Petersen, C.; Déprés, C., Structural materials for T-breeding blankets in fusion reactors: Mastering their in-service properties via irradiation in fission reactors. Technical meeting on research reactor support needed for innovative nuclear power reactors and fuel cycles, Vienna (AT), 20-22 Nov 2006. Unpublished.

4 System analysis

4.1 EFDA-TIMES

P. E. Grohnheit

Since end of 2004 the EFDA and the Associations are developing a multi-region global long-term energy modelling framework called EFDA-TIMES starting from an initial version developed by an external consortium. The initial version has shown several needs for revisions, updates and improvements, which are ongoing within EFDA and several other programmes, e.g. IEA-ETSAP, EU Research Programmes (NEEDS Project), in which Risø is participating.

After a successful Expression of Interest for the call in August 2006 (TW6-TRE-ETM-UPS, etc.), Risø is now participating in the further development of the EFDA-TIMES model under the SERF Programme. Risø will contribute to the development of the upstream sector (fossil resources, refineries, renewable potentials, etc.). The contribution by Risø shall focus on technology vintages based on technology learning as well as contribution to the overall development of the model and use of the database software.

A kick-off meeting was held in Garching in February 2007 together with an EFDA-TIMES Steering Group meeting (Risø Member P. E. Grohnheit). Abstract for a paper "Fusion as new vector in long term energy studies" from the modelling team was submitted to the International Energy Workshop (IEW) in Stanford, California, June 2007. The time horizon for the current Risø contribution is mid 2007.

5 ITER and Danish industry activities

S. B. Korsholm and H. Bindslev
soeren.korsholm@risoe.dk

For several years it has been a priority for Risø to expand the industrial involvement of Danish companies in fusion research. Following the ITER site decision on June 28th 2005, a group was formed consisting of Risø National Laboratory, The Confederation of Danish Industries, The Trade Council of Denmark and the Ministry of Ministry of Science, Technology and Innovation. With Risø being the main driver an initiative was launched to inspire Danish companies and make them aware of the possibilities of being a supplier to the construction of ITER. This effort was initiated in 2005 (see Chapter 4 of Ref. 1), and has been further developed in 2006.

The entry gate to the initiative for Danish companies is a website http://www.risoe.dk/iter built at Risø and further developed during 2006. The website contains information on the coming tasks at ITER, background information, news and announcements of workshops etc., links to relevant international websites, description of experiences of other Danish companies, and an online database, where companies can present their fusion relevant competences and their interests in ITER tasks.

Apart from the fully public ITER and industry website, a site with restricted access is maintained. Companies may request a password to access the site that contains tender action material such as the EFDA and JET calls for expression of interest.

In parallel to these efforts, a mailing list have been maintained and extended. This is an important way of distributing news and advertising tender actions. Currently, over 50 companies and organizations are on the mailing list, and just over 20 companies have registered in the database (http://www.risoe.dk/iter/Database/Competences-Danish-companies.pdf).

A key element of the effort to prepare Danish companies and research institutes for ITER tasks has been the formation of the Danish ITER Industrial Network (http://www.risoe.dk/iter/DKnetvaerk/DKindustrinetvaerk.htm). It was started on the initiative of two companies and the non-exclusive group currently has 14 members consisting of interested companies and public research organisations. Risø has supported the initiative through the whole process and is chairing the network. The purpose of the network is sharing of information, preparation and forming of specific interest groups that may eventually converge into consortia. During 2006 the network formed eight such specialised groups.

The Remote Handling group organised a half day workshop on remote handling issues in collaboration with Risø. More than 20 companies participated.

A delegation of companies from the Network participated in an excursion to EFDA-JET in Oxford, UK, in late November 2006. The visit was organised in collaboration between EFDA-JET and Risø, and included visits to most JET facilities including the torus hall and the remote handling control room. JET scientists and engineers gave lectures and with the concluding debate the trip was great success, giving the companies a good impression on what is required in order to be a supplier for a fusion experiment. The delegation was joined by the science editor of the News Magazine Ingeniøren, who later featured a full page article about the Network and the visit to JET[2].

In February 2007, representing Risø Søren B Korsholm participated in the ITER Industrial Liaison Officers (ILO) meeting in Finland. The purpose of the meeting was to clarify the roles of ILO's and to pave the ground for forming international company networks, eventually becoming consortia.

The effort of preparing Danish companies and research organisations to the future ITER tasks will continue in 2007 and will be adapted to the available resources.

1. Risø-R-1579(EN) Association Euratom - Risø National Laboratory Annual Progress Report 2005, http://www.risoe.dk/rispubl/ofd/ofdpdf/ris-r-1579.pdf, edited by H. Bindslev and B.N. Singh.

2. Ingeniøren, 1 December 2006, page 16.

Risø's research is aimed at solving concrete
problems in the society.

Research targets are set through continuous
dialogue with business, the political system and
researchers.

The effects of our research are sustainable energy
supply and new technology for the health
sector.